uOttawa

L'Université canadienne
Canada's university

FACULTÉ DES ÉTUDES SUPÉRIEURES ET POSTOCTORALES

uOttawa

L'Université canadienne
Canada's university

FACULTY OF GRADUATE AND POSDOCTORAL STUDIES

Hazem Awad

AUTEUR DE LA THÈSE / AUTHOR OF THESIS

M.A.Sc. (Electrical Engineering)

GRADE / DEGREE

School of Information Technology and Engineering

FACULTÉ, ÉCOLE, DÉPARTEMENT / FACULTY, SCHOOL, DEPARTMENT

Competitive Optics Circuits for All-optical Signal-processing Applications

TITRE DE LA THÈSE / TITLE OF THESIS

Trevor Hall

DIRECTEUR (DIRECTRICE) DE LA THÈSE / THESIS SUPERVISOR

CO-DIRECTEUR (CO-DIRECTRICE) DE LA THÈSE / THESIS CO-SUPERVISOR

EXAMINATEURS (EXAMINATRICES) DE LA THÈSE / THESIS EXAMINERS

J. Yao

R. Gauthier

Gary W. Slater

Le Doyen de la Faculté des études supérieures et postdoctorales / Dean of the Faculty of Graduate and Postdoctoral Studies

Competitive Optics Circuits for All-Optical Signal-Processing Applications

Hazem Awad

Thesis submitted to the
Faculty of Graduate and Postdoctoral Studies
In partial fulfillment of the requirements
For the MASc degree in Electrical Engineering

School of Information Technology and Engineering
Faculty of Engineering
University of Ottawa

Your file Votre référence
ISBN: 978-0-494-18394-6
Our file Notre référence
ISBN: 978-0-494-18394-6

Dedication

To my family

Acknowledgments

First, I would like to acknowledge and sincerely thank my supervisor, Dr. Trevor J. Hall who has helped, guided and inspired me throughout my graduate studies. His support, encouragement, and kindness have been instrumental in helping me to bring this work to life.

I would also like to express my great thanks to Dr. Martin T. Hill of COBRA Research Institute, Technische Universiteit Eindhoven for his excellent support and correspondence. I would also like to express my thanks to Dr Lu at NRC for his interesting discussions.

I would further like to thank Mr. Marcio Fertias of Optiwave Corporation for his help in the development of the numerical model used in this work.

I would also like to give my sincere thanks and gratitude to Dr. Miroslaw Florjanczyk for his suggestions and help in the editing of this work and to Michelle Thorman for her excellent help in all administration-related matters.

I would like to express my sincere thanks and gratitude to all the employees of BTI Photonic Systems Inc., in particular Dr Paul Vella and Dr Ahmad Atieh for their exceptional help and support during the experimental phase of the thesis and for giving me the opportunity to use BTI laboratories and equipment.

I would also like to express my sincere thanks to all my great friends and colleagues at the University of Ottawa. In particular I would like to thank Rami, Moh Badri, Moh Kadri, Nizar and others at the SMR and GEMS research labs, Ahmed, Nic, Ben, Pino and others at the Center for Research in Photonics (CRP) for all the help, laughter, support and encouragement.

Finally, I would like to express my greatest gratitude and thanks to everyone in my family for all their tremendous help, love, and encouragement thought my entire life.

Abstract

This thesis details the simulation and experimental validation of several all-optical signal-processing configurations that utilise competitive optics principles. Competitive optics refers to any number of optical systems where different optical modes or wavelengths compete for a limited system resource, such as the optical gain of some common gain medium, in order to receive amplification. The gain medium can utilise different materials including photorefractive materials (e.g. $BaTO_3$ crystals) and saturated gain material (e.g. semiconductor optical amplifiers). Competitive optics configurations are capable of sophisticated all-optical signal processing functions ranging from all-optical wavelength conversion to optical logic and storage.

This thesis will present a series of simulated competitive optics configurations that utilise a semiconductor ring laser a basic competitive optics structure. These simulations will prove the viability and validity of competitive optics configurations that utilise saturated gain material, specifically the Semiconductor Optical Amplifier. The thesis will demonstrate the application of the Lotka-Volterra mathematical model of competitive interactions to the modelling of some of aforementioned configurations. Finally, experimental investigations of different semiconductor ring lasers configurations are presented and analysed from a competitive optics point of view.

Contents

List of Figures

List of Acronyms

ASE: Amplified Spontaneous Emission.

BS: Beam Splitter.

C-SOA: Semiconductor Optical Amplifier optimized for C-band operation.

CW: Continuous Wave.

DWDM: Dense Wavelength Division Multiplexing.

EDF: Erbium Doped Fibre.

EDFRL: Erbium Doped Fibre Ring Laser.

F-SFRL: Filter based Semiconductor Fibre Ring Laser.

FWM: Four Wave Mixing.

L-K: Lotka-Volterra competitive model.

OC: Optical Coupler.

PC: Polarization Controller.

PDG: Polarization Dependant Gain.

PDL: Polarization Dependant Loss.

PM: Polarization Maintaining Fibre.

P-SFRL: Polarization based Semiconductor Fibre Ring Laser.

RO: Relaxation Oscillations.

SFRL: Semiconductor Fibre Ring Laser.

SRL: Semiconductor Ring Laser.

SOA: Semiconductor Optical Amplifier

SOP: State of Polarization.

S-SOA: Semiconductor Optical Amplifier optimized for S-band operation.

WTA: Winner Take All.

XGM: Cross Gain Modulation.

XPM: Cross Phase Modulation.

VP: Voting Paradox.

Chapter 1 Introduction

1.1 Historical Background

Humans have been concerned with gathering, sharing, and exchange of information since early-recorded history. It is therefore reasonable to classify previous human societies are in as information societies. A more strict definition of an information society however, stipulates a society with the infrastructure to allow anyone to access any piece of desired information almost instantaneously.

The advent of the Internet, along with its related services, brought tremendous and fundamental changes in all of the societies that have access to it. Terms such as the "information revolution" and the "information superhighway" have emerged to address the impact the Internet has had and continues to have on human existence. It is often remarked that almost every piece of human knowledge resides somewhere in the Internet domain. The current information society is gradually being replaced by the Internet society where high capacity pervasive telecommunication networks form the backbone. The capacity of optical fibre networks has increased greatly over the past decade. Current networks employing the technology of Dense Wavelength Division Multiplexing (DWDM) have capacities that exceed terabit/s. As more and more people use the Internet, the demand for better, faster, and more accurate communication networks continues to rise.

Unfortunately, the recent market downturn has greatly affected the demand for IP traffic. The optimistic growth predictions before the downturn did not materialise as expected. Instead, the IP traffic levels have more or less stabilized at the same levels they were just before the market downturn. Still the demand for traffic is present and as the market recovers, it is expected that the demand will increase again.

In order to cope with current and future levels of IP and Voice traffic, DWDM continues to be extensively employed in almost all of the optical communication networks backbone. Furthermore, in order to reduce cost and increase profit, a greater number of wavelengths are used.

Several kinds of transmission impairments have emerged as dominant obstacles to performance in current and future optical communication networks. Some of these impairments occur in the optical fibre itself. These include an appreciable increase in both the attenuation and the inter-channel cross-talk level caused by the various nonlinear phenomena that occur in currently deployed optical fibres.

Some of the most important types of these phenomena include Cross Phase Modulation (XPM), Four Wave Mixing (FWM), Self Phase Modulation (SPM), Stimulated Brillouni Scattering (SBS), Stimulated Raman Scattering (SRS) and Polarisation Mode Dispersion (PMD). These phenomena have a detrimental effect on the optical signal's shape and integrity and can lead to a high increase in the Bit Error Rate (BER) up to a point where reliable transmission is no longer possible.

Another type of impairment affects the optical amplifiers deployed throughout the optical network. Examples of such impairments include Amplified Spontaneous Noise (ASE), noise amplification and accumulation, where the optical amplifier amplifies the signal as well as any noise present in it, and a non-flat gain profile. A third type of transmission impairment affects optical switches, the most serious of these impairments include the inter-channel cross talk and inter-symbol-interference (ISI).

The above transmission impairments significantly degrade the Optical Signal-to-Noise Ratio (OSNR) of the fibre links in the networks. This results in a significant reduction of the number of nodes through which optical signals can pass without suffering fatal degradation and sets severe limitations in the maximum transmission distance which results in an overall reduction of the network's scale and scalability.

The overall effect of the aforementioned impairments is a significant increase in the optical networks cost since vendors are forced to deploy more nodes and more fibre to serve the necessary traffic levels.

Electronic regenerators were historically used to correct all of these transmission impairments. These regenerators however, required the use of Optical-to-Electronic-to-Optical (OEO) conversion, which happens to be a very expensive process, and significantly slows down the networks performance. Since optics is many orders of magnitude faster than electronics, an electronic bottleneck is created in the network.

The advent of the optical fibre amplifier in the 1990s fundamentally altered the landscape of optical communication networks. The Erbium Doped Fibre Amplifier (EDFA) has proven extremely successful in handling the attenuation impairment problem in optical networks. The existing optical amplifiers however, are still imperfect with several undesirable features that need to be eliminated or reduced (such as ASE amplification and non-flat gain to name a few).Therefore future optical networks will require improved optical amplifiers as well as the introduction of new amplifier types and configurations.

The other transmission impairments however, are not resolved by optical amplifiers and must be addressed if future optical networks are to remain viable and profitable. The best and most efficient way to address these impairments is via the use of 3R regenerators (Retiming, Reshaping, and Re-amplification) modules. Currently a combination of sporadic use of electronic regenerators and higher layer control is used to perform 3R functions but in electrical domain. Obviously, this approach suffers from the electronic bottleneck problem. It has barely been able to cope with current network traffic and almost certainly will be not adequate for future networks where we need to deal with the transmission impairments mostly at the physical layer without the use of electronic regenerators. Therefore, future optical networks will require all optical 3R regenerators.

Another important issue that future optical networks will face is a limited number of useable wavelengths. There are situations where some wavelengths cannot be used within a certain part of the network. Wavelength conversion (with its associated add-drop functions) is the best way to deal with such a situation. Therefore future optical networks will require simple and efficient all optical wavelength conversion devices.

Finally, all current and future optical networks have to cope with issues such as packet switching, packet header processing and packet contention. This inherently requires logical operations (e.g. the XOR operation) and memory (e.g. lookup tables). Currently this is done electrically, which slows the network down considerably. Therefore, future optical networks will require efficient and practical all-optical logic circuits as well as some sort of reliable optical memory/buffers.

We can conclude that some of the key enabling technologies for the next generation of photonic networks include:

- New and improved optical amplifiers,
- All-optical logic gates and memory,
- All-optical 3R Regenerators and wavelength converters.

1.2 Motivation

From the preceding discussion, it is clear that current photonic networks are facing greater problems dealing with increasing traffic demands while remaining sufficiently profitable. The main issue is the increasing cost of maintaining and deploying electronic devices that are used for network operations such as regeneration, retiming and packet contention resolution. Furthermore, the O-E-O process poses serious restrictions on the network's speed and efficiency. One of the most efficient ways to eliminate or reduce these problems is to move as much of the network's operations and functions as possible into the optical domain.

The main motivation for this work is to address some of the above concerns by suggesting new technologies and methods and to provide a poof-of-concept for some of the aforementioned future photonic networks key technologies. More specifically, the overall goal of the this work is to present competitive optics principles and their associated structures as suitable and viable means for the realisations of some of the key technologies of future photonic networks.

1.3 Objectives

The objectives of this thesis include:

- To examine current approaches for addressing the main issues facing future photonic networks.
- To present competitive optics principles and structures and illustrate the viability and advantages competitive optics structures can bring about for the realisation of some key technologies for future photonic networks.
- To illustrate by simulations, the viability of the Semiconductor Ring Laser (SRL), a fundamental competitive optics structure, for several high-speed all-optical applications (such as wavelength conversion at high data rates).
- To carry out experimental investigations of different SFRL configurations and explain their operation and performance from a competitive optics point of view.

1.4 Summary of contributions

- The Semiconductor Fibre Ring laser (SFRL) was introduced as a fundamental competitive optics structure. A competitive Lotka-Volttera mathematical model of the SFRL was derived.
- Dynamical properties of Filter-based SFRL (F-SFRL) were numerically investigated using VPI's TransmissionMaker™ and ComponentMaker™:Active Photonics commercial optical simulation software packages.
- Verification of some of the numerical results obtained using VPI was carried out using MATLAB.
- The effects of parameters such as cavity delay, SOA bias current, power levels of the competing optical wavelengths and data modulation rates, on the time-domain output of the F-SFRL were numerically investigated.
- The distortion of the F-SFRL output pulses (e.g. Relaxation Oscillations (RO) and gain overshoots) was numerically investigated.
- Correct operation at both 2.5 and 10 Gbit/s data modulation rates was numerically demonstrated for F-SFRL.

- Experimental characterizations of two commercially available SOAs (one optimized for C-band operation and another for S-band) were carried out.
- Experimental investigations of the spectral properties of Polarization-based SFRL (P-SFRL) were carried out.
- The effects of parameters such as wavelength-dependant cavity looses, role of Polarization Marinating (PM) fibres, Polarization Dependant Gain (PDG) of SOA and Polarization Controller (PC) settings, on the spectral properties of P-SFRL was experimentally investigated.
- A P-SFRL lasing in the C-band wavelength regime was experimentally demonstrated utilising the C-band SOA as the competitive gain medium. A similar P-SFRL configuration utilising the S-band SOA was experimentally demonstrated, also lasing in the C-band.
- A modified version of the P-SFRL configuration utilising the S-band SOA but lasing in the S-band was experimentally demonstrated. Single and multiwavelength operation was demonstrated.

1.5 Structure of Thesis

This thesis is organised into seven chapters. Chapter 1 provides the introduction and overall structure of the thesis and lists the major accomplishments. Chapter 2 introduces the Semiconductor Optical Amplifier (SOA) and presents a brief comparison of some of its rate equation models described in the literature. Chapter 3 provides an overview of some of the most promising all-optical technologies for future photonics networks. Chapter 4 introduces the concept of competitive optics and presents a modified version of the Lotka-Volterra model that is suitable for modelling competitive optics processes and structures. Chapter 5 introduces the Semiconductor Ring Laser (SRL) and illustrates its operating principle (gain competition in SOA) from the competitive optics point of view. Chapter 6 presents several experimental investigations of SFRLs. Chapter 7 concludes the thesis and offers additional suggestions for future work.

Chapter 2 The Semiconductor Optical Amplifier

2.1 Introduction and History

The first semiconductor optical amplifiers (SOA) were invented in 1964, approximately two years after the demonstration of the first semiconductor laser diode (LD). Both of these early devices utilised GaAs homo-junctions and were operated at low temperatures [Con'02]. The invention of the double junction structure in 1969 greatly improved the properties of both the LD and the SOA. Currently, the PN double heterostructure is the most preferred means of optical guiding and carrier confinement and all SOA structures are based on it [Occ'02].

The SOA has gone through a tremendous change during the 1970s-1990s. Early SOA devices were simply LDs operated under threshold. These early devices were called Fabry-Perot SOA (FP-SOA) since the reflectivity of their end-facets was significant. FP-SOAs have ripples in their gain spectrum (due to the presence of cavity resonance) and are very sensitive to fluctuations in important SOA parameters such as bias current, signal polarisation and temperature [Con'02]. Other drawbacks, such as low Band-Width (BW), make FP-SOA a poor choice for WDM/DWDM systems [Agr'95].

The introduction of Anti-Reflection coatings (AR) has allowed the development of a true Travelling Wave SOA (TW-SOA). These SOAs have very low end facet reflectivity ($\sim 10^{-4}$). This greatly reduces (or eliminates) feedback reflections in the SOA cavity resulting in a strong suppression of cavity resonance. TW-SOA are less sensitive to fluctuations in bias current, temperature and signal polarisation compared to FP-SOA and they also have a higher bandwidth. This makes them more suitable for amplifications purposes in DWDM systems [Con'02].

The SOA is a very complex device with many areas of the engineering sciences contributing to its theory (such as material science, device physics, and optical engineering, numerical modelling). The purpose of this chapter is to introduce a selected few SOA -related issues that are fundamental to this work. This chapter is by no means a comprehensive review of

the complete SOA theory. Many references exist that provide such a review [Con'02], [Occ'02], [Agr'95].

The rest of this chapter is organised as follows: section 2.2 briefly discusses the origin of the nonlinear phenomena that exist in SOAs. Section 2.3 discusses the differences in materials and performance of bulk, QW and QD SOAs. Section 2.4 introduces the rate equation model of the SOA and highlights its importance in SOA modelling and in the underlying physical phenomena utilised in this work (competitive optics/gain competition). Finally, section 2.5 concludes this chapter.

2.2 SOA Nonlinear Phenomena

The SOA is a highly nonlinear device. Whenever an input signal is present in the SOA, it modifies/modulates its carrier density. Furthermore, since the SOA's material gain spectrum is homogenously broadened, any carrier density changes or modulations will affect all of the input signals of the SOA. These carrier density modulations give rise to the various nonlinear phenomena's present in the SOA.

There are six main SOA nonlinearities: Cross-Gain Modulation (XGM), Cross-Phase Modulation (XPM), Four-Wave Mixing (FWM), Self-Gain Modulation (SGM), Self-Phase Modulation (SPM), and Polarisation Rotation. All of these phenomena's can be used in various novel optical signal-processing schemes [Con'02], [Occ'02], [Cal'05]. Chapter 3 provides a more detailed description of some of these phenomenon and the schemes that employ them for all optical signal processing.

2.3 SOA materials

As is the case in semiconductor laser diodes, SOAs require the use of direct bandgap III-V materials for their active region. The most popular of these III-V semiconductor compounds are InGaAs, InP, InGaAsP, AlGaAs, and InAlGaAs. With these materials, it is possible to construct SOAs for both the 1.3 μ and 1.55 μ wavelengths range for use in photonic

communication networks (InGaAsP and AlGaAs can use for 0.7 μ – 1.6 μ range and InAlGaAs/InP can be used for 1.5 μ) [Con'02], [Occ'02].

The SOA structure greatly affects many of the SOA's important parameters such as material gain, small signal gain, Noise Figure (NF), optical confinement factor, and output saturation power. The classification of an SOA as bulk or Multiple QW (MQW) or QD is based on the nature of the SOA's active region and its dimensions. A bulk-type SOA has an active region dimensions that are much greater than the deBroglie wavelength defined as $\lambda_B = \frac{h}{p}$ where p is carrier momentum. A QW-type SOA has one or more of its active region dimensions on the order of the deBroglie wavelength. Finally, a QD-type SOA has its active regions dimensions much smaller than [Con'02], [Mør'03], [Led'00].

The most illustrative way to understand the differences between bulk, QW, and QD structures is to examine their state density functions. In bulk structures, state density function is continuous with respect to energy. On the other hand, QW structures exhibit a staircase state density function. Finally, QD structures have discrete and localised state density functions with respect to energy [Led'00] [Con'02], [Mør'03]. Figure 2-1 provides an illustration of the differences between state densities of bulk, QW, and QD structures.

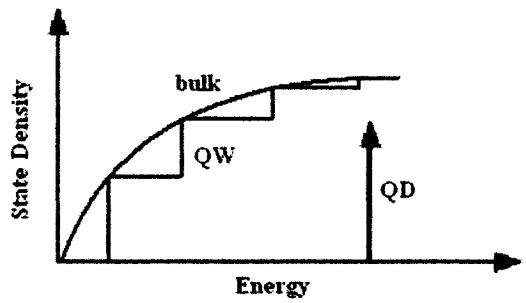

Figure 2-1 Density of states for bulk, QW and QD structures with respect to energy.

2.3.1 QD structures for next generation SOAs

Both Bulk and QW structures suffer from several important problems that could limit their deployment in future photonic networks. Some of the most prominent problems include low saturation power and pattern effects (at 2.5 and 10 Gbit/s) which are caused by the inherently slow response of gain saturation in bulk and QW SOAs. By having QDs as the active region of an SOA (hence the QD-SOA), many of these problems can be overcome and additional benefits (such as very alpha factors) can be realised. [Sug'03], [Mør'03].

Impressive progress has been made in fabrication of low dimensional semiconductor structures particularly during the last 20 years. Researchers were able to progress from the fabrication of bulk, 3-D devices to quasi 2-D quantum-well (QW) devices, to quasi 1-D quantum wire devices and finally during the early 1990s to quasi zero-D quantum-dots (QD).

Quantum Dots (QD) therefore, represent the ultimate example in size quantization in solids. QD are small conductive semiconductor crystals only nanometres in size, coherently inserted in larger semiconductor bandgap matrices. The electronic and optical properties of these QD resemble those of single atoms.

The main advantage of using size-quantized heterostructure in lasers and SOAs originates from the increase in the density of states for charge carriers near the band edges. When used as the active media of the laser/SOA, we acquire a concentration of most of the injected non-equilibrium carriers in an increasingly narrow energy range near the bottom of the conduction and and/or the top of the valence band. As a result, the maximum material gain is enhanced. In structures with size quantization in more than one direction, such as a QD, a singularity in the density of states occurs as shown in Figure. 2-1.This further improves device characteristics [Led'00].

2.4 Rate Equation model of the SOA

The complex nature of the SOA prompted intense theoretical and experimental research in an attempt to understand and accurately predict its behaviour. This resulted in the development of a very wide variety of theoretical models for the SOA [Con'02]. The models can broadly be classified as steady state and dynamic models and can further be subdivided into analytical and numerical models. Analytical models are limited in application because they often make many simplifying assumptions (to reduce the model's equations to a form amiable to analytical solutions). This limits both their accuracy and their operating range [Con'02]. [Occ'02], [Agr'95], [Adm'85], [Hen'85].

Currently, the majority of SOA models are numerical in nature. Numerical models are significantly more accurate due to the limited number of assumptions they make about the SOAs various parameters and phenomenon (many of which are often ignored in analytical solutions). This also greatly increases their applicability since they can accurately predict the SOA performance over a wide range of operating regimes [Con'02], [Adm'85], [Hen'85], [Low'88], [Mor'93], [Nie'00], [Bog'03], [Con'01], [Con'02a], [Won'00]. These numerical models are often quite sophisticated and incorporate many nonlinear effects including such as spatial hole burning (SPH) and sub-picoseconds pulse amplification.

We performed simulations of several SOA-based competitive circuits (chapter 5). One set of these simulations were carried out using a commercial general-purpose optical simulator suite from Virtual Photonic Incorporated (VPI). The particular simulator engine used is called VPIcomponentMaker™: Active Photonics. The SOA model in the VPI simulator is based on the Transmission Laser Line Model [Low'88], [VPI'05]. The model is quite sophisticated and incorporates many of the physical phenomena present in the SOA.

A second set of similar simulations were carried out using a simpler SOA model, which was simulated in the technical computing programming language MATLAB. The SOA model was based on the models present in [Con'01], [Con'02], and [Con'02a]. This was carried out because we did not have access to the details of the SOA model in VPIcomponentMaker™: Active Photonics and hence, it was difficult to explain some of the erroneous results that

were obtained with the simulator (this is the so-called 'black-box' problem). Furthermore, we needed to verify the results obtained with VPIcomponentMaker™: Active Photonics with those from MATLAB model that, while is simpler in nature, still provides reasonably accurate insight into the behaviour of SOA competitive circuits.

2.4.1 MATLAB model of the SOA

In [Con'01], [Con'02], and [Con'02a], a steady state and dynamic model of a bulk InP-InGaAsP homogeneous buried ridge stripe SOA is presented in detail. The amplifier structure and bulk material gain is calculated in detail (i.e. the model does not make use of the simple cubic equations for calculating the material gain, see chapter 5). Furthermore, the travelling wave equations for both the signal fields and ASE are modelled in detail. The numerical algorithm used is very efficient and the simulation results agree very well with experimental measurements [Con'01], [Con'02], and [Con'02a].

A model of a SOA was implemented in MATLAB [Fer'05] based on a (modified) implementation of the SOA model created by Connelly [Con'01], [Con'02], and [Con'02a]. Several versions of the model were implemented to simulate different SOA configurations. The configurations simulated included co-propagating XGM, counter-propagating XGM and multi-input XGM. The model was modified to simulate a SOA-based ring laser (chapter 5). The detailed equations of the model are identical to those in [Con'01], [Con'02], and [Con'02a] and will not be elaborated on further. We only need to mention that the modelling of ASE was not included in the MATLAB model used in this work. This was purely the result of timing constraints imposed by difficulties faced in the implementation of ASE in the model. The results presented in this work are still valid however, since all of the simulated configurations involved XGM in SOA, which is not highly dependant on ASE (functionally speaking at least). Hence, we can be confident in the validity of the presented simulations but expect some additional signal distortions in the output waveforms (due to ASE). This has been confirmed by comparing the simulation results from VPIcomponentMaker™: Active Photonics (which include ASE modelling) with those obtained from MATLAB (chapter 5).

2.5 Conclusion

The history and role of the SOA were briefly presented. The major nonlinear phenomenons in the SOA were described and their physical causes were highlighted. SOA materials (bulk, QW and QD) were described and contrasted with each other and it was found that QD SOA posses superior properties over both bulk and MQW SOAs. A qualitative description of a rate equation based SOA model implemented in MATLAB was described. This model is used in this work to simulate several SOA-based competitive optics circuits and configurations.

Chapter 3 Overview of Future Photonic Networks Key Technologies

3.1 Introduction

Future photonic networks must contend with increasing traffic demands. This will lead to an increase of the transmission rates which results in greater impairment penalties. Furthermore, the increase in data traffic and the related increase in the bit rate puts greater strain on the electronics currently deployed within photonic networks (which is can handle bit rates up to 40 Gbit/s). Therefore, there is a great need for all optical processing functions to alleviate the impairment and electronic bottleneck issues facing current and future photonic networks.

3.2 Key Technologies for Future Photonic Networks

As discussed in chapter 1, four different but related all optical technologies are needed for current and future photonic networks. This section provides an overview of some of the demonstrations of these technologies.

3.2.1 New and improved optical amplifiers

Traditional DWDM systems that utilise optical amplification used sophisticated and relatively expensive gain-flattened EDFA for amplifying a broad range of wavelengths. This proved successful and profitable as DWDM systems were initially deployed in backbone communication networks. These networks did not require rapid and/or frequent reconfiguration. [Zim'04].

The success of DWDM systems prompted their introduction and deployment in metropolitan networks. These networks differ fundamentally from backbone networks in that they require reconfigured much more frequently. Important functions such as wavelength routing, optical switching, and path protection become dominant in metropolitan networks. The Optical Amplifiers (OA) used in these networks must be able to suppress dynamical effects such as transient crosstalk between the amplified wavelengths.

Future photonic networks will have the deployment cost of the network (including components cost) as their top priority. It is therefore essential that we increase the deployment of new and cheap kinds of OAs (often referred to in literature as Amplets) in future photonic networks to reduce their overall cost. These new OAs will help supplement the larger, more complex, and more expensive EDFA.

There are several kinds of amplets currently available. They are classified as Erbium-based and semiconductor-based amplets. Erbium-based amplets include EDFA (Erbium Doped Fibre Amplifier) and EDWA (Erbium Doped Waveguide Amplifier) amplets. The Semiconductor Optical Amplifier (SOA) falls under the category of semiconductor-based amplets. The SOA is in-fact a small, low cost device with moderate-to-good performance and hence qualifies as an amplet.

The main distinguishing feature of the amplet (from the more complex DWDM OA) is their cost vs. performance ratio. Amplets sacrifice some of the performance features of traditional DWDM amplifiers in order to reduce overall cost. For example, an EDFA amplet will typically be able to amplify 4-8 ITU channels vs. 32-40 channels for the traditional broadband EDFA. However, due to its low cost, multiple EDFA amplets may be used to amplify the same 40 channels that a single large EDFA amplifies and still maintain an overall lower cost. Furthermore, deploying multiples of small and cheap identical EDFA amplets can lead to other advantages such as simpler network reconfigurations. EDWA amplets have the advantage that they can be integrated along with other components (such as pump lasers, Variable Optical Attenuators...etc) onto Photonic ICs that are easily mass-produced. [Zim'04].

SOAs were initially abandoned as potential WDM/DWDM due to their severe nonlinearities, especially the Cross Gain Modulation, XGM, effect that induces channel crosstalk. SOAs however, were used in increasingly more sophisticated all-optical signal processing applications. Examples include all optical logic, wavelength conversion, regeneration, and switching to name a few [Ber'01], [Con'02].

Alcatel has a developed a different kind of SOAs, called the Gain-Clamped SOA (GC-SOA) [Ber'01]. It solves the channel crosstalk problem by stabilizing the amplifiers gain and thus reduces/eliminates XGM.

Future photonic networks will make more and more use of amplets for their low cost and good performance vs. price ratio. It is expected that amplets will penetrate deep into future photonic networks and replace expensive OA for most applications. This will greatly reduce the overall cost of the network and provide additional benefits as previously discussed.

3.2.2 All optical logic

Research in optical logic began as far back as the late 70's, early 80's when Bell Laboratories scientists and engineers where working on early all-optical logical devices. To this day however, electronics remains the dominant logical processing technology (e.g. header recognition, packet contention resolution, and memory) in current photonic networks. Optical signal processing is yet to be widely deployed within these networks. There are many reasons for this, the most important of which is that efficient, all-optical processing is still not realisable on a practical and profitable scale. Almost all of the breakthroughs that occurred in the optical logic field have been in building single stage devices and gates such as the NOT, AND, OR and other familiar logic gates. Larger, multi-stage logical devices, which are required for processing, switching, storing, and routing traffic within the photonic networks, have not yet been satisfactorily demonstrated.

Electronics on the other hand, is a far more mature field. Extremely large and complex electronics systems have been constructed and because of advances in the electronics and CAD technologies, much larger and more complex systems continue to be developed. Electronics is well suited for performing all of the aforementioned tasks reliably and inexpensively. This is especially true in the case of memory-based functions in photonic networks (such as lookup tables, i.e. associative memory).

Another important fact to consider is the associated cost of all optical signal-processing circuits. The majority of the fabrication foundries currently operating produce and process Si which, as of yet, cannot be used in building optical logic due to its non-direct band-gap nature which makes it ill suited for manipulating light. The manipulation of light can be efficiently accomplished in direct band-gap materials (e.g. III-V materials, GaAs, and InP). III-V material processing however is not as mature as Si processing (Si wafers can come in 12-inch size while GaAs wafers come in 6-inch only) and not as reliable (lower yield).

Furthermore, photonics currently suffer from low integration levels, comparable to those of vacuum tube era. This does not allow for highly automated assembly procedures [Stu'00]. All of the above translates to higher construction costs for all optical processing circuits.

None of the above factors however, diminishes the fact that optical processing is essential for future photonic technologies due to the speed limitations of electronics and the high (and soon to be prohibitive) costs of O-E-O conversion. As a result, massive research efforts continue in that field.

Most forms of optical logic are based on some nonlinearity that might exist in the optical medium. Several optical mediums exist that exhibit suitable optical nonlinearities. Examples include photorefractive materials and saturated gain material (e.g. SOA). We will review some of the fundamental optical logic approaches based on SOA nonlinearities.
The SOA exhibits several kinds of nonlinearities that are primarily caused by changes in its carrier density (see chapter 2). These changes are induced by the input signals of the SOA, which modulate its carrier density give rise to several kinds of nonlinear phenomena

3.2.2.1 Cross Gain Modulation (XGM)

XGM is perhaps, the simplest technique that can be used to perform logical operations in the optical domain. It utilises the Semiconductor Optical Amplifier (SOA) as the basic building block for all of the logical devices that it can create.

XGM is a phenomenon that exists in SOAs when two or more inputs exist. These inputs compete for the limited carrier pool in the SOA. The stronger input, the pump signal, it saturates the SOA, and hence because the modulation of the weaker input, called the probe, which experiences a gain drop due, saturation of the SOA by the pump input and hence inverts. Several signal graphs as shown in Figure 3-1 to illustrate this.

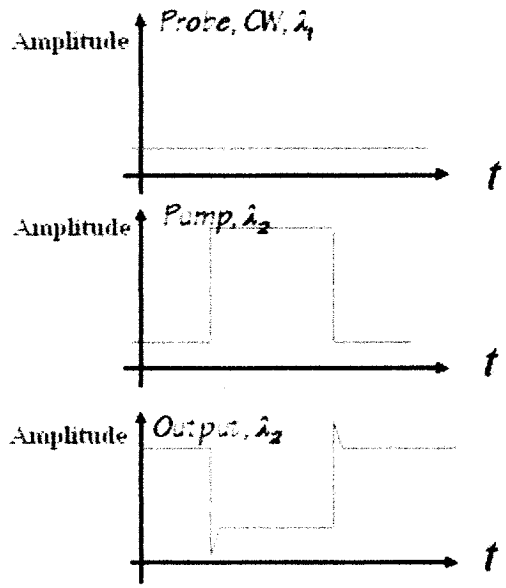

Figure 3-1 Pump, probe and output signals for XGM in a SOA.

All of the basic logical gates such as AND, OR and NOT have been implemented using XGM. Furthermore, other circuits such as wavelength converters and RZ to NRZ converters have been implemented using XGM. [Stu'00].

XGM however, does suffer from several problems. Both of the modulated probe and original pump inputs are present at the output so we would require a filter to remove the unwanted pump signal. In addition, there is a large signal chirp present at the output. XGM however, is very robust and has good conversion efficiency [Con'02], [Stu'00], and forms the basis for the majority of the optical logic gates developed to date. In this work, XGM is utilised to perform various optical signal-processing functions.

3.2.2.2 Cross Phase Modulation (XPM)

XPM is another technique that is used to perform logical operation in the optical domain. It is more complex than XGM but does offer several advantages such as superior performance, and more importantly, a wider range of parameters exist that can alter to optimize the performance.

The basic element in XPM-based system is the Mach-Zender interferometer (MZI). The MZI consists of two SOAs in a Mach-Zender loop configuration. This configuration is illustrated in Figure 3-2.

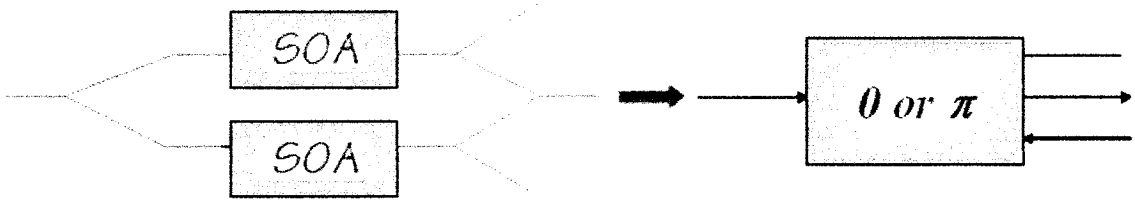

Figure 3-2 XPM Mach-Zender configuration and corresponding block symbol.

Because the MZI configuration on the left hand side of Figure 3-2 is cumbersome to draw, it is customary to replace it in circuit; diagrams with the configuration shown on the right had side. It is important to note that some MZI configuration use only one SOA in either the upper or the lower arms. This configuration proved unstable however and almost all of the XPM circuits utilise two SOAs in both of the MZ arms. Also, note that by using a directional coupler at the input port of the MZI, the MZI can function as a two-input device.

The operation of the MZI is based on biasing of two MZ arms to create phase difference between them. This phase difference is controlled by the lengths of the two MZ arms. It can also be controlled by reversing the bias of one or both of the SOAs. This technique however is highly unreliable and so most often the phase difference is solely controlled by the arms lengths.

If we are interested in using MZI are as a logic device, there exist only two different phase-difference values between the two MZ arms are of interest to us: 0° and 180° (π) phase difference. If we bias the MZ arms so that there is a 0°-phase difference between both of them, we would have constructive interference at the output of MZI and the MZI would be called a 0°-device. If on the other hand, we bias the phase difference between the two MZ arms so that we will have destructive interference at the output of the MZI, it would then be called a π -device. We now have constructed an optical device that is capable of producing both a logical high and a logical low depending on the bias state of its arm. Therefore, we are now able to use the MZI to build logic gates and devices.

Figure 3-3 illustrates all possible operational cases for a two-input MZI device (both 0° & π phases).

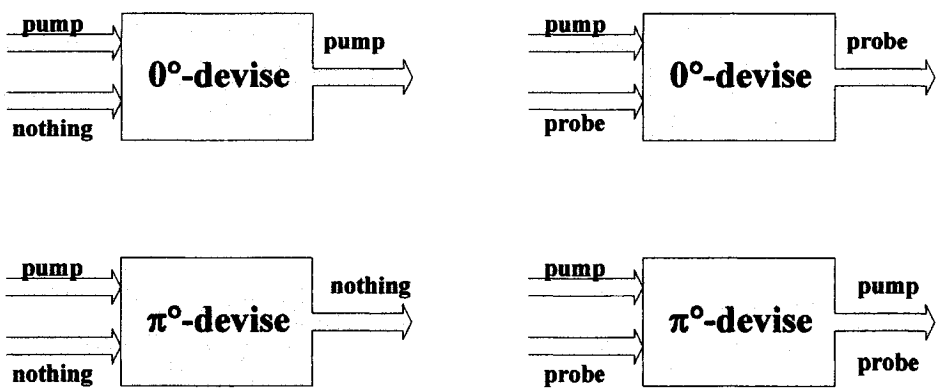

Figure 3-3 Input and output signals of various XPM devices.

Figure 3-3 is self-explanatory. We have four cases to look at:

1) 0°-device with only a pump input: since the device is in the constructive interference mode, the pump will constructively interfere with nothing at the output of the MZI device. Hence, we would expect to the see the pump signal at the output.

2) 0°-device with pump and probe inputs: since the device is in the constructive interference mode, both the pump and probe signals will constructively interfere at the output. Hence, we would expect to see only the probe signal at the output.

3) 0°-device with only a pump input: since the device is in the destructive interference mode, the pump will destructively interfere with nothing and there will be no output.
4) 0°-device with pump and probe input: in this case, both pump and probe will destructively interfere and appear at the output.

XPM can be used to create many logical elements including all the basic logic gates (NOT, AND, OR, NOR, XRO and NAND). More sophisticated logical circuits can also be implemented using XPM [Stu'00]. Furthermore, XPM is potential increases when we combine it with XGM gates or Four Wave Mixing (FWM) gates. This is called mixed-logic style all optical gates.

3.2.2.3 Four Wave Mixing (FWM)

FWM is a nonlinear phenomenon that could arise when two or more frequencies of light propagate simultaneously along optical fibre or inside the SOA cavity. When a condition called phase matching exists (satisfied) within the fibre, new light is generated at new frequencies and different power levels. FWM is a third-order nonlinear process and when it occurs in SOA, it becomes an ultra fast process. FWM can be used to construct SOA-based wavelength converters with bandwidths that exceed the Terahertz range. FWM is a very useful process for the construction of optical logic gates. FWM can take on two different forms: 1) a partially degenerate form and 2) a non-degenerate form.

For most logic operations, we try to avoid the non-degenerate case because it produces too many new wavelengths and hence we would require several filters to remove them. Most often, when using FWM to perform logical operations we try to force the partially degenerate case. Assuming the partially degenerate case, there exists three cases that require further attention. They are illustrated in Figure 3-4.

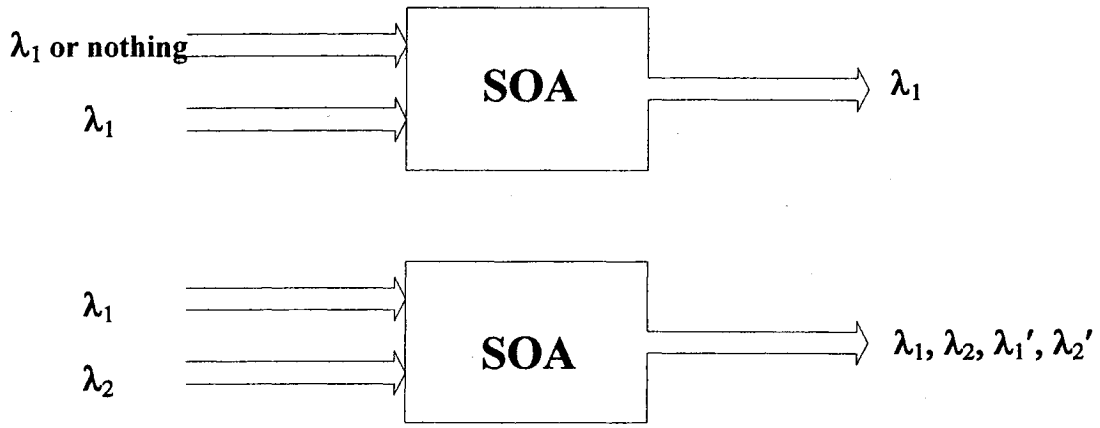

Figure 3-4 Four Wave Mixing phenomena in SOA.

1) One input, wavelength, λ_1: since we only have one input for the SOA, no FWM would occur. The output will be an amplified version of the input.
2) Two inputs, same wavelength, λ_1: since we have two signals with the same λ_1, we now have a degenerate case. No FWM occurs and the output is the same as the inputs.
3) Two inputs, different wavelengths, λ_1 and $\lambda 2$: since we have two inputs with different wavelengths, FWM occurs. The output will be the original inputs plus some extra wavelengths, which are the conjugates of the inputs wavelengths.

FWM can solely be used to implement logic gates. These gates however, are usually more complex than comparable gates implemented using XGM or XPM [Dom'00]. Furthermore, all of the inputs to the FWM gates appear at the outputs so we would require filters to remove them. A variant of FWM called Filter Free FWM (F-FFWM) has been proposed which does not require the use of filters [Dom'00]. The output signal is spatially separated from the input signal. This configuration however, suffers from limitations on its possible wavelength conversion rates.

FWM gates can be used to test if the both of its inputs are equal. This property is often used in the construction of mixed logic gates (discussed in the wavelength-based logic section) and can help facilitate the construction of XOR gates, which have the same functionality [Dom'00], [Stu'00]. All elementary logic gates have been implemented using FWM gates.

By using a combination of FWM and XPM/or XGM, even more powerful logic gates can be implemented (as will be discussed in the wavelength-logic section).

3.2.2.4 Nonlinear Optical Loop Mirrors

The Nonlinear Optical Loop mirror (NOLM) [Dom'00], [Bah'01] is an approach to implement XPM-based circuits using the Sagnac interferometer. The configuration is illustrated in Figure 3-5.

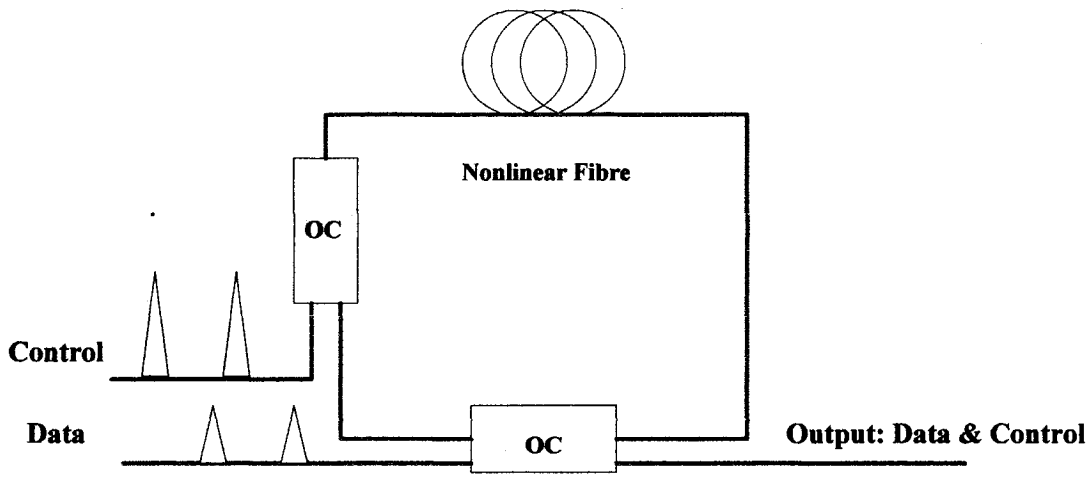

Figure 3-5 NOLM configuration.

As it can be seen from the above the configuration, we have two inputs: data and control. The data signal is split into two signals (via the input coupler) and these two signals travel oppositely through the fibre loop and recombine again). The control pulse is a strong unidirectional pulse and is introduced so that it will affect the phase of the data pulse that travels in the same direction as the control pulse, called the co-propagating data pulse. Hence, when the two data pulses combine at the output, they will be out of phase relative to one another. By carefully controlling that phase difference (via controlling the length of the loop) we can achieve constructive or destructive interference. Hence, we in essence can use the NOLM and set it up to act as a 0- or π device and can therefore perform logic operations with it. To be more precise, the control pulse induces a refractive index change in the co-

propagating data pulse. This index change is what causes the differential phase difference between the two data pulses.

A major disadvantage of NOLM is its incompactness. The effect of the control pulse (i.e. the phase change of the co-propagating data pulse) is nonlinear (hence the term Non-Linear Loop). Furthermore, the physical mechanism that exists in the Sagnac interferometer is termed the Kerr nonlinear effect and is very small in glass. Hence, we would require several kilometres of fibre to induce the necessary phase change and to keep the signal level of the pulses within the loop at acceptable levels. This severely limits our ability to build compact logical elements and devices using NOLM and severely limits our ability to integrate them with other devices.

3.2.2.5 Semiconductor Laser Amplifier in a Loop Mirror Configuration (SLALOMS)

The SLALOMS [Dom'00], [Bah'01] is another loop configuration that is utilises the Sagnac interferometer loop configuration. It is very similar to NOLM; however, it places an extra SOA and places it in an asymmetric position with respect to the centre of the Sagnac loop. This configuration is also know as Terahertz Optical Asymmetric De-multiplexer (TOAD) and is illustrated in Figure 3-6.

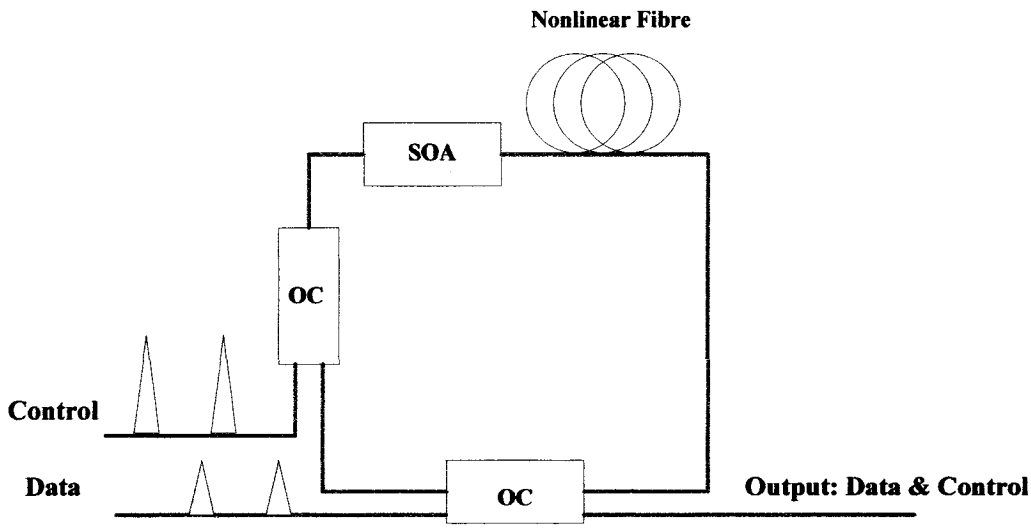

Figure 3-6 TOAD/SLALOMS configuration.

Previous Sagnac interferometer loop configuration suffered from relying on the inter-band carrier life times for the switching function. The problem is that this lifetime is slow (around 100 – 500 ps) and hence a switching rate of 1 GHz is all that could be achieved with such configurations. The solution is to place a SOA in an asymmetric position with respect to the center of the loop. By doing so, our data-switching rate is no longer limited by the inter-band carrier lifetimes. In fact, since the rise time of the carriers is much shorter (around 1ps) than their lifetime, we can now have a switching window of around 10 ps.

All basic logic functions such as AND, OR, NOT, XOR have been implemented with the TOAD. Furthermore, more complicated circuits such as full adders and multiplexers have been implemented with using TOAD configurations [Dom'00], [Bah'01].

3.2.2.6 Ultra fast Nonlinear Interferometer (UNI)

The Ultra Fast Nonlinear Interferometer (UNI) [Dom'00], [Bah'01] is another Sagnac-based configuration however, it uses a single arm only, and hence no loop exists. It is a balanced configuration and hence does not require any external stabilisation of the interferometer arm. The configuration is illustrated in Figure 3-7.

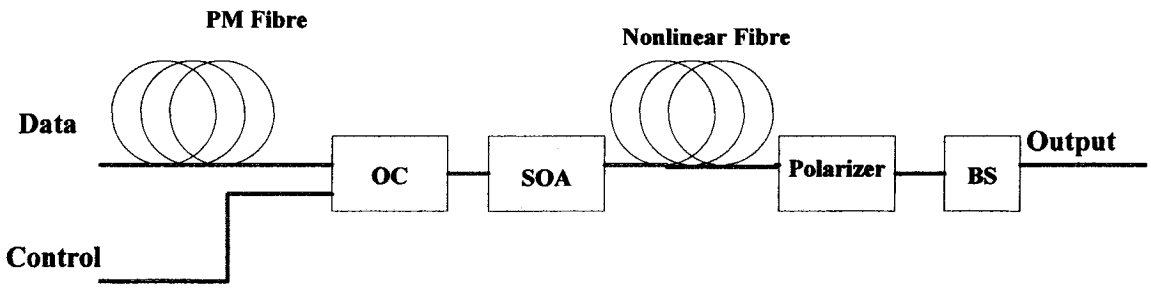

Figure 3-7 UNI configuration.

The data pulse is passed through a birefringent fibre loop. This separates the data pulse into its two orthogonal polarizations components. They then pass through a polarisation insensitive SOA and recombine again via the second birefringent loop. The polarizer combines the two orthogonal polarizations into a single data pulse. This data pulse will have

the logical value of one, i.e. we have generated a high output. If we want to generate a low output, we use a control pulse, which couples with the data pulse and that causes the output data pulse to be of logical low.

We can now use the UNI to build elementary logic gates. Logical functions such as AND, OR, NOT, OR and XOR have been developed. [Ham'01], [Hal'98].

3.2.2.7 Wavelength-based logic

This optical logic technique attempts to overcome the inherent difficulty of relying on the presence or absence of light to represent the different logic states. It is well known in the optical domain that active optical elements, such as SOAs, always produce some level of ASE (which depends on the bias current of the SOA among other things). As a result, optical logic configurations that use SOAs typically do not have a true "off" or "no light" logic state. In other words, there is always some small level of ASE light present in the system.

This ASE level will also be amplified by the SOAs as it propagates through multiple stages within a system. This limits the number of optical logic systems or gates that can be cascaded as the extinction ratio of the optical logic signals decreases dramatically as the number of cascaded stages increases. This is a serious issue for many of the optical logic systems that have been devised so far.

Wavelength-based logic attempts to overcome this problem by representing the different logical levels with different wavelengths [Dom'00]. This could potentially help with the extinction ratio problem because the logical outcome of the circuit is not solely determined by the amplitude of output signal, but rather by the wavelengths of the output signals. An example of a possible truth table for a two-input AND gate based on wavelength-logic is illustrated in Table 3-1.

2-input AND gate; $\lambda_0 = 0, \lambda_1 = 1$		
Input		Output
λ_0	λ_0	λ_0
λ_1	λ_0	λ_0
λ_0	λ_1	λ_0
λ_1	λ_1	λ_1

Table 3-1 AND truth table in wavelength logic domain.

The choice and logical assignment of the various λs is irrelevant from a theoretical standpoint. Of course, depending on which system these logical devices are used in, we may have to favour some λs over others. In the above truth table, we assign λ_0 a logical value zero and λ_1 a logical value of one.

Another important and excellent feature of wavelength-based logic is that all the techniques that utilize XGM, XPM can be implemented using wavelength-based logic. Furthermore, wavelength-based logic allows us to utilize the Four Wave Mixing (FWM) property and FWM logic gates and enables us to combine FWM, XGM, and/or XPM to build more powerful and complex logical gates. These gates are called mixed logic gates [Dom'00].

3.2.2.8 Mixed Gates: FWM + (XGM/XPM)

These optical logic gates combine FWM gates and XGM gates or XPM gates [Dom'00]. The result of such a combination is that we now have a new technique for performing optical logic. In general, these mixed gates have a component count, which is smaller than their comparable gates in FWM and even XPM (in some cases). This advantage of reduced component count for mixed gates is more evident when we are designing complex logic gates. We discuss the NADN logic gate as a typical gate of the mixed logic family.

3.2.2.9 NAND mixed logic gate

This NAND gate [Dom'00] utilises both FWM and XPM gates. Its schematic is illustrated in Figure 3-8.

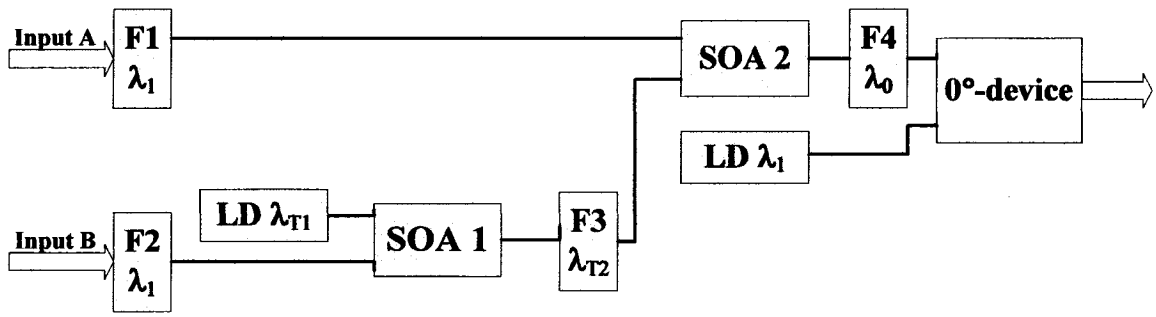

Figure 3-8 Mixed Logic NAND schematic.

The operation of the above NAND gate consists of following four cases (since we have two inputs) (remember λ_0 = zero, λ_1 = one):

1) Input A = λ_0 = Input B: When both inputs are identical and equal in frequency to λ_0, i.e. they are both low, then no signals will be present after filters F1 and F2 (which allows λ_1 only to pass). Therefore, no FWM will occur at SOA1 because there is only one input signal, λ_{T1} from Laser Diode λ_{T1} (LD λ_{T1}). The output of SOA 1 will therefore, be an amplified λ_{T1}, which will be filtered out by F3. Therefore, there will be no signals present at inputs of SOA 2 and hence no output. All this will lead to having a single input, λ_1 from LD λ_1 that will be

present at the input of the 0-device. By referring to case 1 in Fig. 3, we know that the final output the circuit will be λ_1, i.e. high.

2) Input A = λ_1 = Input B: When both inputs are λ_1, i.e. they are both high. FWM of λ_1 and λ_{T1} will then occur at SOA 1 and the output will λ_{T2} after F3. FWM of λ_1 and λ_{T2} will then occur at SOA 2 and the output will λ_2 after F4. Finally, XPM of λ_0 and λ_0 will occur at 0-device and the will be λ_0 (case 2 of Figure 3-3).

3) Input A = λ_1, Input B = λ_0: when Input A is high (λ_1) and Input B is low (λ_0) we will have no signal present after F2. Therefore, no FWM occurs at SOA 1, and its output will be an amplified λ_{T1}, which will be filtered by F3. Therefore, only λ_1 will be present at input of SOA 2. The output of SOA 2 (amplified λ_1) will be filtered by F4. Finally, XPM of λ_1 and nothing 0-device will produce an output λ_1 (case 1 in Figure 3-3).

4) Input A = λ_0 and Input B = λ_1: when input A is low (λ_0), there will be no signal present after F1. Therefore, FWM of λ_{T1} and λ_1 (from input B) will occur at SOA 1, and the output will output λ_{T2} after F3. Hence, only λ_{T2} will be present at input of SOA 2 and the output will be an amplified λ_{T2}, which will be filtered by F4. As a result, XPM of λ_1 and nothing will occur at 0-device and the output will be λ_1 (case one in Figure 3-3).

The operation of this mixed NAND gate is more complicated than other gates but the circuit functions properly and proves the concept that we can combine various techniques such as FWM and XPM to implement an optical logic gate using wavelength-based logic. The component count for this NAND gate is quite high (9 in total) but is equal to the component count of a NAND circuit that utilizes only XPM gates [Dom'00].

3.2.3 All optical 3R regenerators and wavelength converters

As was previously stated, all-optical 3R regeneration is needed in current and future photonic networks to overcome attenuation, avoid the accumulation of noise, crosstalk and

other non-linear fibre distortions and to ensure the best possible signal quality (i.e. the highest OSNR) for transmission of any optical path across the entire network.

Optical 3R regeneration is broken down into three distinct operations (or functions): 1R-Reamplification, 2R-Reamplification, and Retiming, 3R-Reamplification, Retiming and Reshaping. Re-amplification (1R) is currently carried out by Erbium Doped Fibre Amplifiers (EDFA) or in certain cases by SOAs. This operation has the advantage of being bit rate and protocol (i.e. data format) independent and multiple optical signals (i.e. channels) can be simultaneously amplified. Currently, Re-amplification is the most mature operation of 3R regeneration.

The problem with optical amplifiers however, is that any noise and crosstalk present in the optical signal(s) is amplified along with the signal itself. This accumulates as the signal is propagated through multiple amplifier stages and there will come a point where the OSNR of the signal has fatally degraded (i.e. the signal is no longer recognisable). 2R regeneration is used to control and reduce the amount of noise and crosstalk present in the optical signal. 2R regenerators require an optical threshold element (or circuit). One of the most popular circuits for 2R utilizes a wavelength converter based on a non-linear optical gate Figure 3-9.

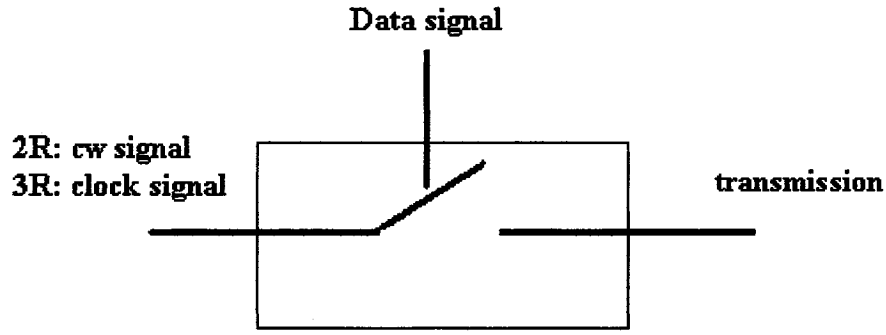

Figure 3-9 Wavelength converter utilizing a non-linear optical gate and its transfer function.

The operation of the above wavelength converter is similar to the XGM phenomena discussed earlier. The Data signal (i.e. optical signal) is used as the control signal for the non-linear gate. Since the noise level present in the optical signal is of such a small value, it has no effect on the non-linear gate. Only the data signal itself have sufficient power to affect the non-linear gate. As a result, only the data signal is transferred (i.e. encoded) to the probe signal (CW) being injected to the non-linear signal. In effect, we filtered out the noise from the data signal. If the probe is of a different λ, then we simultaneous achieved filtering of noise and wavelength conversion of the data signal. 2R regeneration is currently compatible with RZ and NRZ modulation formats and is bit rate transparent but ONLY up to the speed limit of the non-linear gate (hence if the date rate is faster than that speed limit, we would require a different non-linear gate with a higher speed limit to correctly performs 2R regeneration).

3R regeneration differs from 2R in that it requires a clock (optical) to perform the clocked decision process. Clock recovery and decision making element form the two fundamentals blocks of an optical 3R regenerators. In most 3R regeneration techniques, the optical clock needs to be synchronized with the data signal. It is far more attractive to achieve this synchronization optically rather than by the use of electronics. This can be done for mode locked lasers, for example [Sar'01a] .The device is operated via the use of dc currents. If the data rate and clock frequency are close to each other in value (within a certain locking range), the data signal becomes synchronized. This scheme has been successfully demonstrated for 10 and 40 GHz clock signals and has the added advantage the signal emitted from the mode locked laser is very well suited for transmission over long haul [Sar'01].

[Yik'01] presented an all-optical limiting amplifier performs the amplification and reshaping of an optical signal whiles a phase-locked loop (PLL) for the timing recovery. This technique also performs a simultaneous wavelength conversion operation (by 15nm) on the regenerated data. This technique differs from the majority of other optical 3R regeneration techniques (which consist of optical-gating elements and clock-recovery components in two separate blocks). The 3R regenerator is set in specific configuration as a single ring, which

simplifies the system structure. The all-optical limiting amplifier is based on FWM amplification in a piece of dispersion-shifted (DS) fibre. Due to the ring configuration, the only amplification limit results from Kerr response of the fibre, which is ultra fast As a result the data rate for this 3R regenerators can be extended from 10Gbit/s to 40Gbit/s. This 3R regenerator has the added advantage that it can function as a de-multiplexer as well. This occurs if input signal is an integral multiple of the 10Gbit/s data stream.

[Gav'03] demonstrated a 3R regeneration technique based on polarisation switching in Sagnac interferometer that uses a high gain, low polarisation-dependent SOA. Successful trials were conducted for data signals at 10 Gbit/s employing RZ modulation format with pulses that are 20 ps in width. Low power penalties of less than 0.5 dB were observed. This 3R regeneration technique is highly promising (especially due to low power penalty) and can be operated at 40 Gbit/s and beyond.

The 3R regenerator is very similar to the TOAD and consists of a 4-port polarization beam splitter with two arms forming a fibre loop, which incorporates an SOA. An optical clock signal is launched at the input of the polarisation beam splitter (which splits the signal into its two orthogonal polarized components). The two orthogonally polarized clock signals travel in different directions relative to one another (i.e. counter-propagate) in the loop and recombine at the output port of the polarisation beam splitter. The SOA is offset from the loop centre to ensure that the two clock signals are temporally separated and do not overlap as they travel through the SOA. The data signal is synchronized with the clock signal and is coupled into the interferometer. The data signal reaches the SOA before the co-propagating pulse (and after the counter propagating signal has passed through the SOA) [Gav'03].

As a result, the co-propagating clock signal experiences a nonlinear phase shift induced in the SOA by the data pulse. The mismatch of the pulse delays causes the two clock pulses to recombine with different polarizations at the polarization beam splitter. The position of the SOA in the fibre loop mirror determines the switching window of this 3R regenerator [Gav'03].

In order to cascade optical 3R regenerators, the wavelengths of the optical signals must be the same. The optical 3R regenerator discussed here retains the input signal by using a Sagnac interferometer integrated with parallel-amplifier structure (SIPAS). The SIPAS is a Sagnac interferometer with a parallel-amplifier structure (PAS), which is a symmetric MZI having polarization insensitive SOAs in each arm (as discussed in the Optical Logic section [Nip'00].

Since the PAS is asymmetrically placed in the Sagnac loop, the SIPAS operates due to differential-phase-modulation (DPM) between the co-propagating and counter-propagating signal. When the PAS is set in the cross state, the optical signal cannot get into the loop, resulting in filter-free wavelength conversion. The input and regenerated signals are spatially separated without using a filter and as a result, the clock and the input signal can have the same wavelength [Nip'00].

Quantum-dot SOAs (QD-SOAs) have superior features over traditional Quantum Well SOAs (QW-SOA). One of the most distinct features of QD-SOA is their gain recovery speed, which is much faster than that of QW-SOA. This allows QD-SOA based 3R regenerator to be used up to 160 Gbit/s, compared to only 80 Gbit/s for QW-SOAs [Sug'02].

3.3 Conclusion

In this chapter, we have highlighted some of the important technologies for next generation photonic networks. Invariably, all of these technologies require all optical signal processing. It is expected that future photonic networks will see wide deployment of OA amplets as they posses both compactness, low cost and good performance. In addition, 3R regeneration, wavelength conversion and all optical logic (for header recognition and packet contention resolution) will be needed in future photonic networks. Finally, simple optical memory elements will be required for buffering of optical packets in future photonic networks.

Chapter 4 Competitive Optics for All-optical signal processing

4.1 Introduction

Competitive Optics is a term coined by Dana Anderson and Claus Benkert [Ben'91] to describe the phenomena of competition between optical modes. Competitive-based systems and processes however, are not just limited to the optical domain. They occur in a wide variety of fields including artificial neural networks, computer and wireless networks, ad-hoc networks, biological systems, and natural phenomena such as hurricanes [Ben'91]. One of the most basic and illustrative examples of an optical competitive system is the multimode laser (where the various modes within the laser cavity compete with each other to determine which one will be oscillating at a given time).

Generally speaking, competitive-based systems (more precisely, competitive-based interactions) naturally have decision-making abilities. The human brain for example, is a dynamical system composed of a massive neural network with competitive (as well as cooperative) dynamics with decision making capabilities [Ben'91].

Dana Anderson and Claus Benkert pioneered the use of competitive optics principles, specifically, mode competition in photorefractive media [Hal'03]. Utilising the photorefractive ring oscillator as a basic building block, Anderson was able to realise a variety of important all optical signal processing functions. Examples include photorefractive Flip-Flop [And'91], optical neural networks functions such as Winner-Take-All and Voting-Paradox [Ben'91], [Hal'03], and various optical self-organising processes [Hal'03].

The rest of this chapter is organised as follows: section 4.2 will discuss the Lotka-Volterra model, which provides a mathematical description of some of the photorefractive competitive optics circuits developed by Anderson (and others). Section 4.3 will demonstrate how mode competition could be applied to saturated gain media (most notably SOA) to construct all optical signal-processing circuits based competitive optics principles and

highlight the similarities between them and Anderson's photorefractive circuits. Section 4.4 concludes this chapter.

4.2 Photorefractive Competitive Optics Circuits

Using the phenomenon of mode competition in photorefractive ring oscillator, Anderson and others successfully constructed and demonstrated a variety of all optical signal-processing circuits. In particular, Anderson was able to construct all optical neural networks composed of multiple, coupled photorefractive ring oscillators. The modes of these oscillators competed for the gain provided by the BaTiO3 crystals (an example of photorefractive media) which in turn led to the realisation of several neural network functionalities such as the Winner-Take-All (WTA) and the Voting-Paradox (VP) neural networks [And'90] ,[Ben'91].

The basic mathematical model for a competitive system is the Lotka-Volterra model. The model, developed by A. J. Lotka and V. Volterra [Lot'25], [Vol'31], was initially used to describe predator-prey dynamics. Despite its simplicity, the Lotka-Volterra model and is widely used in the majority of population dynamics models and in almost all dynamical systems that exhibit competitive behaviour between its variables.

A simple form of the Lotka-Volterra model is suitable for describing several of Anderson competitive optics schemes (such as WTA and VP optical neural networks). The model used consisted of a set of coupled differential equations of the following form [Ben'91]:

$$\frac{d}{dt}I_j = \alpha_j I_j - \sum_{k=1}^{N} \theta_{jk} I_k I_j, \qquad j = 1,...,N \qquad 4.1$$

Where:

- I_j and I_k represent the j_{th} and k_{th} competing modes,
- α_j represents the linear gain for the j_{th} competing mode,
- θ_{jk} represents the cross-saturation coefficient for the j_{th} and k_{th} competing modes,
- N represents the number of competing modes in the system.

With Equation 4.1, we can model competitive optics systems and gain insight into their internal behaviour and dynamics. We describe two general competitive systems that highlight the principle of mode competition in signal processing/decision making systems. These systems are Winner-Take-All and Voting-Paradox systems. It is worth mentioning that the dynamics of the competitive system, modelled by Equation 4.1, are primarily dependant on θ_{jk}, the cross-saturation coefficient parameter. Depending on the chosen value of θ_{jk}, one can for example, change a WTA system into a VP system and vice versa [Ben'91].

4.2.1 Winner-Take-All optical neural network

The WTA optical neural network [Ben'91] is a multi-state system that provides a good example of the basic principles of Anderson's signal processing schemes based on mode competition in BaTiO3 crystals. Typically, the competing modes are in the form of dynamic holograms [Hal'03]. Anderson's work involved single and/or multiple $BaTiO_3$ crystals interconnected with multimode fibres [Dam'01]. Several gain and loss mechanisms exist in these photorefractive crystals including two-wave mixing and phase conjugation. These mechanisms provide differing amounts of (saturable) gain and/or loss to the various competing modes. The value of the gain/loss provided depends on the initial intensities of the competing modes. The strong oscillation of one of the modes within the crystal provides a loss pump for the two-beam coupling of the other modes (those with weaker intensities/oscillations). When this happens, the passive loss of the crystal imposed upon these weaker modes exceeds their gain and they cease oscillating. Therefore, the mode with strongest intensity (strongest oscillation within the crystal) dominates and suppresses the other modes becoming the steady-state output of the WTA neural network [Ben'91], [And'90].

In order to use Equation 4.1 to model the WTA neural network, we must determine all values of the cross saturation coefficient, θ_{jk}. Given N competing modes in a WTA system, θ_{jk} will be an N x N matrix of the form [Ben'91]:

$$\Theta = \begin{bmatrix} \beta & \theta & \dots & \dots & \theta \\ \theta & \beta & & & \vdots \\ \vdots & & \ddots & & \vdots \\ \vdots & & & \ddots & \theta \\ \theta & \dots & \dots & \theta & \beta \end{bmatrix} \quad j,k = 1...N \qquad 4.2$$

Where:

- β_{jj} represents the self-saturation coefficient for the j^{th} competing mode,
- θ_{jk} represents the cross-saturation coefficient for the j^{th} and k^{th} competing modes.

Equation 4.1 can be solved with the aid of 4.2 to determine the intensity of any of the competing modes in a competitive system at any given time. In particular, we are interested in the steady state output of the WTA system to determine which particular mode dominates and suppresses the oscillation of all the other modes (i.e. which mode 'wins' the competition). Several steady state solutions of Equation 4.1 exist and their stability is based on the values of α, β and θ parameters [Ben'91]:

$$I_j = \begin{cases} 0 & if \ \alpha < 0 \quad for \ all \ j, \qquad 4.3 \\ \dfrac{\alpha}{\beta + \theta(N-1)} & if \ \theta \approx 0 \quad for \ all \ j, \qquad 4.4 \\ \dfrac{\alpha}{\beta}, I_k = 0 & if \ \theta > \beta \quad for \ all \ k \neq j \quad 4.5 \end{cases}$$

Equation 4.3 represents the simplest and most intuitive steady state solution. Suppose that all αs are equal and less than zero (i.e. $\alpha_j < 0$ for all j). Then all of the competing modes in the system experience no net gain (they actually experience a net loss since they receive less than zero amplification by a crystal that has passive losses). As a result, none of the competing modes will be able to oscillate and the output of the system will simply be zero, as represented by Equation 4.3. Therefore, we must ensure that the condition $\alpha_j > 0$ for all j is satisfied for all j in order to perform any useful function with our competitive system. For the remainder of this discussion we shall assume, that α_j has the same (nonzero) value for all

modes. In reality, different modes may experience different linear gains by the gain media (see section 4.3). Furthermore, assume that the cross-saturation parameters for all the competing modes are equal, i.e. $\theta_{jk} = \theta$ [Ben'91].

The value of the cross-saturation parameter,θ dictates weather Equation 4.4 or 4.5 describes the output of the competitive system. Equation 4.4 suggests that the system's output is not dominated by single mode but in fact, all the competing modes oscillate simultaneously and with equal intensity. This situation arises when the competing modes' oscillation is independent of each other which happens when the value of the cross-saturation parameter is low, i.e. $\theta \approx 0$.

If θ is large, then the intensity of a competing modes is highly dependant on the intensities of all other modes in the system (i.e. there is strong coupling between the oscillating modes in the system). Furthermore, if $\theta > \beta$, then strong competition between the modes is present in the system and not all modes can oscillate simultaneously (as is the case in Equation 4.4). The mode with the strongest intensity 'wins' the competition and suppresses the oscillation for all other modes. This is illustrated in Equation 4.5 that in fact represents a WTA competitive system.

It is hence clear, that the parameters of a competitive system dictate its behaviour. For a competitive system modelled by Equations 4.1 and 4.2, we can achieve WTA dynamics if choose the cross saturation parameter is greater than the self-saturation parameter of the system (i.e. $\theta > \beta$).

We carried out simulations of Equations 4.1 and 4.2 in MATLAB to illustrate the aforementioned arguments. Figures 4.1 and 4-2 plot the output of the competitive system for theα, β and θ parameters to illustrate some of the steady solutions described by Equations 4.3 to 4.5.

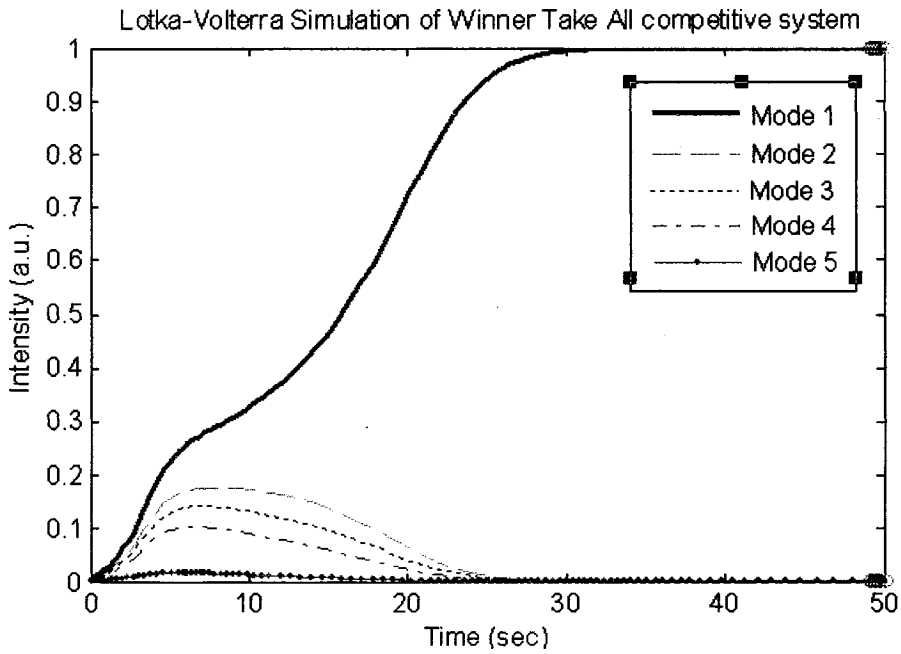

Figure 4-1 N = 5, $\alpha = 1$, $\beta = 1$, $\theta = 1.5$. Initial mode intensities chosen randomly from the interval [0, 0.001].

It is evident from the above Figure 4-1 that the Lotka-Volterra model, Equations 4.1 and 4.2 does indeed describe a WTA neural network. *The winning mode is chosen by the system based on the initial intensities of the competing modes.* The mode with strongest initial intensity (oscillating within the $BaTiO_3$ crystal) rapidly increases in intensity at the expense of the remaining modes. Eventually, the strongest mode consumes all the available energy in the system (i.e. consumes all the available gain provided by the crystal). This leads to the suppression of the oscillation of the remaining modes and their intensities drop to zero. As a result, a WTA dynamic is achieved (Figure 4.1). A physical realisation of the WTA using photorefractive crystals is discussed in [Ben'91]. The important thing to note is that the system in [Ben'91] can be optically switched to select a desired mode as the output of the WTA. The injection of an optical signal into that desired mode, will force the WTA to select that particular mode as the winner [Ben'91]. This has important a ramification for WTA circuit implemented using saturated gain media (for example, in SOA) since it implies high-speed switching operation is possible [Hil'02].

WTA neural networks can find several applications in photonic networks. They can be used for header recognition for example. A WTA neural network can be trained (by setting the appropriate synaptic connections weights) to recognise a certain bit pattern of optical packets. Once the pattern is recognised, the packet can then be routed to the appropriate location. WTA neural networks can also be used to implement simple optical logical operations such as XOR with very high contrast ratios (~100:1) [Hil'02].

4.2.2 Voting-Paradox neural network

Another competitive system that can be described by the Lotka-Volterra equations is the Voting-Paradox (VP) neural network. VP dynamics have inherent contradictions within them, unlike WTA dynamics. The best way to illustrate this is by drawing an analogy to a simple voting process (and hence the name). Assuming there are three (or more) groups and each group holds veto power over other groups (i.e. group 1 has veto power over 2, group 2 has veto power over group 3, and group 3 has veto power over group 1). If all of these groups have mutually conflicting interests, then the voting process will be deadlocked, as no consensus can be reached due to the voting powers each group posses.

An optical neural network system with such characteristics will therefore not have a final stable steady state solution. The output will continuously cycle between the competing modes in the system in a sequential manner (i.e. each mode has a chance to oscillate for a certain period and then is replaced by another mode, which also oscillates for another period and so on). These oscillations can be maintained indefinitely (provided the system has sufficient input power).

The Lotka-Volterra model can also be used to describe a VP system. Equation (2) must be modified however, in order to reflect the contradictory dynamics of VP. The fact that the output of the VP cycles through a sequence of the oscillatory modes in the system implies that the each mode in the system (positively) stimulates the next mode to start oscillating.

The aforementioned argument implies that neighbouring modes (say j, j+1) *cooperate* with each other (mode j provides a positive stimulus to kick-start the oscillation of mode j+1) while competing with *all* other modes (i.e. mode j suppresses the oscillation of all other modes except that of mode j+1). Therefore, the energy in a VP system moves from one mode to the next in a timed manner. Such cooperation is represented in the cross-saturation matrix of the system [Ben'91].

$$\Theta = \begin{bmatrix} \beta & \theta & \dots & \dots & \theta \\ \theta & \beta & & & \vdots \\ \vdots & & \ddots & & \vdots \\ \vdots & & & \ddots & \theta \\ \theta & \dots & \dots & \theta & \beta \end{bmatrix} - \begin{bmatrix} 0 & 0 & \dots & 0 & \delta \\ \delta & 0 & & & 0 \\ 0 & \delta & \ddots & & \vdots \\ \vdots & & \ddots & \ddots & 0 \\ 0 & \dots & 0 & \delta & 0 \end{bmatrix}$$

$$\Theta = \begin{bmatrix} \beta & \theta & \dots & \theta & \theta-\delta \\ \theta-\delta & \beta & \theta & \cdots & \theta \\ \theta & \theta-\delta & \ddots & \ddots & \\ \vdots & & \ddots & \ddots & \theta \\ \theta & \cdots & \theta & \theta-\delta & \beta \end{bmatrix} \qquad 4.7$$

Figure 4-2 illustrates the output of a VP process based on MATLA simulations of Equation 4.7. Clearly, the VP steady state output does not have a single, stable value (or mode). Instead, the output cycles through all the modes in the system. A VP can find application for recalling a certain timed-sequence of data [Ben'91].

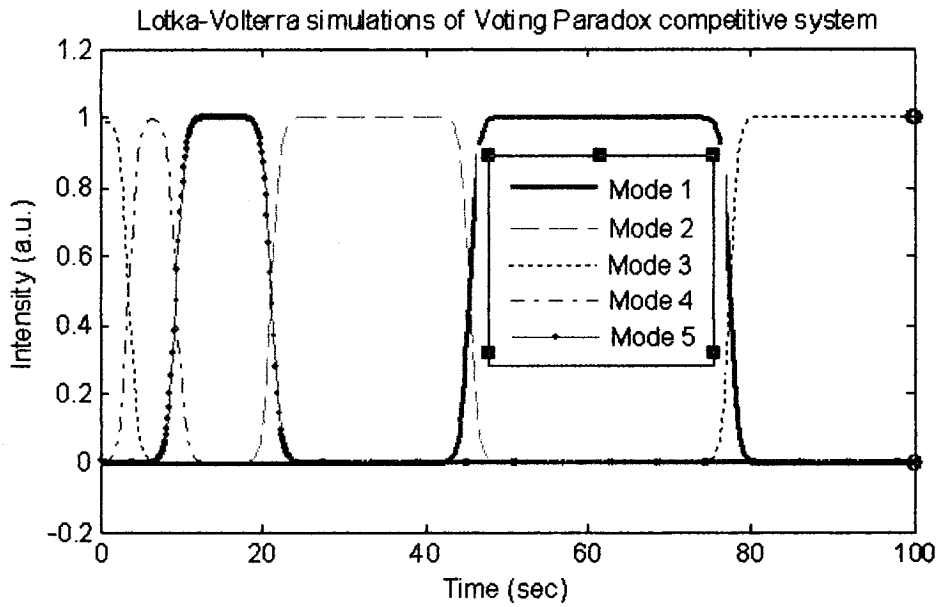

Figure 4-2 Lotka-Volterra Simulation of Voting-Paradox System.

4.3 Competitive Optics in Saturated Gain Media

The work by Anderson and others has highlighted the importance of competitive optics in all optical signal decision-making. A wide variety of important signal-processing functions has been demonstrated in photorefractive media. Some of these functions, such as Flip Flop, WTA neural networks, ring counters, and others can find many applications in current and future photonic networks [Hal'03].

The major drawback of the aforementioned work however, is its operating speed. Time constants for some of these photorefractive circuits are in the range of 0.001-10 seconds [Ben'91]. This is mainly due to the dielectric nature of photorefractive material and the bulk nature of the. Hence, competitive optics circuits in photorefractive media are unsuitable for deployment in photonic networks.

The competitive optics principle however, is media independent. As previously mentioned in section 4.1, Hall has proposed that competitive optics can be applied, via different nonlinear mechanisms to other material and could therefore function at different speed and wavelength regimes (depending on the underlying physics of the media) [Hal'03]. Hall and others have successfully demonstrated this concept using Four Wave Mixing in saturated gain grating (such as Nd:YAG) [Hal'03].

Martin Hill and others used XGM in SOA to perform all optical signal processing functions (such as Flip Flop, WTA neural networks, variable optical buffers) [Hil'01], [Hil'02], [Liu'02], [Liu'03], [Liu'03a], [Zha'04]. By coupling semiconductor ring lasers (analogous of photorefractive ring oscillators) and controlling the intensities of the competing modes within the rings cavity (by providing them with different satiable gains and losses), Hill was able to demonstrate the application of competitive optics circuits in SOA (a form of saturated gain media).

One can draw notice several similarities between Hill and Anderson's work. Anderson utilised two-beam coupling (a competitive physical process) in $BaTiO_3$ photorefractive crystals while Hill used XGM (another competitive physical process) in SOA. By constructing optical circuits where different optical modes (or wavelengths) are sharing the same gain medium (BaTiO3 or SOA), both authors were able to perform several important all-optical signal processing functions utilising the same basic principles of competitive optics.

The work by Hill and others is very significant because it has direct relevance and application to current and future photonic circuits. Competitive optics circuits based on SOAs ring lasers offer a number of advantages over their photorefractive ring oscillator counterparts. SOA are mature, cheap and can be easily integrated. SOA based ring lasers (and circuits based on them) do not suffer from any of the phase alignment problems that plague photorefractive circuits. XGM in SOA is primarily an intensity-based phenomenon and hence the phase of the competing signals plays a minimal role in the overall operation (as compared to photorefractive circuits operations). Finally, SOAs have a reputation for

high-speed operation. As a result, all-optical signal processing circuits based on competitive optics in SOA are very suitable for current and future photonic networks.

4.4 Conclusion

Competitive optics is an important physical phenomenon that finds many applications in decision-making schemes. Anderson and others have created a variety of useful all optical circuits using competitive optics principles in photorefractive crystals including photorefractive flip flop, WTA and VP neural networks. The drawback of Anderson's schemes is its bulkiness and very low speeds. Hall and others have extended Anderson's work to staurable gain media (such as Nd:YAG) with much higher speeds but with bulkiness and alignment issues. Hill and others extended Anderson's work to SOA and solved the alignment problem by utilising an intensity based physical phenomena (XGM in SOA) to alleviate the need for precise round trip phase matching.

Chapter 5 Fundamental Competitive Optics Structure: The Semiconductor Ring Laser (SRL)

5.1 Introduction

The ring resonator cavity was proposed shortly after the demonstration of the first practical laser. Unlike the Fabry-Perot cavity in which the light experiences repetitive reflections between two partially reflecting mirrors, the ring cavity employs three (and often more) mirrors that propagate the light in a unidirectional (clockwise or counter-clockwise) manner. These two cavity structures are often used in many laser intra-cavity configurations (e.g. gas, dye and semiconductor lasers). We will use the terms SRL to refer to unidirectional Semiconductor ring lasers where the semiconductor gain media is a SOA.

Figures 5-1 and 5-2 show the schematics of the Fabry-Perot and ring resonator cavities, respectively [Num'04].

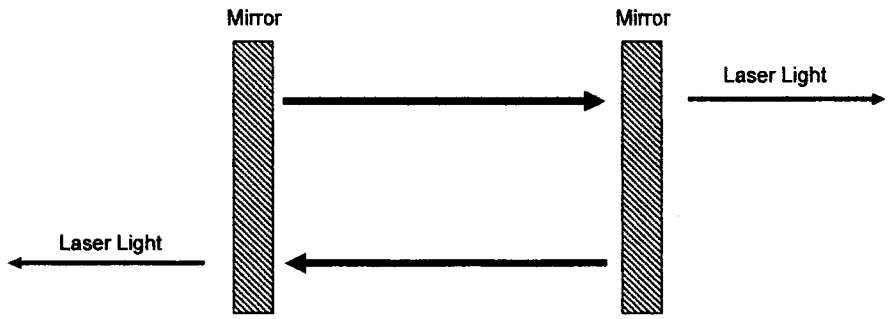

Figure 5-1 Fabry-Perot resonator cavity

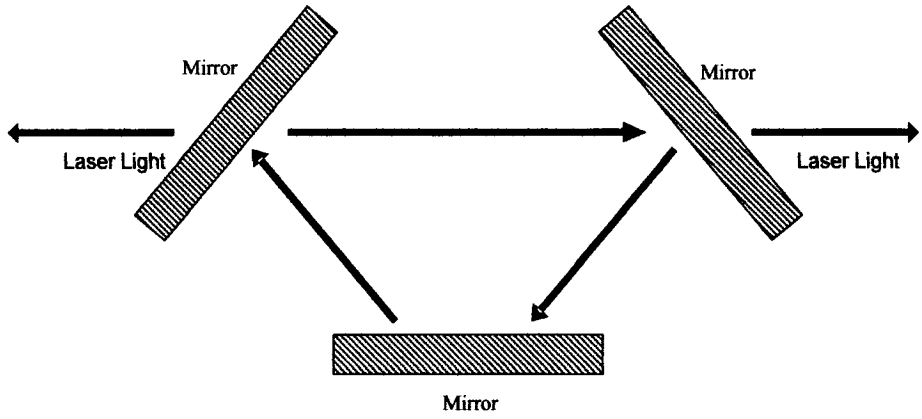

Figure 5-2 Ring resonator cavity

It follows naturally that the ring resonator was also employed in the laser's extra-cavity configurations. Many applications have arisen from placing a gain medium in a ring configuration, the so-called Ring Laser configuration. The gain media can vary but the two most common media are Erbium Doped Fibre (EDF) and Saturated Gain Media such as Semiconductor devises (either lasers or SOA). We refer to Erbium Doped Fibre Ring Lasers as EDFRL where as we use the SFRL acronym to refer to Semiconductor Fibre Ring Lasers that use SOA as the gain medium.

Ring lasers can be mode locked (actively or passively), injection locked, and (rational) harmonic locked [Xu'03], [Pen'02], [Zoi'00], [Wu'00]. A chief advantage of the ring laser structure lies in the fact that it can be mode-locked without suffering from the detrimental effects of Spatial Hole Burning (SHB) which can cause damage to mode locked FP and DFP lasers.

The SFRL provides an alternative to the widely used EDFRL [Hab'00]. Recent theoretical and experimental research into the SFRL has led to the development of several SFRL configurations that have edged comparable EDFRL configuration in terms of performance and speed [Xu'03]. Furthermore, SFRL-based devices can perform a wide variety of all-optical high-speed applications that are not possible with EDFRL, primarily due to the slow carrier lifetime of Erbium, which is in the order of a few ms. The SOA on the other hand has

the attractive characteristic of very fast response times (due to its short carrier lifetimes, in the order of a few ns or less).

The SFRL has found many applications in photonic networks. Some of the traditional SFRL applications include ultra short pulse generation, multiwavelength optical sources, tuneable laser sources, and all-optical clock recovery [Xu'03]. Recently, SFRL were used as all-optical memory elements and buffers, all-optical neural networks, and simple all-optical logic gates [Hil'01], [Hil'01a], [Hil'02], [Hil'04], [Hal'03], [Lin'04], [Liu'02], [Liu'03], [Liu'03a], and [Zha'05].

One of the main advantages of SOA-based ring lasers is their ease of integration (compared to EDF-based ring lasers). The SOA naturally lends itself to integration and the fibre interconnections could be replaced with waveguides. This could result in a very small and compact device with numerous applications [Sor'03]. From now on, we will refer SOA ring lasers with waveguide interconnections as simply Semiconductor Ring lasers (SRL).

The rest of this chapter is organised as follows, in sections 5.2.1 and 5.2.2 we will provide a qualitative description of the operation of an externally injected SRL. This device forms a basic unit that operates on competitive optics (gain competition) principles. Section 5.2.3 introduces a simple dynamic model of the SRL based on rate and signal-propagation equations. Section 5.3 presents simulations of several all-optical signal processing applications using the SRL. The simulations were performed with a commercial photonic circuit software package, VPIcomponentMaker™: Active Photonics. Additional simulations of the dynamic model in section 5.2.3 were performed in MATLAB. Section 5.4 concludes the chapter and provides a brief summary.

5.2 Semiconductor Ring Lasers

It is important to note that, due to the bidirectional nature of the SOA, the SRL is inherently a bidirectional device as well. Hence, there will be two laser light beams propagating the SRL cavity in opposite directions (a clockwise beam and a counter-clockwise laser beam).

This significantly complicates the theoretical and practical operation of the SRL but does gives rise to several interesting, and potentially useful, phenomenon [Sor'03].

The work presented here however, does not require or make use of the bidirectional nature of the SRL. To achieve unidirectional operation, an isolator is placed in the ring cavity to ensure the unidirectional propagation of light in the ring cavity. This simplifies the modelling and simulation of the SRL but does not limit its potential applications.

5.2.1 SRL with External Injection

Figure 5-3 presents a typical physical setup of an externally injected SRL. We can identify main components that make up the SRL structure; 1) a SOA (bulk, QW, or QD active region material) serves as the nonlinear gain medium of the SRL. 2) A laser transmitter (TX) serves as the external input signal to the SRL. 3) Coupler 1 couples the external light signal into the SRL cavity while Coupler 2 extracts the output light signal from the SRL cavity. 4) A filter selects the output wavelength of the SRL from the Amplified Spontaneous Emission (ASE) spectrum of the SOA. 5) An isolator ensures the unidirectional propagation of light inside the SRL cavity. In the simulation environment, Null and Gnd refer to the unused input port of Coupler 2 and the unused output port of Coupler 1, respectively. Optical waveguides interconnect the SRL components and the output is viewed using an Optical Spectrum Analyzer (OSA) or Optical Scope (to view time-domain pulses).

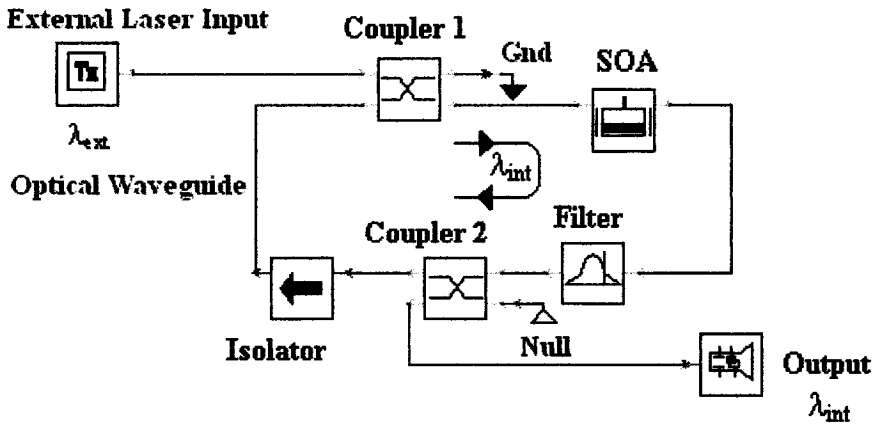

Figure 5-3 Externally injected (co-propagation) SRL physical setup.

The difference between the SFRL and SRL is that the former is a bulk device employing relatively long lengths of fibre (~ 10 m or more) which form the optical cavity of the ring laser. The SRL on the other hand is an integrated device that replaces the fibre with waveguides that are much shorter in length (~ mm or even less). The ring cavity length sets an upper limit on the speed of the ring laser structure [Hal'03], which implies that the SRL is a much faster device the SFRL. Both devices have their applications however, but for the purposes of all-optical signal processing and decision-making, the SRL is a more applicable building block as it offers both a small size and high speed.

The main objective of this work is to prove the competitive optics concept in saturated gain media. We achieve this aim by simulating several SRL-based all-optical signal-processing circuits. In modelling the SRL however, we only consider the temporal effects of the interconnecting waveguides. In our simulations, we ignore other detrimental effects, such as optical mode confinement and cross coupling of light to and from other nearby structures. Correct operation of SRL-based all-optical circuits is heavily dependant on the SRL cavity delay (section 5.3.1.1). On the other hand, other waveguides effects usually have a more limited impact on the *temporal and functional operation of the SRL*. Hence, it is justifiable to ignore such effects for the purposes of this work. Of course, these effects must be considered if we wish to carry out experimental verification of the presented simulations. [Sor'03] provides a comprehensive review of waveguide effects in integrated SRL.

5.3 Principle of Operation

The basic operation of the SRL can be broken down into two distinct cases: 1) Solitary SRL operation and 2) SRL operation with external injection. We discuss both in detail.

5.3.1.1 Solitary SRL operation

Figure 5-4 shows the physical setup of a solitary SRL. In the solitary case, no externally injected signal is applied to the SOA. As a result, the SOA's (bidirectional) output is purely

ASE. The isolator only permits unidirectional propagation of light inside the SRL ring cavity and forces the ASE to circulate the cavity in its direction (clockwise in Figure 5-4).

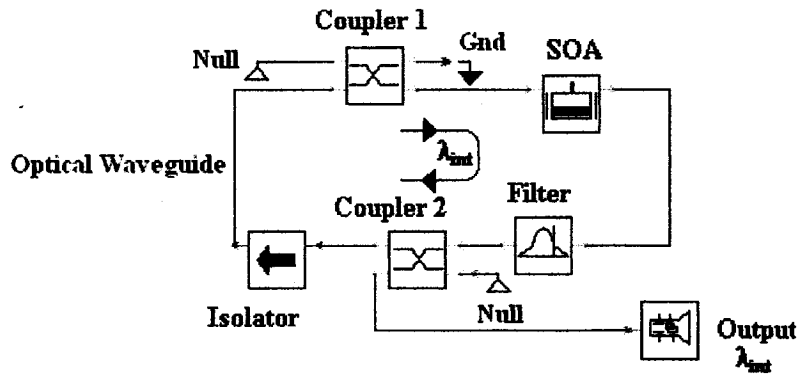

Figure 5-4 Solitary SRL physical setup.

For the purposes of all-optical signal processing, we are usually interested in SRLs with single longitudinal mode outputs [Hil'01], [Hil'02], [Lin'04], [Zho'05], and [Zoi'02]. This can be achieved by placing a filtering element in the SRL cavity. The filter, depending on its bandwidth, then selects a single longitudinal mode from the SOA's ASE bandwidth. This single longitudinal mode then circulates the SRL ring cavity continuously and receives amplification each time it passes through the SOA, building up in amplitude and coherence. The result is a coherent beam of light whose wavelength is specified by the filter's transmission-peak wavelength. This represents the internal lasing signal of the SRL and we denote its wavelength as λ_{int}. Coupler 2 extracts a portion of the SRL's internal lasing signal λ_{int}, for viewing on an oscilloscope and further processing. We will now discuss the case where external injection is present.

5.3.1.2 Externally injected SRL operation

An external input signal can also be injected into the SRL cavity via a coupler as shown in Figure 5-3 (using Coupler 1). The concept of injecting external radiation into a (fibre) ring laser has extensively been studied in literature. For the purposes of this work however, it is important to make a clear distinction between the different types of external injection into a ring laser.

Injecting the output of a laser into the input of another laser creates a Master-Slave laser system [Hil'01]. In most cases, the injection of the Master's laser radiation into the Slave laser alters the Slave laser's frequency to a value (closely) equal to the Master's laser frequency. In essence, the Master laser 'locks' the frequency of the Slave laser to its own frequency. This process is referred to as injection or active mode locking [Lu'04].

If we use the same injection-locking technique but only allow the Slave laser to oscillate in the ring cavity (by placing a filtering element tuned to the Slave laser's frequency) a new situation arises, often referred to gain suppression (or gain quenching) [Hil'02], [Lu'04], [Pen'92]. The SRL presented in this work falls under this category.

With reference to Figure 5-3, the laser transmitter (TX) injects an input signal of wavelength λ_{ext} into the SRL (via Coupler 1). As a result, the SOA will now serve as the gain medium for two separate signals: the externally injected signal, λ_{ext}, and the SRL internal lasing signal, λ_{int}. If we assume that the SOA gain is uniform in the spectral range covering both wavelengths, the SOA will amplify both signals with similar gain.

The injection of an electrical current into the SOA creates a reservoir (or pool) of carriers that occupy the conduction band of the SOA active region. In the solitary SRL case (Figure 5-4); the carrier reservoir is used for the amplification of *only* one signal, the SRL internal lasing signal, λ_{int}. With the introduction of the external signal, λ_{ext} into the SRL cavity, (Figure 5-3); two signals now share the SOA carrier reservoir. As λ_{ext} and λ_{int} propagate through the SOA, they will both attempt to receive amplification from the SOA by consuming its carrier reservoir (the process of optical amplification). Now, both λ_{ext} and λ_{int} will have to compete with one another for the *limited* supply of SOA carriers and in essence, will end up competing for the *limited* SOA gain. This situation gives rise to the Cross Gain Modulation (XGM) effect, discussed in section 3.2.2.1.

XGM provides an excellent illustration of the competitive optics/gain competition principle in saturated gain media (in this case, the SOA). The signal with the strongest power will 'win' this competition and deny the weaker signal access to SOA carrier reservoir. The

weaker signal therefore receives no amplification from the SOA and is ultimately suppressed (or quenched) by the stronger signal.

From the above description, we can conclude that an externally injected SRL functions as an all-optical wavelength converter. When the (modulated) external signal, λ_{ext}, is high in power, it essential wins the competition for the SOA gain and suppresses the oscillation of the SRL internal signal, λ_{int}. Furthermore, since λ_{ext} does not make a full roundtrip across the ring cavity (it is prevented from doing so by the filter which is set to allow λ_{int}), no further oscillations will be present inside the SRL cavity and as a result, no light will be generated from the SRL output (Coupler 2). On the other hand, when external signal, λ_{ext}, is low in power, it is unable to suppress the oscillation of the SRL internal signal, λ_{int}, in the ring cavity and as a result, the SRL will output light with a wavelength of λ_{int}. In effect, the information in the external signal λ_{ext}, is inverted in amplitude and converted into the SRL internal signal wavelength, λ_{ext}. The SRL therefore functions as a basic *inverting* wavelength converter.

The external signal, λ_{ext} can be CW or time varying (modulated) and so can the solitary SRL signal, λ_{int}, by direct modulation of the SOA injection current. The optical circuits presented in this work all have constant SOA injection currents (hence CW λ_{int}) with modulated external inputs.

5.3.2 Theoretical Model

The main component of the SRL is the SOA; the SRL theoretical model is often obtained by modifying the SOA model to take into the account the presence of the two signals (external signal, λ_{ext} and SRL lasing signal, λ_{int}). Many SRL models exist in the literature [Pen'92], [Hil'01], [Hil'02], [Lin'04], [Lu'04], [Sor'03], [Pen'02], [Xu'03], [Zoi'02], and [Xin'04]. The most relevant models to this work is [Lin'04], and [Xin'04] and they shall form the basis of the SRL model presented here. All simulations were carried out using bulk SOA parameters (section 5.3).

We first present a steady-state model that describes the SRL threshold conditions (i.e. minimum gain required to start laser oscillation). A dynamic model is then presented to describe the evolution of the SRL output and describe its output pulses temporal behaviour. Finally, a Lotka-Volterra competitive model is presented to describe the SRL operation from a competitive optics point of view. The models given below were used to simulate the SRL structure in MATLAB. VPI used more complex (and often propriety) models to simulate the SRL structure.

5.3.2.1 Steady-State Model

With reference to Figure 5-3, let the external (time-varying) signal power be denoted by P_{ext} and let the solitary SRL internal lasing power be denoted by P_{int}. Furthermore, let the output signal power of the SRL (which is extracted from the SRL cavity by Coupler 2) be denoted P_{out} as shown in Figure 5-5.

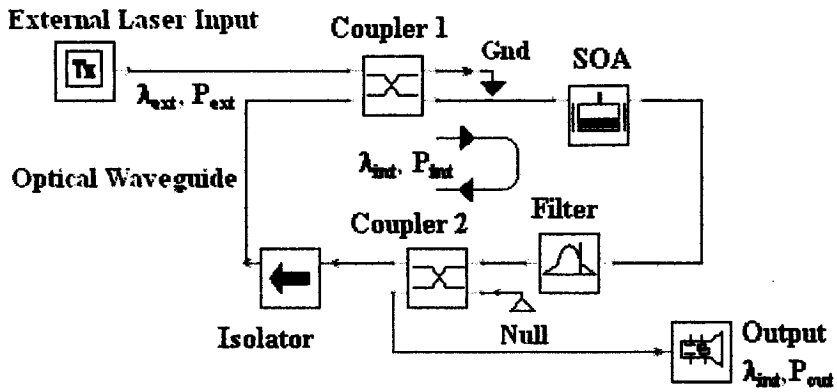

Figure 5-5 Externally injected SRL schematic with signals powers and wavelengths.

The solitary (i.e. no external injection present) SRL will not start lasing until the SOA provides enough gain to the internal lasing light, λ_{int} to overcome all losses in the ring cavity. In other words, lasing will only occur if the λ_{int} receives enough amplification from the SOA to be able to make a full roundtrip in the SRL cavity. This is simply the threshold condition of the ring laser. The minimum SOA gain that satisfies the above condition is referred to as the SRL's threshold gain, G_{th}.

The threshold gain will depend on the various losses incurred by the λ_{int} signal as it traverses the ring cavity. These losses will include all of insertion losses of the passive components that make up the SRL (isolator, filter, and two couplers) as illustrated in Equation 5.1 [Xin'04]:

$$G_{th} = \sum_{i=1}^{i=N} \varepsilon_i(\lambda) \qquad 5.1$$

Where,

- G_{th} is the threshold gain of the SRL,
- ε_i (λ) is the insertion loss of the i^{th} passive components in the SRL cavity N is the total number of passive components in the SRL,
- N is the total number of passive components in the SRL.

In reality, the amount of insertion loss that a passive component imposes on a signal is wavelength dependent. However, for the purposes of this work, such wavelength dependency is ignored since both the external and internal signals' wavelengths are chosen to be close enough to each other to experience relatively the same gain by the SOA. Hence, we assume that all passive components in the SRL impose the same insertion loss on both the external and internal signals.

The feedback nature of the SRL implies the existence of a boundary condition that relates the SRL's internal signal input power, P_{int} with the SRL's output power, P_{out}. With the aid of Figure 5-5 (and dropping loss wavelength dependence), we can derive such a boundary condition [Xin'04]:

$$P_{\text{int}} = P_{out} \times \sum_{i=1}^{N} \varepsilon_i \qquad 5.2$$

Where,

- P_{int} is the SRL internal signal power,
- P_{out} is the SRL output signal power,
- ε_i is the insertion loss of the i^{th} passive components in the SRL cavity,
- N is the total number of passive components in the SRL.

Referring to Figure 5-5, we have five passive components (i.e. N = 5) and hence 5 insertion-loss terms in Equations 5.1 and 5.2. The passive components include the isolator, two couplers, filter, and interconnecting waveguides.

It is also important to mention the phase relationship requirement for a ring cavity. The ring cavity is resonant at certain frequencies only given, i.e. only those frequencies can be supported (i.e. can oscillate/lase) in the ring cavity. The spacing, $\Delta\lambda$, between adjacent wavelengths that satisfy the resonant condition of the cavity is given by $\Delta\lambda = \frac{\lambda^2}{n_g L_r}$, where n_g represents the refractive index of the ring cavity and L_r represents the length of the ring cavity.

5.3.2.2 Dynamic Model, Co-propagation configuration

As was previously discussed in section 2.4, we can use the SOA rate equation model to determine the dynamic properties of the SOA and invariably those of the SRL as well. The carrier density in the SOA cavity is time and space dependent, this makes the rate equation a partial differential equation. However, we often assume a constant carrier density throughout the SOA cavity. This allows us to drop the carrier density space-dependency and express it as a differential equation in terms of time only [Num'04]. This assumption is valid in instances where there are light fields propagating through the SOA cavity in both directions thus creating an approximately constant and uniform carrier density distribution [Hil'02]. In a unidirectional SRL however, light propagates in the SOA cavity in one direction only and the assumption of constant carrier density cannot be applied accurately. Therefore, we must keep both the space and time dependency in our rate equation model for the SRL.

In order to accurately (numerically) model such a rate equation, the SOA cavity needs to be subdivided into several small sections of uniform length, ΔL. The rate equation is then solved for each section and the signal fields are propagated from one section to the next until we reach the end of the SOA cavity and obtain our outputs. This is the basic idea of the Transmission Line Laser Model (TLLM) technique [Low'88], [Con'02], [Con'02a] and [Lin'04]. Figure 5-6 shows a representation of the SOA's active region subdivided into N sections with equal lengths of ΔL value.

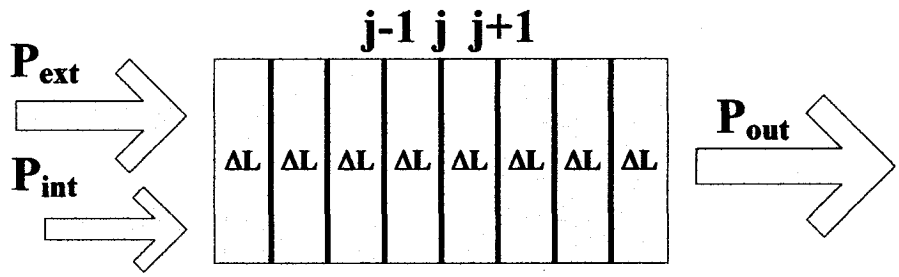

Figure 5-6 SOA cross-section for co-propagation configuration

With the aid of Figure 5-6, we can formulate the carrier-density rate equation for an externally injected SRL. The reduced time variable T ($=t-\frac{z}{V_g}$, V_g represents the group velocity) is often used in order to obtain analytical solutions to the carrier density [Con'02], [Agr'95]. The carrier density for the j^{th} section of the SOA, $N_j(z,T)$, can therefore be expressed as:

$$\frac{\partial N_j(z,T)}{\partial T}=\frac{I}{qV}-\frac{N_j}{\tau_c}-\left[\frac{\Gamma g_{ext,j}(N_j(z,T))}{\hbar w_{ext}A_{cross}}\overline{P}_{ext,j}+\frac{\Gamma g_{int,j}(N_j(z,T))}{\hbar w_{int}A_{cross}}\overline{P}_{int,j}\right] \qquad \textbf{5.3}$$

Where

- z is the space variable,
- T is the reduced time variable, $T=\frac{t-z}{V_g}$,
- N_j is the carrier density distribution in the SOA j^{th} section,
- $\overline{P}_{ext,j}$ is the average power of the external signal in the SOA j^{th} section,
- $\overline{P}_{int,j}$ is the average power of the SRL internal lasing signal in the SOA j^{th} section.
- $g_{ext,j}$ is the material gain coefficient for the external signal in the SOA j^{th} section,
- $g_{int,j}$ is the material gain coefficient for the SRL internal lasing signal in the SOA j^{th} section,
- I is the injection current,
- q is the electron charge,
- V is the volume of the SOA's active region,
- τ_c is the carrier lifetime,
- is the optical confinement factor of the SOA active region,
- $\hbar$ is the reduced Planck's constant,
- ω_{ext} is the angular frequency of the external signal,
- ω_{int} is the angular frequency of the internal signal,
- A_{cross} is the cross sectional area of the SOA's active region.

The material gain coefficient is one of the most important SOA parameters. It dedicates the SOA gain spectrum and its wavelength dependency. Many models for the gain coefficient exist with varying degrees of accuracy. A simple cubic formula is often used to describe the asymmetric gain for both the external and SRL lasing signals [Lin'04]:

$$g_{ext,j} = a_1(N_j - N_0) - a_2(\lambda_{ext} - \lambda_{Nj})^2 + a_3(\lambda_{ext} - \lambda_{Nj})^3 \qquad \textbf{5. 4}$$

$$g_{int,j} = a_1(N_j - N_0) - a_2(\lambda_{int} - \lambda_{Nj})^2 + a_3(\lambda_{int} - \lambda_{Nj})^3 \qquad \textbf{5. 5}$$

$$\lambda_N = \lambda_0 - a_4(N_j - N_0) \qquad \textbf{5. 6}$$

Where

- $g_{ext,j}$ is the gain coefficient for the external signal in the j^{th} section of the SOA,
- $g_{int,j}$ is the gain coefficient for the SRL internal lasing signal in the j^{th} section of the SOA,
- N_j is the carrier density in the j^{th} section of the SOA.
- N_0 is the transparency carrier density for the SOA,
- λ_{ext} is the external signal wavelength,
- λ_{int} is the SRL internal lasing signal wavelength,
- λ_{Nj} is the corresponding wavelength for SOA's peak gain,
- a_1 is the differential gain coefficient of the SOA,
- a_2 is an empirical constant characterising the width of the SOA gain profile,
- a_3 is an empirical constant characterising the asymmetry of the SOA gain profile,
- a_4 is an empirical constant characterising the shift in SOA's gain peak.

Signals travelling through the SOA cavity experience different amplification depending on their position along the cavity. This behaviour is modelled with signal's power propagation equations. We need two such equations; one for the external signal power, P_{ext}, and another one for the SRL internal lasing signal power, P_{int} [Lin'04]:

$$\frac{\partial P_{ext,j}(z,T)}{\partial z} = \Gamma(g_{ext,j}(N_j(z,T)) - \alpha_{int})P_{ext,j}(z,T) \qquad \textbf{5.7}$$

$$\frac{\partial P_{int,j}(z,T)}{\partial z} = \Gamma(g_{int,j}(N_j(z,T)) - \alpha_{int})P_{int,j}(z,T) \qquad \textbf{5.8}$$

Where

- $P_{ext,j}$ is the power of the time varying external signal in the j^{th} section of SOA,
- $P_{int,j}$ is the power of the time varying SRL internal lasing signal in the j^{th} section of the SOA,
- Γ represents the SOA active region confinement factor,
- α_{int} represents the SOA internal losses.

Now that we have the propagation powers, we can compute the average (position-dependant) powers (for both the external and internal signals) inside the SOA. For j[th] section of the SOA, we have (refer to Figure 5-6):

$$\overline{P}_{ext,j} = \frac{1}{\Delta L}\int_{(j+1)\Delta L}^{\Delta L} P_{ext,j-1} e^{(\Gamma g_{ext,j}(N_j)-\alpha_{int})z}\,dz = \frac{G_{ext,j}-1}{\ln(G_{ext,j})} P_{ext,j-1} \qquad \textbf{5. 9}$$

$$G_{ext,j} = e^{(\Gamma g_{ext,j}(N_j)-\alpha_{int})\Delta L} \qquad \textbf{5. 10}$$

$$\overline{P}_{int,j} = \frac{1}{\Delta L}\int_{(j-1)\Delta L}^{j\Delta L} P_{int,j-1} e^{(\Gamma g_{int,j}(N_j)-\alpha_{int})z}\,dz = \frac{G_{int,j}-1}{\ln(G_{int,j})} P_{int,j-1} \qquad \textbf{5. 11}$$

$$G_{int,j} = e^{(\Gamma g_{int,j}(N_j)-\alpha_{int})\Delta L} \qquad \textbf{5. 12}$$

Where

- $\overline{P}_{ext,j}$ is the average power of the external signal in the SOA's j[th] section,
- $\overline{P}_{int,j}$ is the average power of the SRL internal lasing signal in the SOA's j[th] section,
- $G_{ext,j}$ is the gain of the external signal in the SOA's j[th] section,
- $G_{int,j}$ is the gain of the internal signal in the SOA's j[th] section,
- ΔL represents the length of a SOA section.

Equations 5.3 to 5.12 provide a simple dynamical model of a co-propagating externally injected SRL. Simulations of these equations using MATLAB allow us to gain insight into the fundamental operations of the SRL. Furthermore, the MATLAB simulations can be used to verify the accuracy of commercial photonic circuit software simulations.

5.3.2.3 Dynamic model, counter-propagation configuration

Since the SOA is a bidirectional device, we can construct two basic SRL configurations: the co-propagation configuration, Figure 5-3, or the counter-propagation configuration, Figure 5-7. In the co-propagation configuration, both external signal and SRL internal lasing signal

enter the SOA from the same facet unlike the counter-propagating configuration where they enter the SOA from opposite facets.

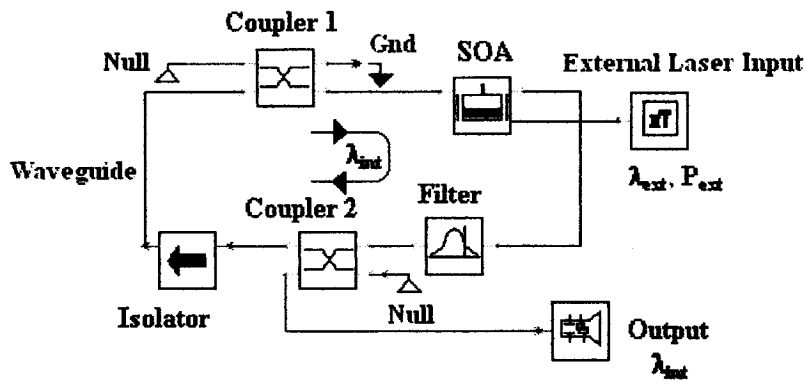

Figure 5-7 Externally injected counter-propagation SRL physical setup.

In order to obtain a dynamical model for the counter-propagating SRL, we need to modify the external signal's (λ_{ext} with power P_{ext}) propagation and average power equations, Equations 5.7 and 5.9 respectively, to reflect the counter-propagation situation. A minus sign is added to Equation 5.7 to indicate the external signal's opposite propagation direction (with respect to the SRL internal lasing signal), yielding Equation 5.13. The integration limits of Equation 5.9 are also changed to reflect the external signal's propagation direction, yielding Equation 5.14. All other equations are identical for the co- and counter-propagating configurations. Figure 5-8 depicts the SOA cross-section in the counter-propagation configuration.

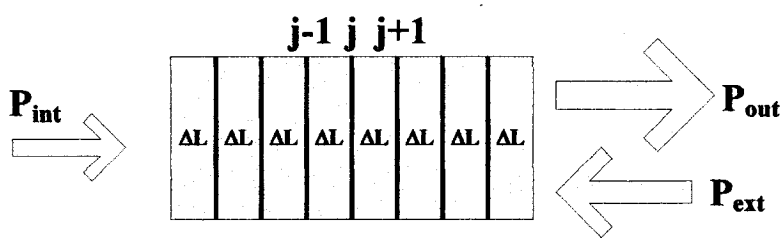

Figure 5-8 SOA cross-section for counter-propagation configuration

$$\frac{\partial P_{ext,j}(z,T)}{\partial z} = -\Gamma(g_{ext,j}(N_j(z,T)) - \alpha_{\text{int}})P_{ext,j}(z,T) \qquad \textbf{5. 13}$$

$$\overline{P}_{ext,j} = \frac{1}{\Delta L}\int_{(j+1)\Delta L}^{\Delta L} P_{ext,j+1} e^{(\Gamma g_{ext,j}(N_j)-\alpha_{\text{int}})z} dz = \frac{G_{ext,j}-1}{\ln(G_{ext,j})} P_{ext,j+1} \qquad \textbf{5. 14}$$

The above model does not incorporate the SOA ASE. To do so, we must include an additional power propagation equation for the ASE and include its contribution to the SOA carrier density distribution in Equation 5.3 [Con'01], [Con'02], and [Con'02a]. Due to difficulties encountered in the MATLAB implementation of the ASE noise process, ASE effects were not included in the MATLAB simulations. In order to generate the solitary SRL lasing signal (generated by the SOA ASE, see section 5.3.1.1), we introduced a small, low power seed signal to 'kick-start' the SRL internal signal oscillation. We will later demonstrate (by comparing the MATLAB and VPI simulations) that the exclusion of the ASE process from the MATLAB simulations did not have a detrimental effect on the accuracy of these simulations.

5.3.2.4 Lotka-Volterra competitive system model

As previously discussed (section 5.3.1.2), the XGM phenomenon is an inherently competitive process. In the SRL, both the external signal, λ_{ext}, and the SRL internal lasing signal λ_{int}, propagate along the SOA competing for the its gain (by competing for its carrier reservoir) in order to receive amplification from the SOA.

We can use the Lotka-Volterra model presented in section 4.2 to model the SRL. The SRL can be modelled as a Winner-Take-All system where there is one external mode (external signal, λ_{ext}) and an internal mode (SRL internal lasing signal, λ_{int}) competing for the gain provided by a nonlinear gain medium (the SOA). In the initial state of the system (provided threshold conditions have been met, section 5.3.2.1), the internal mode, λ_{int}, is oscillating within the gain medium (SOA). The introduction of the external signal λ_{ext} however, creates a competitive situation within the SOA. The external signal consumes the SOA gain and forces the internal mode/signal to cease oscillating. Due to the presence of the filtering

element in the SRL cavity, the external signal cannot also oscillate within the SRL cavity and the system's output is zero.

The Lotka-Volterra coupled differential equations model for a WTA system is restated here for convenience (see section 4.2):

$$\frac{d}{dt}I_j = \alpha_j I_j - \sum_{k=1}^{N} \theta_{jk} I_k I_j, \qquad j = 1,\ldots,N \quad \textbf{5. 15}$$

Where

- I_j and I_k represent the j^{th} and k^{th} competing modes,
- α_j represents the linear gain for the j^{th} competing mode,
- θ_{jk} represents the cross-saturation coefficient for the j^{th} and k^{th} competing modes,
- N represents the number of competing modes in the system.

$$\Theta = \begin{bmatrix} \beta & \theta & \cdots & \cdots & \theta \\ \theta & \beta & & & \vdots \\ \vdots & & \ddots & & \vdots \\ \vdots & & & \ddots & \theta \\ \theta & \cdots & \cdots & \theta & \beta \end{bmatrix} \qquad j,k = 1\ldots N \quad \textbf{5. 16}$$

Where

- β_{jj} represents the self-saturation coefficient for the j^{th} competing mode,
- θ_{jk} represents the cross-saturation coefficient for the j^{th} and k^{th} competing modes.

We can derive the equivalent Lotka-Volterra model for the externally injected SRL by making appropriate variable substitutions to Equations 5.15 and 5.16. From the SRL model (Equations 5.1 to 5.14) we have two competing modes, the external signal/mode I_1 and the signal/internal mode I_2. The linear gain (of the gain medium, i.e. SOA) for these two modes is given by G_{ext} and G_{int} respectively, dropping the j^{th} subscript.

In equation 5.16, β_{11} represent the SOA saturation power in the presence of the external signal/mode only. Similarly, β_{22} represent the SOA saturation power in the presence of the internal signal/mode only. Finally, θ_{12} and θ_{21} represents the SOA saturation power in the presence of the external mode/signal *and* internal mode/signal. Therefore, the Lotka-Volterra model for an externally injected SRL is expressed as:

$$\frac{d}{dt}I_1 = G_{ext}I_1 - (\theta_{11}I_1I_1 + \theta_{12}I_2I_1) \quad \textbf{5.17}$$

$$\frac{d}{dt}I_2 = G_{int}I_2 - (\theta_{21}I_1I_2 + \theta_{22}I_2I_2) \quad \textbf{5.18}$$

With the SRL models developed, we can now illustrate via simulations, some SRL-based all-optical signal processing circuits. We will present simulations of the SRL obtained using a commercial photonic devices simulator, VPIcomponentMaker™: Active Photonics and compare them with MATLAB simulations of Equations 5.1 to 5.14.

5.4 SRL All-Optical applications

The SRL is a very versatile device that can perform a wide variety of applications. SRL-based circuits can be used as all-optical wavelength converters, memory and packet buffering elements, threshold elements and logical gates [Hil'01], [Hil'01a], [Hil'02], [Hil'02], [Hil'04], [Lin'04], [Liu'02], [Liu'03], [Liu'03a], [Xin'04], and [Zha'04]. We perform simulations of SRL wavelength converters using VPIcomponentMaker™: Active Photonics and/or MATLAB simulations of Equations 5.1 to 5.14.

VPIcomponentMaker™: Active Photonics uses an advanced proprietary model for modelling the SOA [VPI'05]. The algorithm is based on the Transmission Line Laser Model (TLLM) [Low'88]. The basic SOA model was roughly outlined in [VPI'05] but the numerical details were hidden. This made it difficult to verify the simulations and made the analysis of erroneous data more challenging (since the governing equations for the model were not readily available). To remedy this situation, a second set of simulations were

carried out in MATLAB for some of the all-optical circuits presented in this work. These simulations were based on the theoretical model (Equations 5.1 to 5.14) presented in section 5.3.2 and were compared with the simulations obtained from VPIcomponentMaker™: Active Photonics.

5.4.1 Simulation parameters

Tables 5-1 and 5-2 outline the active and passive components parameters used in the simulations presented in this work. These parameters were kept the same throughout most simulations to facilitate meaningful comparisons of performance. However, in certain cases, the parameters were altered to achieve correct circuit operation. Whenever this is the case, it will be clearly stated in the following.

Table 5-1 Active components physical parameters

Devise	Parameter	Value	Units
SOA	Chip Length	350.0e-6	m
	Active Region Width	2.5e-6	m
	Active Region Thickness	0.2e-6	m
	Confinement Factor	0.45	
	Left Facet Reflectivity	1.0e-4	
	Right Facet Reflectivity	1.0e-4	
	Fixed Internal Loss	3000	
	Alpha factor	5	
	Linear Material gain coefficient	3.0e-20	m^2
	Linear radiative recombination coeff.	0.00	s^{-1}
	Bimolecular recombination coeff.	1.0e-16	m^3s^{-1}
	Auger recombination coeff.	1.3e-41	m^6s^{-1}
	Nonlinear time constant	100e-15	s
	Initial carrier density	1.0e+24	m^{-3}
	Injection Current	250e-3	A
	Transparency carrier density	1.5e+24	m^{-3}
	Nonlinear gain constant	10e-23	m^3
TX	Emission frequency	193.1e12	Hz
	Emission wavelength	1552.52e-9	m
	Average Power	1e-3	W

Table 5-2 Passive Components physical parameters

Devise	Parameter	Value	Units
BP Filter	Gaussian Order Centre wavelength Centre Frequency Bandwidth	1 1552.52e-9 193.25e12 10e9	 nm Hz m
Coupler 1	Coupling Ratio	0.99	
Coupler 2	Coupling Ratio	0.5	
Isolator	Insertion Loss	1	dB
Waveguide	Delay	1.5625e-12	s

5.4.2 Externally injected SRL as an inverting Wavelength Converter (co-propagating configuration)

As previously mentioned, the externally injected SRL is an inverting wavelength converter. It inverts the information present in the external signal (wavelength λ_{ext}), and converts it to the wavelength of the SRL internal signal, λ_{int}. This is possible in both the co- and counter-propagating configurations of the SRL.

We performed a simulation of a co-propagating SRL wavelength converter in VPIcomponentMaker™: Active Photonics at external signal data rates of 2.5 Gbit/s and 10 Gbit/s. We also performed the same simulations in MATLAB for the 10 Gbit/s. For convenience, the simulation setup schematic is shown in Figure 5-9.

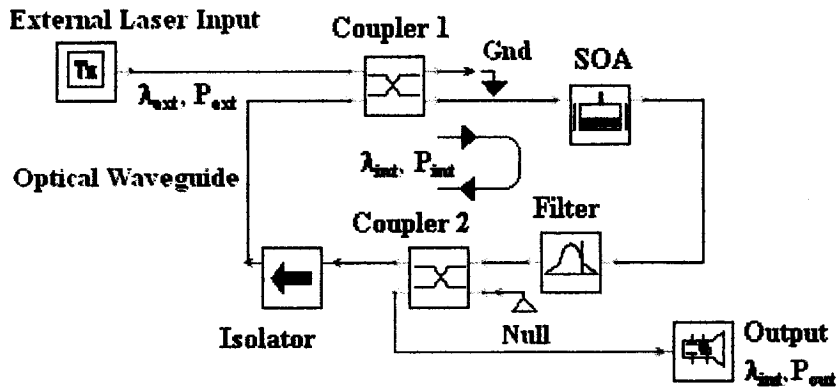

Figure 5-9 Simulation Schematic of Co-propagation SRL wavelength converter.

5.4.2.1 VPIcomponentMaker™: Active Photonics simulations at 2.5 Gbit/s

We used an externally modulated laser transmitter (TX) as the input for the SRL (Figure 5-10). The transmitter uses a Pseudo Random Bit Sequence (PRBS) generator to generate the external signal's bit sequence. The bit sequence is then converted to the Return-to-Zero (RZ) format and its rise time is adjusted to simulate realistic situations. A Mach-Zender Modulator (MZI) is finally used to modulate a CW laser (λ_{ext} = 1552.52 nm, = P_{ext} = 1mW, 0dBm) and the RZ bit sequence to give us the external signal.

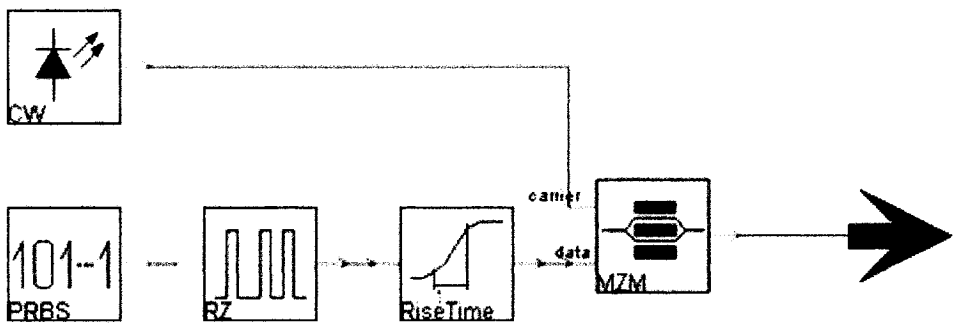

Figure 5-10 RZ external laser transmitter setup in VPIcomponentMaker™: Active Photonics

Figure 5-11 shows the input external signal (λ_{ext} = 1552.52 nm), the SRL output signal (λ_{out} = 1551.32 nm) and the SOA's carrier density distribution. The carrier density distribution cannot be measured experimentally. However, its behaviour is well known theoretically and can be verified by comparing the theoretical carrier density plot with the experimental output

plot, in the sense of our numerical experiment, since the output of the SOA depends on the carrier density distribution within its active region.

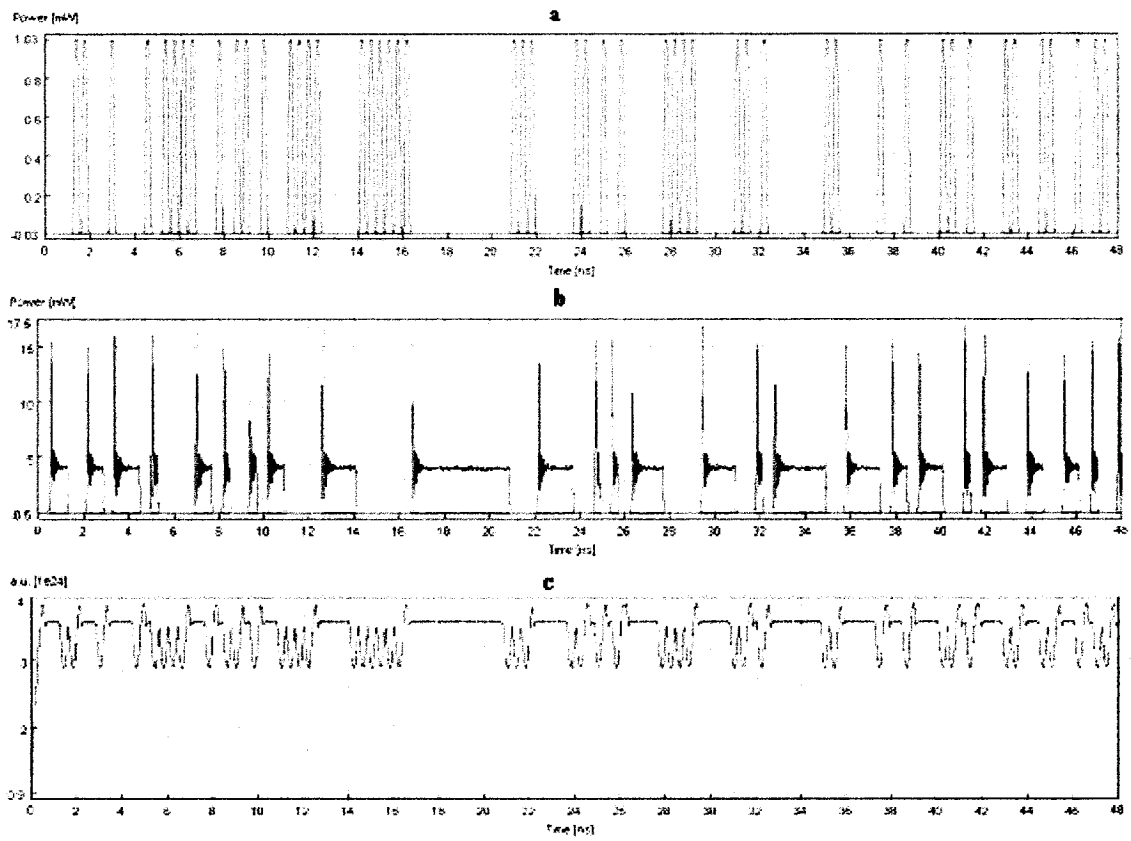

Figure 5-11 a) External input signal, b) SRL output signal, c) and carrier density plots of a co-propagating SRL wavelength converter in VPI.

Figure 5-11 demonstrates the correct operation of the SRL wavelength converter and highlights some of its important advantages. The SRL was able to successfully perform an inverted and amplified wavelength conversion function between two optical signals that are separated by only 1.2 nm in wavelength (spacing of three 50 GHz ITU channels). The external signal (λ_{ext} = 1552.52 nm, P_{ext} = 1mW) is inverted, amplified, and converted to the SRL output signal, (λ_{out} = 1551.32 nm, $P_{out} \approx$ 5mW). Furthermore, the wavelength conversion range, set by the difference between external and output wavelength, is primarily determined by the filter's bandwidth. This provides us with the ability to tune the wavelength range by changing the filter's bandwidth to a desired (narrower or wider) value. Also, since the output wavelength of the SRL is determined by the peak transmission

frequency of the filter in the SRL cavity, it can be used as a tuneable wavelength converter by using a tuneable filter in its cavity instead of a fixed one.

Examining Figure 5-11(a) and Figure 5-11(b) reveals another interesting feature of the SRL. Noticing that the external signal (Figure 5-11(a)) is in RZ format, while the SRL output signal (Figure 5-11(b)) is in NZR format, implies that the SRL is also a RZ-to-NRZ converter. We can deduce the reason behind this phenomenon by computing the SOA's carrier lifetime (τ_c) and comparing it with the 'zero-amplitude' time between any two consecutive 1's in the RZ signal (roughly <<1 ns, Figure 5-11(a)).

The SOA carrier lifetime τ_c ($= \frac{1}{A + BN + CN^2}$) depends on the carrier density (N), the linear radiative recombination coefficient (A), the bimolecular recombination coefficient (B), and the Auger recombination coefficient (C). Assuming an average carrier density of 3.42e+24 (arbitrary units, Figure 5-11(c)), and using the values given in Table 5-1 we obtain a carrier lifetime value of approximately 3ns (τ_c =3ns). Since the SOA carrier lifetime is greater than the 'zero-amplitude' time of between any two consecutive 1's in a RZ signal (<<1ns), the SOA will not have sufficient time to build the corresponding output pulse. More specifically, the SOA carrier density does not have sufficient time to build up in amplitude to produce an output pulse that satisfies the threshold conditions as illustrated in Figure 5-11(c).

The SRL output signal, however, suffers from some distortions. By inspecting Figure 5-11 (a), (b), and (c) we see that an overshoot/spike occurs in the SRL output (Figure 5-11(b)) whenever the external signal (Figure 5-11(a)) is low. We know from semiconductor laser physics that such an overshoot/spike occurs at the onset of laser oscillation (i.e. when the laser is 'turned-on', usually by supplying electrical injection current) [Num'04]. A similar phenomenon occurs in the SRL when it is 'tuned-on' optically, which happens whenever the external signal is low and as a result the SRL has spikes in its output. To get a better understanding of what is happening, we zoom-in on specific time duration in Figure 5-11 (say 10-22ns) as shown in Figure 5-12.

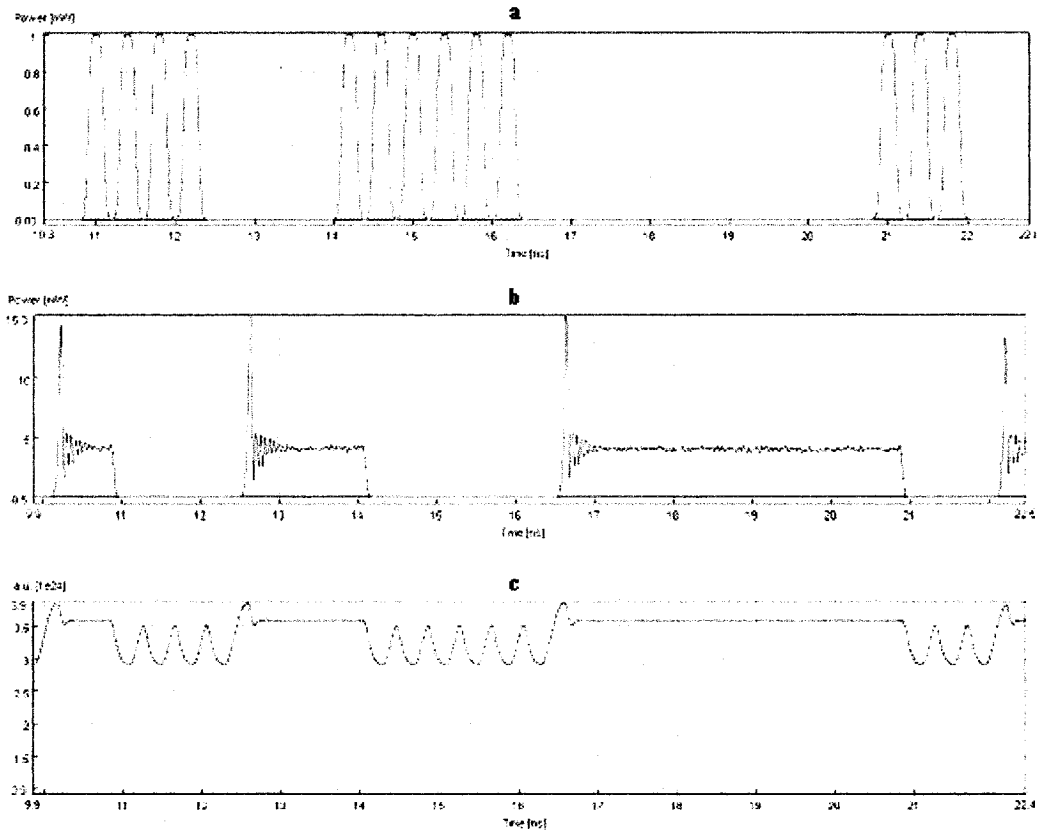

Figure 5-12 External input signal (a), output signal (b) and carrier density (c) plots of a SRL wavelength converter for time range 10-22ns in VPI.

Small variations in the steady-state value of the SRL output signal are present in Figure 5-12 (b) in the form of small oscillations. These oscillations could be the result of a variety of sources, most notably Relaxation Oscillations (RO) and Amplified Spontaneous Emission (ASE) noise, or a combination of both. Relaxation oscillations accompany the initial spike in the SRL or laser output and have a specific frequency, $f_r = \frac{1}{2\pi}\sqrt{\frac{1}{\tau_c \tau_p} \bullet \frac{J}{J_{th} - 1}}$ (where τ_p represents the photon lifetime. determined by the cavity length, J and J_{th} represent the current and threshold current densities respectively).

ASE on the other hand, is a random process and hence any oscillations induced by ASE would be random as well. Therefore, if the oscillations in Figure 5-12 (b) were due to ASE, their periods would be random. If on the other hand, Relaxation oscillations were the cause of these variations, then the oscillation period would be the same for the entire duration of

the output pulse (set by the f_r). Figure 5-13 provides a zoom-in plot of Figure 5-11(b) for the time duration of 12-14 ns.

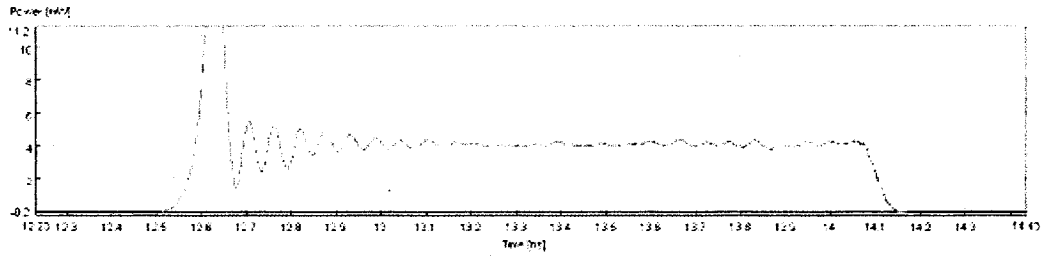

Figure 5-13 SRL output signal for time duration 12-14 ns in VPI.

By inspecting the plot of Figure 5-13, we note that consecutive oscillation peaks occur regularly with a period of approximately 0.07 ns. We can therefore conclude that these oscillations are the result of RO and that the period of RO is approximately 0.07 ns. Furthermore, these oscillations decay exponentially which further confirms that they are indeed relaxation oscillations resulting from turning the SRL 'on' optically.

Figure 5-14 illustrates the same set of simulations for the SRL wavelength converter but with a NRZ transmitter (Figure 5-15) used as the external input signal. Clearly, the two operations are almost identical to one another in terms of performance. This implies that the SRL is data format independent and further enhances its case for deployment in photonic networks.

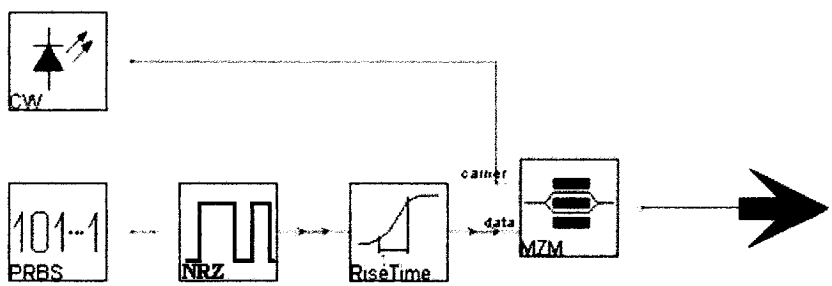

Figure 5-14 NRZ external laser transmitter setup in VPIcomponentMaker™: Active Photonics

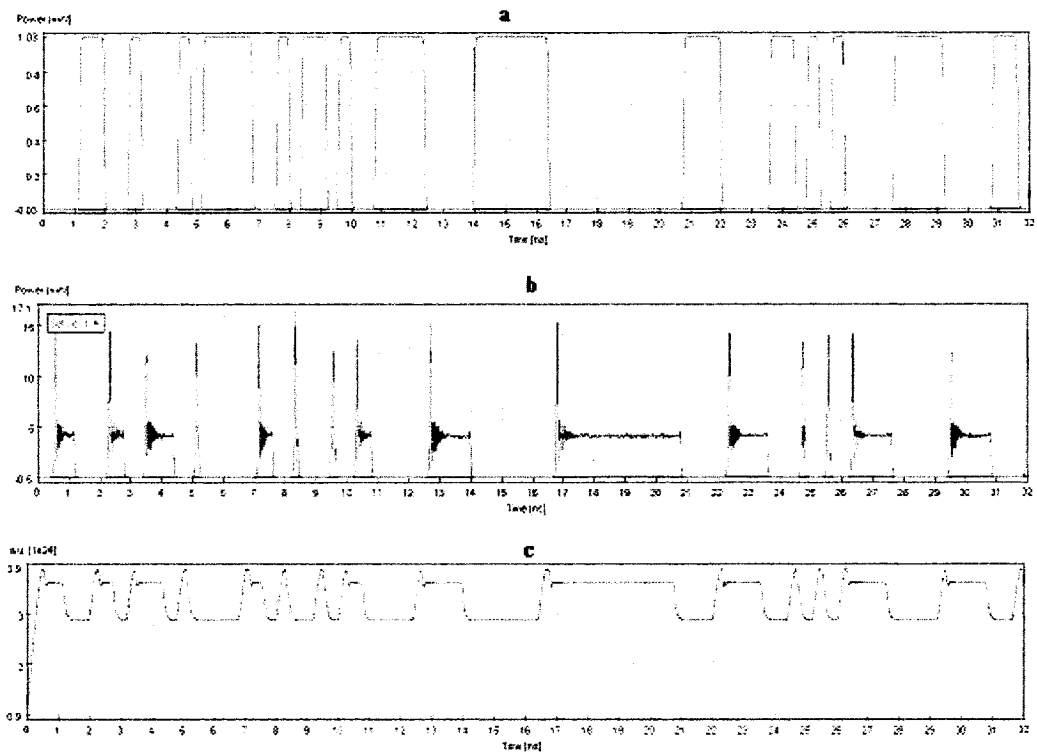

Figure 5-15 External input signal (a), output signal (b) and carrier density (c) plots of a SRL 2.5 Gbit/s NRZ wavelength converter for time range 10-22ns in VPI.

5.4.2.2 VPIcomponentMaker™: Active Photonics simulations 10 Gbit/s

We have also performed simulations of SRL with an externally injected signal at 10 Gbit/s data rate. This was done to demonstrate the viability of SRL as a wavelength converter in current photonic networks operating at 10 Gbit/s rates. Furthermore, these simulations can help us predict the SRL behaviour (and limitations) at even higher data rates of 40 Gbit/s and above.

Fig 5-16 shows the results of simulations of SRL wavelength converter with a 10 Gbit/ NRZ input signal in VPIcomponentMaker™: Active Photonics. The same setup and parameters as for the 2.5 Gbit/s SRL were used.

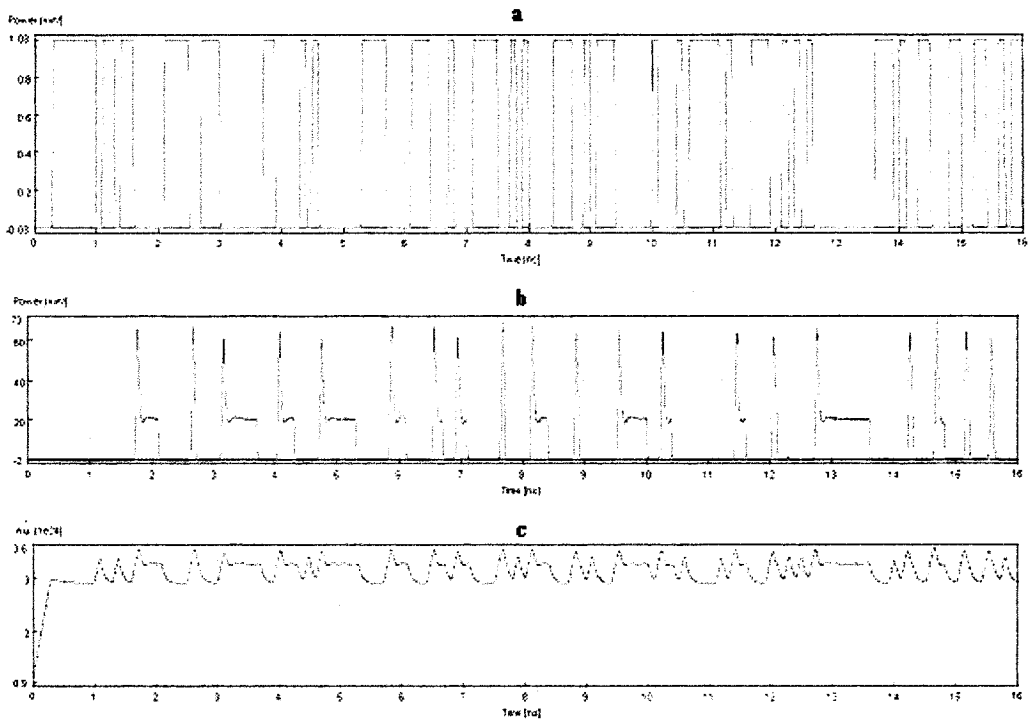

Figure 5-16 (Incorrect) SRL wavelength converter operation with NRZ input at 10 Gbit/s in VPI, external input signal (a), output signal (b) and carrier density (c).

As can be seen, the SRL does not function correctly. For example, the SRL is unable to detect the presence of 0's between the two consecutive sequences of 1's for the time duration 0.5-1.5 ns. As a result, the SRL at 10 Gbit/s (given the parameters used for the 2.5 Gbit/s rate) operation is not error free.

There are two possible reasons for this incorrect behaviour. The duration of the '0' bit (between the consecutive 1's bits) may be shorter than the SRL cavity delay and as a result, the presence of the '0' bit may not be detected by the SRL. A second reason could be that the SRL does not have sufficient time to form the correct output pulse (logical '1') for the corresponding input pulse (logical '0') due to the very short duration of the '0' input bit. This case is very similar to the case in Figure 5-11, where the SRL was not able to respond to the 'zero-amplitude' pulses present between any consecutive RZ pulses.

A possible solution is to decrease the SRL cavity delay and/or increase the SRL gain by increasing the SOA injection current. That way we provide a longer time for the output pulse to build up in amplitude by decreasing SRL delay and increase its build up speed by providing more gain from the SRL. An additional solution could be to reduce the external input power so we are not suppressing the SRL lasing signal far below the SOA threshold and hence the output pulse build up will take shorter time since output pulse will now build up from a higher amplitude. Figure 5-17 shows simulation results for the same SRL but with an input power of 0.5 mW instead of 1mW and cavity delay of 0.78125 ps instead of 1.52625 ps. As can be seen, correct operation at 10 Gbit/s is achieved.

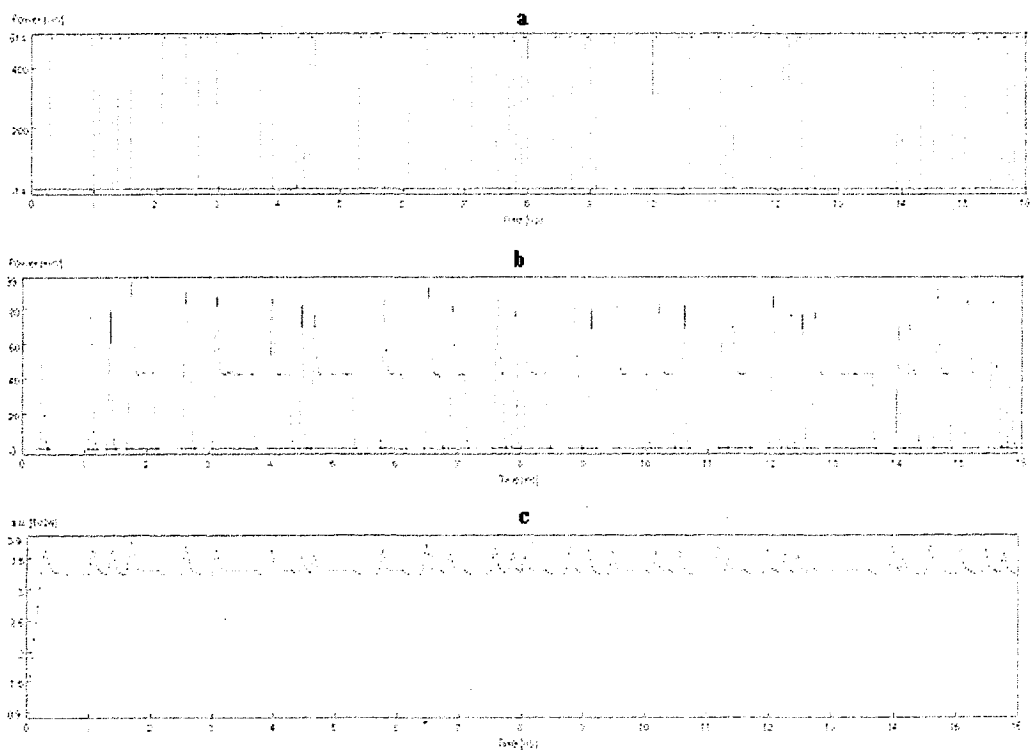

Figure 5-17 Correct operation of SRL at 10 Gbit/s in VPI, external input signal (a), output signal (b) and carrier density (c).

5.4.2.3 MATLAB simulations

Simulations of Equations 5.1 to 5.12 (co-propagating SRL wavelength converter) were carried out in MATLAB. These simulations were used to verify the accuracy of the simulations performed with VPIcomponentMaker™: Active Photonics whose SOA model is proprietary. The SOA model simulated in MATLAB [Fer'05] did not include ASE as previously discussed. Furthermore, the material gain model in [Fer'05] was based on [Con'02] and hence was more accurate than the cubic gain model presented in Equations (3-4) [Lin'04]. Figure 5-18 shows the simulation results for a co-propagating SRL wavelength converter with 10 Gbit/s NRZ external input.

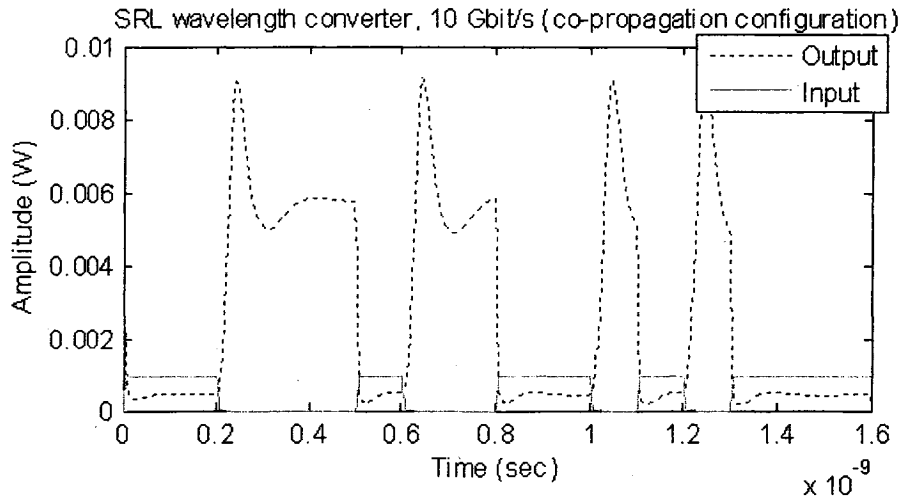

Figure 5-18 10 Gbit/s NRZ SRL wavelength converter simulation in MATLAB

As can be seen from Figure 5-18, the SRL performs error free wavelength conversion with inversion. In addition, there is also an overshoot in the output of the SRL, which confirms the presence of RO in SRL.

5.4.3 SRL as a Wavelength Converter (counter-propagating configuration)

An alternative SRL configuration (counter-propagation) is shown in Figure 5-19. In principle, it does not require the use of a filter since the signals enter the SOA from the opposite side. However, since the SRL already has a filter by default, the counter-

propagating configuration offers no additional advantages over the co-propagating configuration at least in terms of component count.

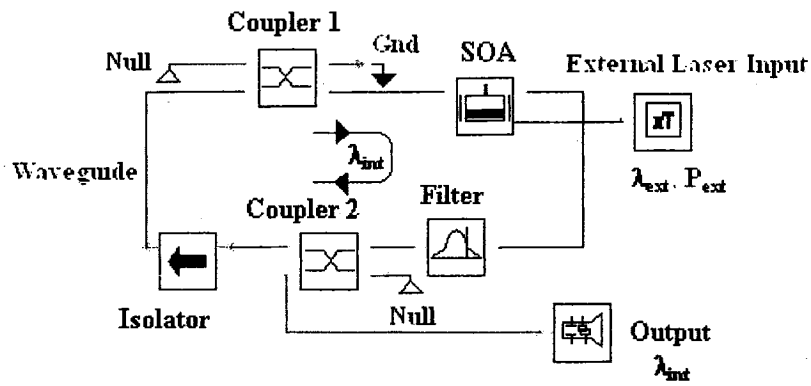

Figure 5-19 Counter-propagating SRL wavelength converter schematic

5.4.3.1 VPI simulations (counter-propagating SRL) 2.5 Gbit/s

Figure 5-20 shows the external input signal (a), the SRL output signal (b), and the SOA carrier density (c) of the SRL. It does not appear to be much difference between the co-propagating and counter-propagating schemes, at least in terms of performance. This could be due to the fact the simulator engine does not completely model all of the effects that might lead to such differences (the counter-propagation configuration offers slightly inferior noise performance compared to co-propagation [Con'02]) or that the SRL itself is indifferent to co or counter propagating external injection.

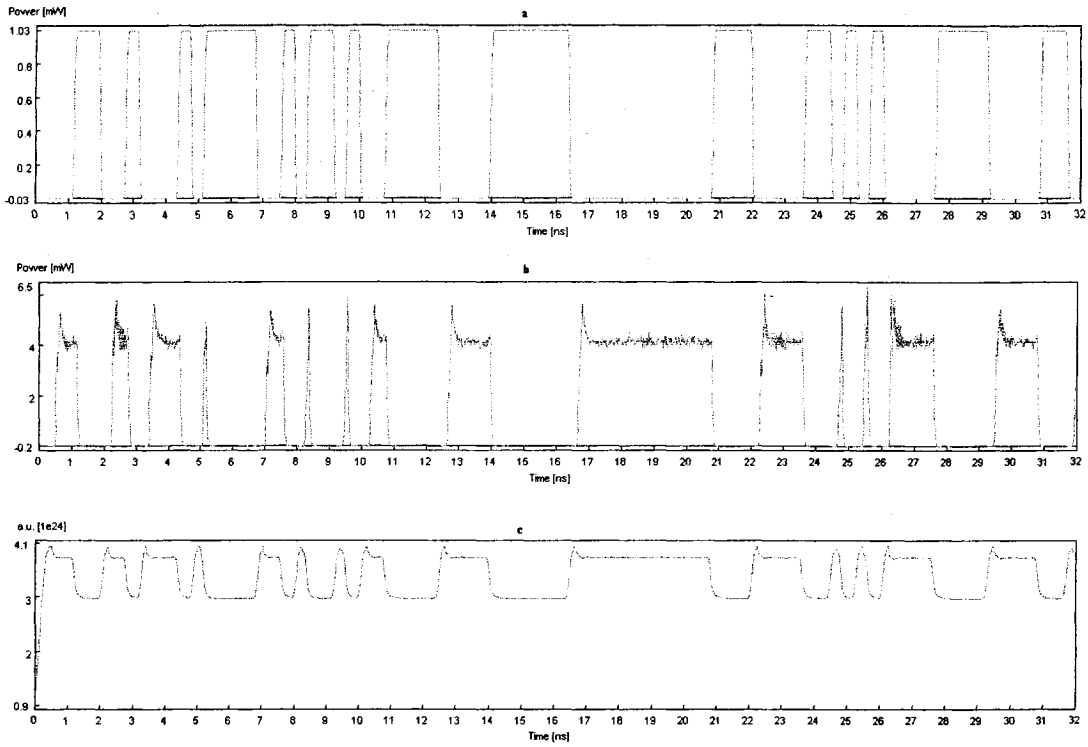

Figure 5-20 SRL counter propagating wavelength converter, 2.5 Gbit/s in VPI.

We again do a zoom in and look at RO in the output of the SRL. Figure 5-21 shows such a plot for time duration of 12-26 ns. Little difference is observed between the co- and counter propagating schemes. In the absence of experimental verification, we conclude that the co- and counter propagating configuration for a SRL wavelength converter are comparable in performance.

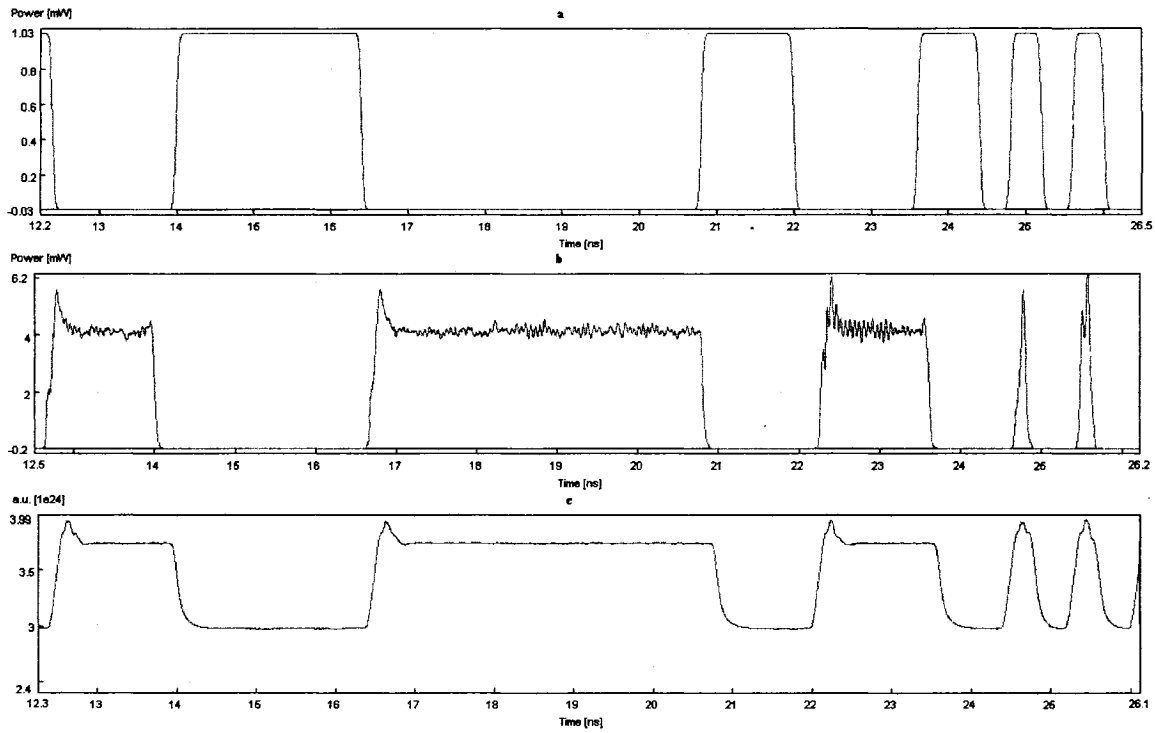

Figure 5-21 SRL wavelength converter output for time duration 12-26 ns.

5.4.3.2 MATLAB simulations SRL counter-propagating 10 Gbit/s

We also performed MATLAB simulations of the counter-propagation SRL configuration. As was previously discussed in section 5.3.2.3, the model for a counter-propagating SRL wavelength converter is given by Equations 5.1 to 5.6, 5.8, and 5.11 to 5.14. The results are shown in Figure 5-22. There is very little difference in performance between the co- and counter- propagating SRLs as predicted by the VPIcomponentMaker™: Active Photonics simulations (Figures 5-13 and 5-22).

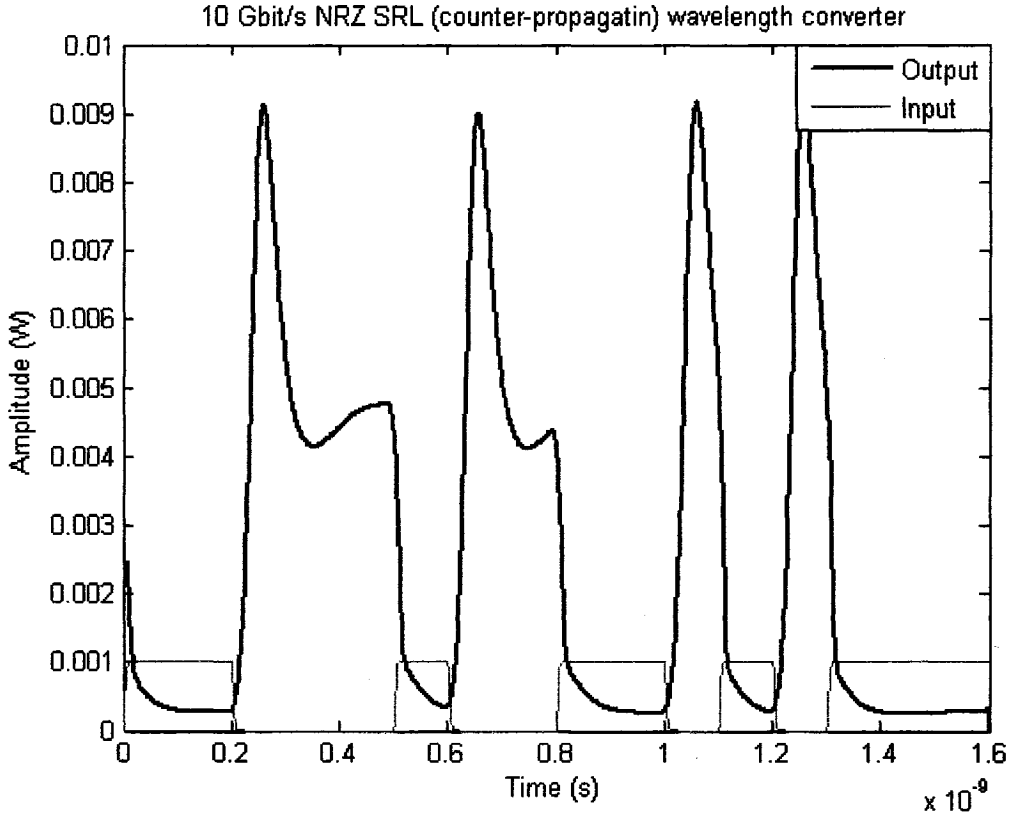

Figure 5-22 10 Gbit/s NRZ counter-propagating wavelength converter simulation in MATLAB.

5.4.4 Cascaded SRL

SRL circuits need to be cascadable if they are to be deployed in photonic networks. This is very important, especially if the SRL is to be used as a building block for all-optical logical gates, the SRL must be able to drive other SRL-based circuits for it to be useful in photonic networks. Figure 5-23 depicts the schematic of two cascaded SRLs.

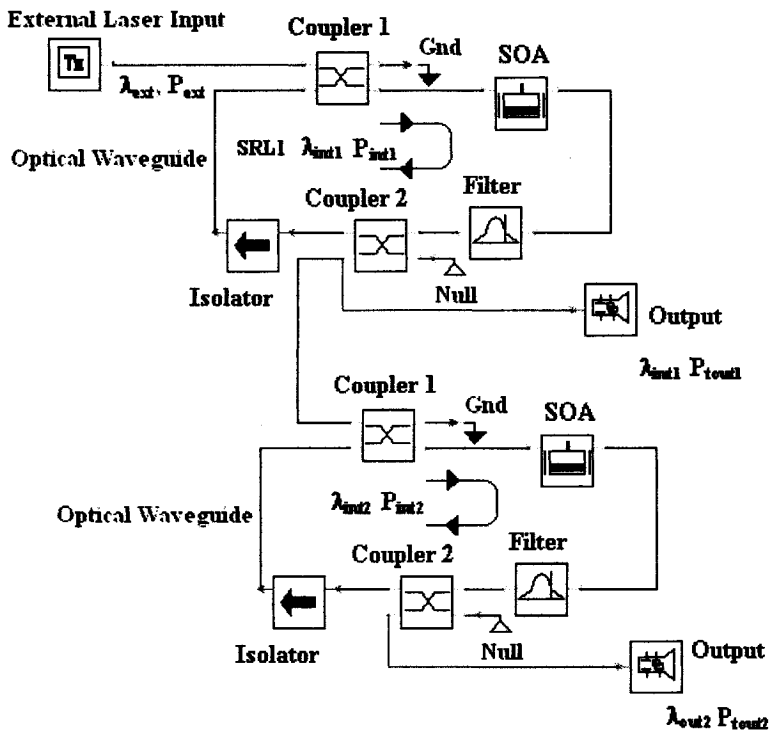

Figure 5-23 Schematic of two-cascaded SRLs

We performed simulations of two-cascaded SRL wavelength converters using VPIcomponentMaker™: Active Photonics Figure 5-24 shows input external signal (a), the output signal of SRL 1(b), and the output signal of SRL 2(c).

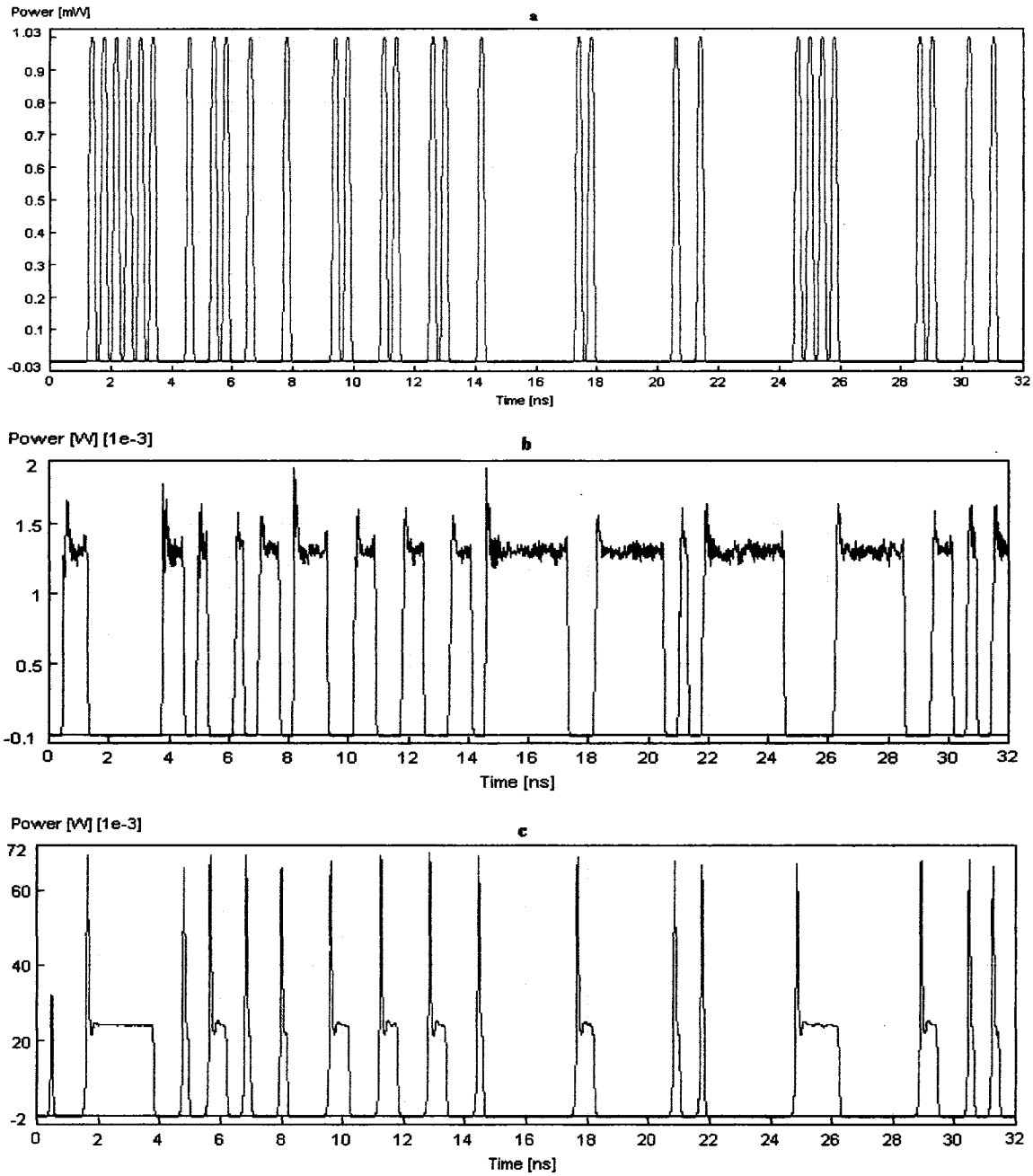

Figure 5-24 External signal (a), SRL 1 output (b), SRL 2 output (c).

From Figure 5-24, we can observe correct operation. SRL 1 inverts and amplifies the external signal (λ_{ext} = 1552.52 nm) and wavelength-converts it to its internal signal wavelength (λ_{int1} = 1551.32 nm). λ_{int1} then serves as the input to SRL 2 (whose filter centre frequency is set at 193.4 THz). Again, SRL 2 inverts, amplifies and wavelength-converts

λ_{int1} to its own output signal, λ_{int2} (1550.12 nm). Note that λ_{int2} and λ_{ext} have the same information but with different wavelengths and powers.

Note that the output of SRL 2 also suffers from overshoots. Furthermore, this overshoot is greater than the overshoot in the output of SRL 1. This is because the input of SRL 2 (λ_{int1}, output of SRL 1) already suffers from an overshoot, unlike the external signal, λ_{ext}, and hence the situation is worsened. Also, note that there are no minimal distortions in the steady-state value of the output of SRL 2 as compared to output of SRL 1. This is because the SOA of SRL 2 is saturated and hence any variations/oscillations that are present in its input of SRL 2 do not have an effect on its response.

Figure 5-25 shows a zoomed plot of the output of SRL 2. Note that the output pulses suffer a single oscillation before quickly settling down to a steady-state value which indicates that the RO decays much faster than the RO in output of SRL 1, again this is due to the fact the SRL 2 is already gain saturated.

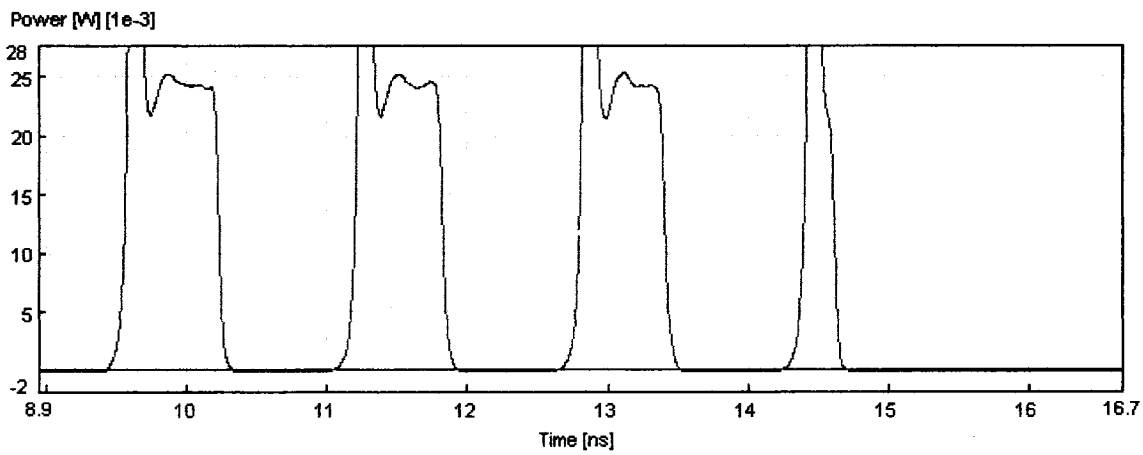

Figure 5-25 SRL 2 output for time duration 9-16 ns.

5.5 Conclusion

The results presented in this chapter clearly demonstrate the viability of competitive optics circuits based on SRL for all optical signal processing. Anderson's competitive optics schemes have been successfully applied to saturated gain media but for much shorter time scales (nanoseconds and picoseconds compared to milliseconds for photorefractive materials). Coupled with the fact that the SRL is a highly compact device, SRL-based all-optical signal processing circuits are well suited for applications in future photonic networks. Only a small number of SRL based applications have been demonstrated in this chapter however, and several questions remain open, such as the suppression of RO.

Chapter 6 Experimental Investigations

6.1 Introduction

Semiconductor Fibre Ring Lasers (SFRL) have been extensively studied experimentally for their many potential applications such as wavelength converters, optical (multistate) memories, optical logic elements, tuneable, multi-wavelength and ultrashort optical pulse sources to name a few [Che'04], [Cho'02], [Hill'01], [Hil'01a], [Hil'02], [Lin'04], [Lu'04], [Pen'92], [Xin'04], [Xu'02], [Xu'03], [Wu'00], [Yao'05], [Zha'04], [Zha'05], [Zha'05a], [Zho'98], [Zoi'00], [Zoi'05]. The operating principle of most SFRL configurations is the mode competition between the possible longitudinal modes supported by the ring cavity (determined by the usual cavity resonance conditions) for the gain of the SOA. The mode (or group of modes) which are able to experience the highest possible gain from the SOA (alternatively, experience the lowest loss from the system) dominate (i.e. win the competition) and suppress the oscillation of the remaining modes. In turn, they become the SFRL's final output (Chapter 5). *We can therefore classify most SFRL configurations as Winner Take All (WTA) competitive systems.*

We often need to control the competition process and its dynamics in a competitive optics system in order to realise useful (all-optical) functions. A simple way to control the competition between the longitudinal modes in the SFRL is to include a filtering element in the ring's cavity. We refer to such a structure as Filter-based SFRL (F-SFRL). The filter provides different losses for all the longitudinal modes of the SFRL. Those longitudinal modes which experience the least loss (i.e. those whose frequencies fall within the filter's transmission bandwidth), become the output of the SFRL. Other longitudinal modes, whose frequencies lie outside of the filter's transmission bandwidth, suffer significant attenuation. As a result, the power of these filtered longitudinal modes is not strong enough to access the carrier reservoir pool of the SOA and therefore they experience no amplification. Thus, they are unable to sustain their oscillation within the SFRL cavity and eventually cease lasing.

Alternatively, we can base the control of the competition process of the longitudinal modes in the SFRL on their State Of Polarization, SOP (as opposed to their intensity levels as is the case in F-SFRL) [Xu'02], [Zho'98]. We refer to this structure as Polarization-based SFRL, P-SFRL.

6.2 Experimental Investigation of Semiconductor Fibre Ring Lasers

One of the main goals of experimental work is to validate the theoretical models developed for a particular system or component by comparing the theoretical simulation results with those obtained experimentally. Therefore, it was natural to attempt to perform experimental validations of some of the SRL structures simulated in Chapter 5. The SRL is an integrated devise however and therefore required specialized photonic-circuit foundries for its construction, something that was not available to us. As a result, we attempted to perform experimental investigations of the bulk cousins of SRL, specifically, the F-SFRL.

Another issue emerged when we attempted to investigate the temporal dynamics of F-SFRL (as to validate the results obtained in Chapter 5). For successful temporal operation of F-SFRL, the frequency of the external input signal must be a near integer multiple of the fundamental frequency of the ring cavity [Lee'03], [Lin'04], [Lu'04], [Pen'92], [Xin'04], [Yao'05], [Zha'04], [Zha'05], [Zha'05a], [Zoi'00], [Zoi'05]. This proved to be a very difficult condition to satisfy in our experimental investigation. The F-SFRL we constructed had a large cavity length, in excess of 30 meters, which made it very sensitive to environmental perturbations. As a result, the value of the fundamental frequency of the ring cavity fluctuated and it was not possible to match the frequency of the external input to that of the fundamental of the ring. As a result, the output pulses of the F-SFRL were significantly distorted and could not be compared with the simulations results (which assume the satisfaction of the frequency matching condition).

The importance of satisfying the frequency matching condition cannot be overstated. A relatively small mismatch (on the order several hundred kHz) between the external input frequency and the fundamental frequency of the ring causes significant distortions to the

output of the F-SFRL [Lee'03]. In practice, we can overcome by the use of Optical Delay Lines (ODLs) which can slightly alter/tune the optical length of the ring cavity until a reasonable frequency match is obtained and by making the ring cavity as small as possible to minimise its sensitivity to environmental perturbations. We were unable to acquire any ODLs however, and as a result, the frequency matching condition remained unsatisfied in our experimental investigation.

We therefore decided to focus the experimental portion of this work on P-SFRL. By studying the spectral properties of P-SFRLs, we can alleviate the need for ODLs and frequency matching techniques and at the same time, still gain significant insight into the gain competition behaviour of SFRL. P-SFRLs typically do not make use of a dedicated narrow bandwidth filter in the ring cavity (as F-SFRLs do) and as a result, more than one longitudinal mode can lase/oscillate within the cavity. As a result, P-SFRLs typically display richer mode competition dynamics that makes them better candidate for experimental investigation of competitive optics systems. We carried out several experiments on different P-SFRL structures at BTI Photonic Systems http://www.btiphotonics.com located at 50 Northside Road, Ottawa.

6.3 Polarization-based Semiconductor Fibre Ring Laser Experiment

P-SFRL typically does not employ a dedicated filter in their cavity to determine their output wavelength(s). Instead, P-SFRL structures rely on polarization-dependant gain/loss mechanisms that exist in the SFRL [Xu'02], [Zho'98]. P-SFRL can be used as widely tuneable sources with narrow linewidth [Zho'98] and can exhibit optical bistability through the gain saturation competitive mechanism in SOA [Xu'02]. Furthermore, investigation of P-SFRL structures allows us to gain greater insight into the competitive optics phenomena in SOA since the absence of the filter gives rise to many more possible modes that can oscillate within the SFRL cavity (compared to F-SFRL). Figure 6-1 shows a typical setup of a P-SFRL.

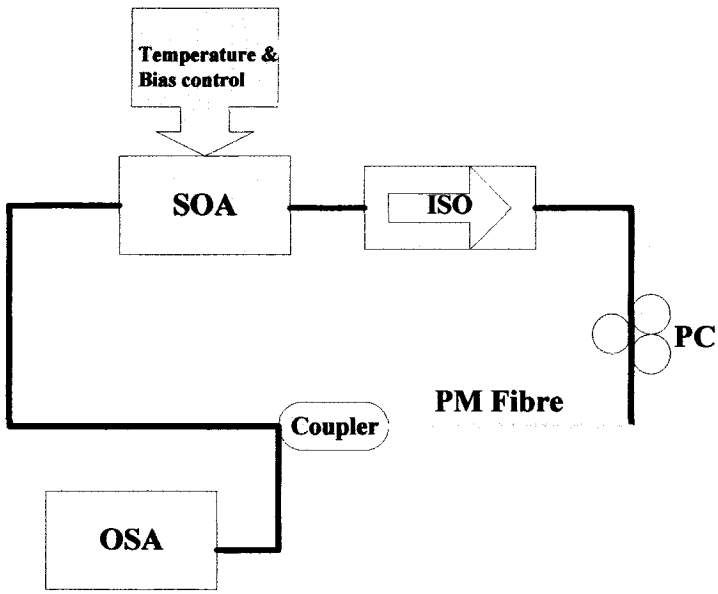

Figure 6-1 Typical experimental setup of a P-SFRL. ISO: Isolator.

Several polarization-dependant gain/loss mechanisms exist in P-SFRL that serve as competitive wavelength selection mechanism including: 1) Optical fibre's birefringence (more pronounced in PM fibre compared to standard SM fibre), 2) Polarization Controllers (PC), 3) PDG of the gain medium, SOA, and 4) Polarization Dependant Loss (PDL) of passive components. These mechanisms serve to favour some of the cavity's longitudinal modes over others. In addition to the usual threshold and ring cavity resonance conditions, the longitudinal modes or wavelengths that can repeat their polarization state at the input of both the SOA and PC after one round trip while also experiencing the lowest overall loss in the cavity represent the final output of the P-SFRL. In essence, these wavelengths win the competition for the SOA gain and suppress the oscillation of all other wavelengths in the cavity. We carried out several experiments to determine the effect of the aforementioned competitive wavelength selection mechanisms on the output of the SFRL.

The above discussion helps illustrate the relationship between P-SFRL and F-SFRL and competitive optics in general. Both of these structures rely on the interplay of several competitive mechanisms to determine their final state (i.e. their output). As a result, we can classify both the P-SFRL and F-SFRL as competitive optics structures or systems.

The active element in the SFRL is the SOA and it greatly influences the overall properties of SFRL. We performed several characterizations of the SOA (i.e. not in a ring configuration) to help in the design of SFRL. Initially, we wanted to build a SFRL that would lase in the C-band, i.e. its output wavelength(s) would lie in the 1530-1565 nm range. We refer to such a SFRL as a C-band SFRL. This dictated our choice for the SOA in the SFRL, and we chose to use a C-band optimized SOA, referred to thereafter as C-SOA, purchased by BTI from Kamelian (now Amphotonix Ltd, http://www.kamelian.com) for use as the active element in the SFRL. We describe its optical characterization next.

6.3.1 C-SOA Characterization

The operation of the SFRL is highly dependant on the properties of the SOA used as the active gain media. In particular, the SOA's gain (wavelength and polarization dependant) influences the SFRL steady-state operation (i.e. the lasing threshold of the SFRL). Other parameters of importance include: 1) the SOA output saturation power, 2) SOA carrier lifetime (which influences the dynamic operation of the SFRL), and 3) the SOA noise figure (which places a limit on how many SFRL can be cascaded together). The C-SOA used was manufactured by Kamelian with integrated isolators and soldered to an evaluation board that controlled its temperature and bias current. The SOA temperature was kept constant at 20 °C.

6.3.1.1 ASE Spectrum

A usual first step in SOA characterization is to determine the ASE spectrum of the SOA under different bias currents. The ASE spectrum gives us a picture of the SOA gain peak and its bandwidth. Since the C-SOA had integrated isolators, only the co-propagating ASE spectrum could be determined. Furthermore, all other SFRL setups that used the C-SOA were carried out in the co-propagating configuration. The experimental setup for determining the co-propagating ASE spectrum of the C-SOA is relatively simple and is shown in Figure 6-2. The ASE spectrum, for different bias currents, is given in Figure 6-3.

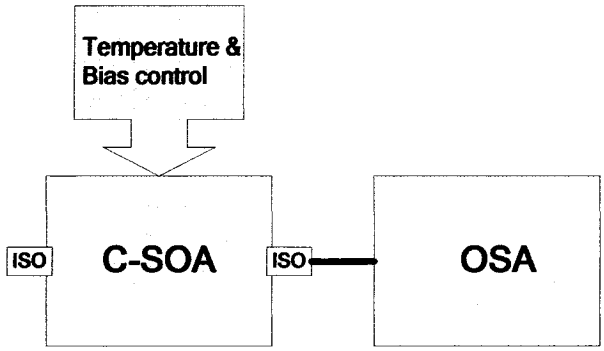

Figure 6-2 Co-propagating ASE experimental spectrum setup for C-SOA. C-SOA: C-band Semiconductor Optical Amplifier with integrated C-band isolators, OSA: Optical Spectrum Analyzer.

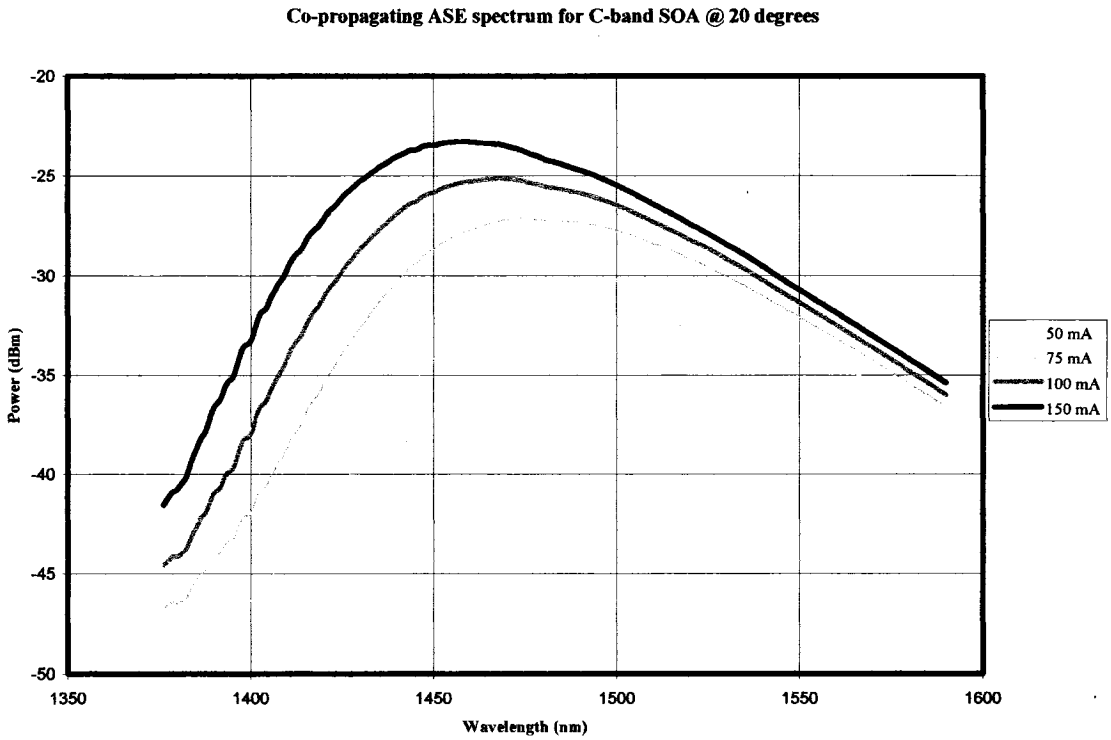

Figure 6-3 Measured Co-propagating ASE spectrum for C-SOA.

Table 6-1 gives the C-SOA gain peak wavelengths and their corresponding power levels for several different bias levels. In order to provide maximum output power, the C-SOA gain peak was shifted by design to lower wavelengths and lies in the S-band (1460-1530 nm) [Kam'03]. The ASE spectrum shows that changing the bias current level changes the gain peak wavelength of the C-SOA and its power.

Bias Current (mA)	Peak Wavelength (nm)	Power (dBm)
50	1494.291	-30.18
75	1473.522	-27.14
100	1468.383	-25.14
150	1458.106	-23.32

Table 6-1 C-SOA peak wavelength and power for different bias currents @ 20 ° C.

6.3.1.2 *SOA gain*

Since the SOA gain is wavelength dependant, it should be characterized for each appropriate wavelength of operation. We decided to characterize the C-SOA gain for 1550 and 1555 nm wavelengths. The experimental setup for measuring the C-SOA gain is shown in Figure 6-4. Figures 6-5 through 6-9 show various measured C-SOA gain-related parameters for both 1550 and 1555 nm CW input signals.

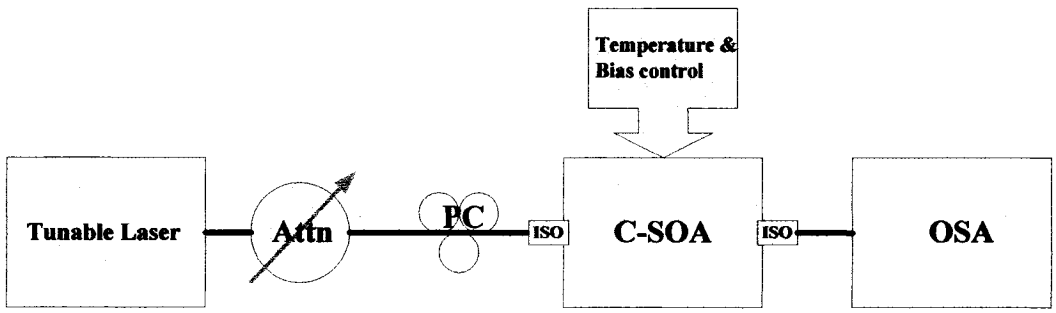

Figure 6-4 Experimental setup for measuring C-SOA polarization dependant gain (PDG). Attn: Digital Optical Attenuator, PC: Polarization Controller.

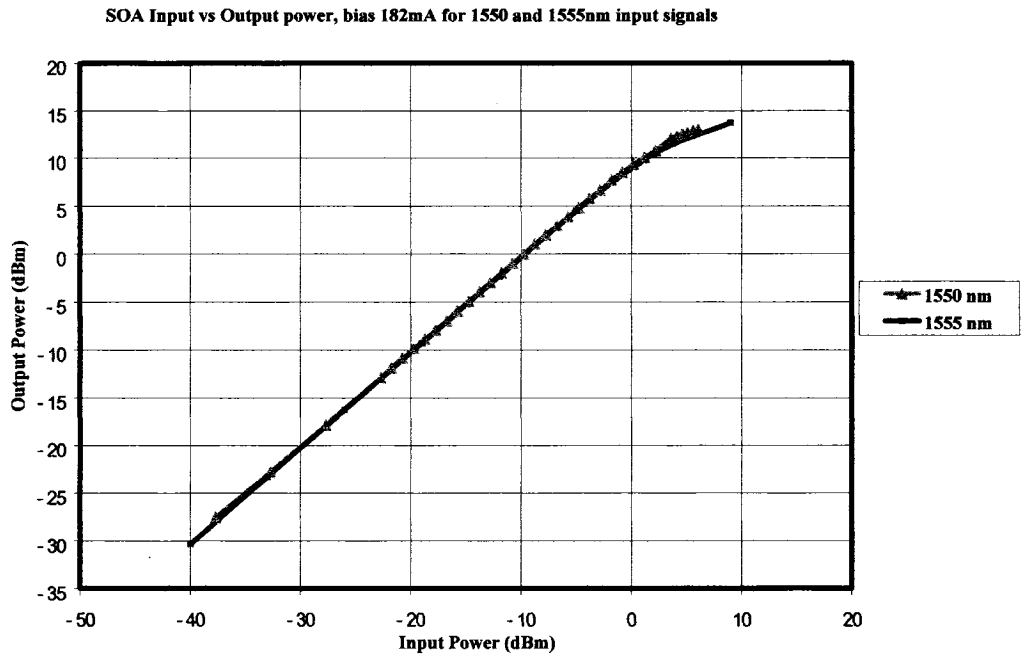

Figure 6-5 C-SOA output vs. input power for 1550 and 1555 nm CW signals at 182 mA bias.

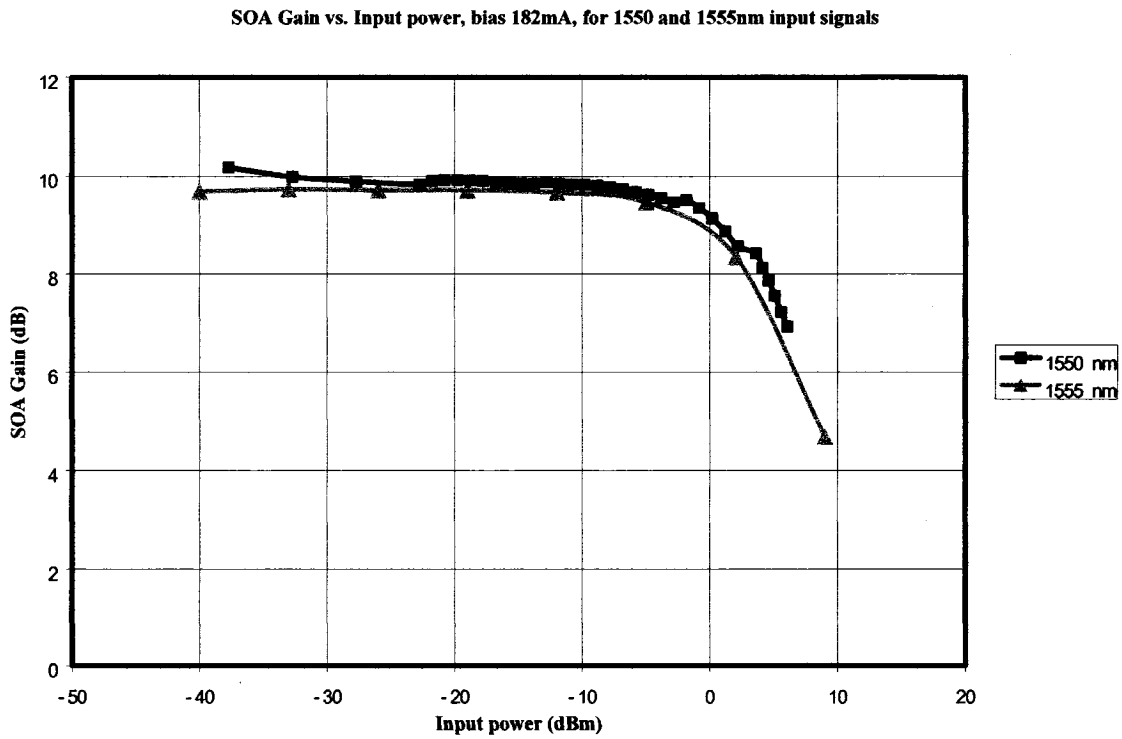

Figure 6-6 C-SOA Gain vs. input power for 1550 and 1555 nm signals at 182 mA bias.

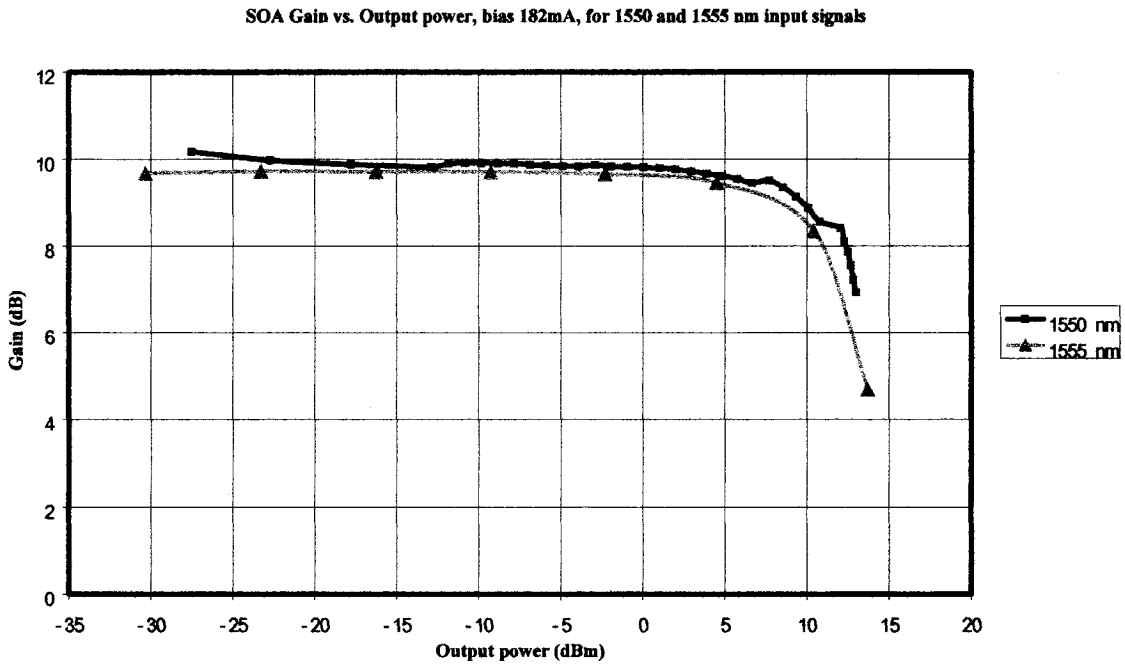

Figure 6-7 C-SOA Gain vs. output power for 1550 and 1555 nm signals at 182 mA bias.

Figures 6-5 to 6-7 show that C-SOA's gain for 1550 nm wavelength is higher than that for 1555 nm wavelength. On average, the 1550 nm signal has 0.3 dB more gain than the 1555 nm. This result is also evident from the C-SOA's ASE spectrum (Figure 6-3). The C-SOA's gain is polarization-dependant however, and such dependence can be large enough to affect the proper design of the SFRL. The experimental setup of Figure 6-4 was used to measure the C-SOA PDG for CW 1550 and 1555 nm wavelengths. We used the PC to change the polarization of the input signals and the OSA recorded the maximum and minimum output powers. Figures 6-8 and 6-9 show the C-SOA PDG for the 1550 and 1555 nm wavelengths respectively. On average, the C-SOA has a 0.7 dB PDG for 1550 and 1555 nm wavelengths.

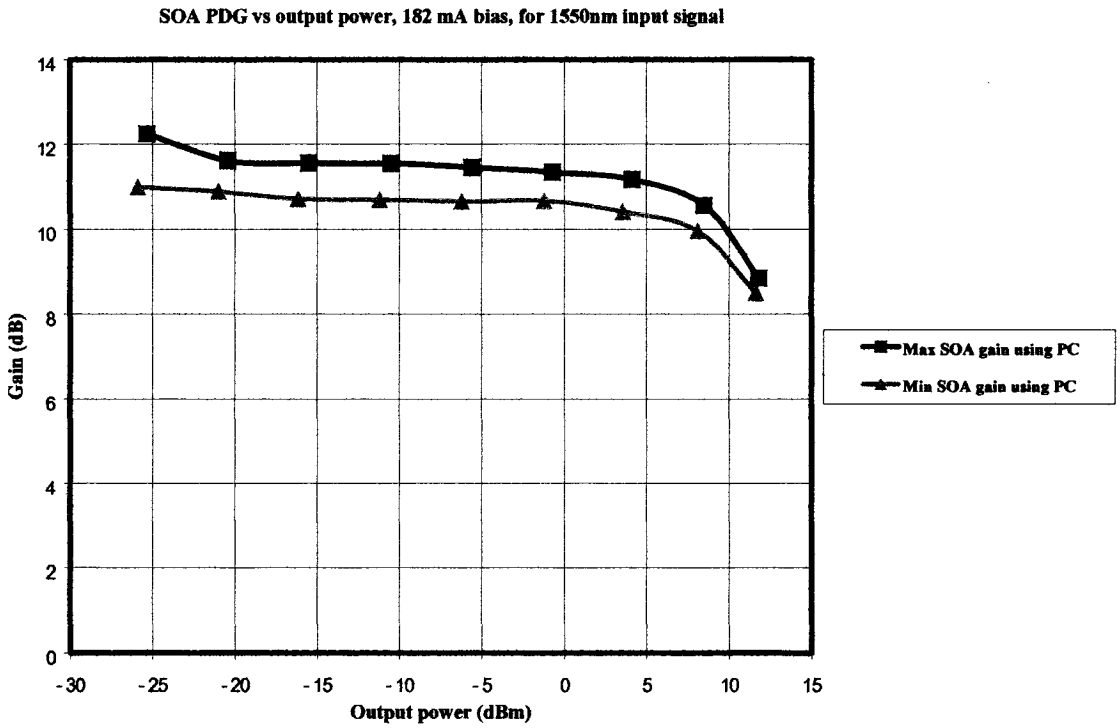

Figure 6-8 C-SOA PDG for CW 1550 nm signal.

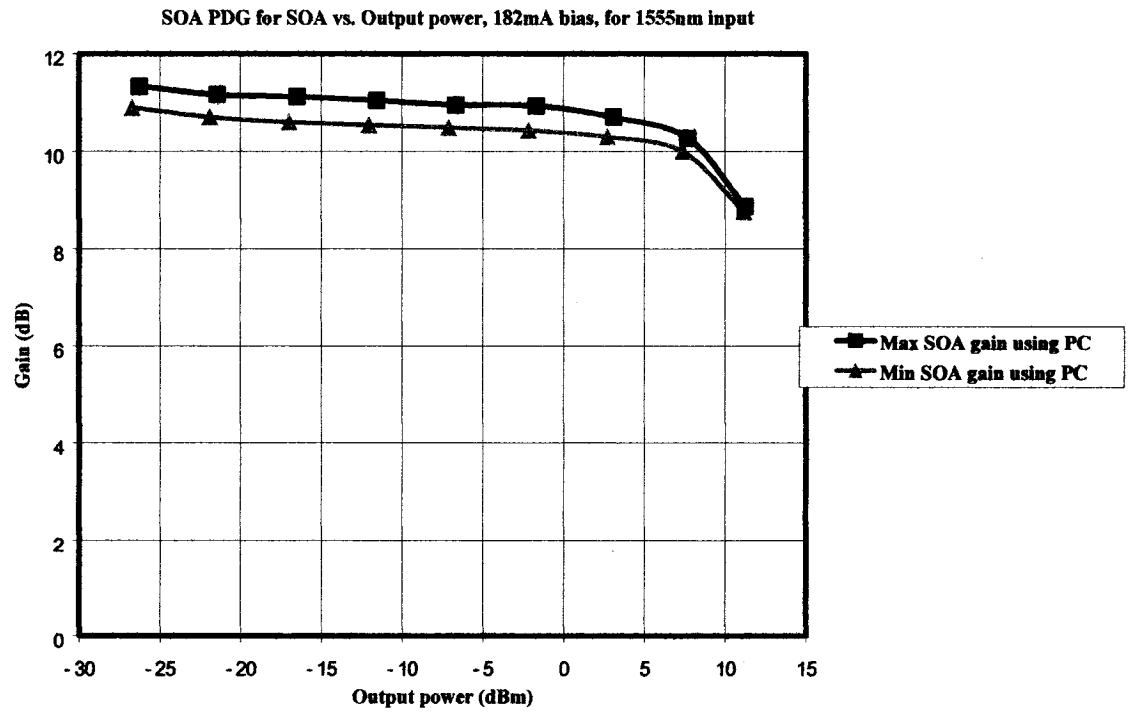

Figure 6-9 C-SOA PDG for CW 1555 nm signal.

6.3.2 C-band P-SFRL experiment

The first series of experiments utilised the Kamelian C-SOA presented in 6.2.1. We investigated two different P-SFRL setups: the setup of figure 6-10 used an all Single Mode (SM) fibre cavity while that shown in 6-12 utilised a 1 m long PM fibre in addition to SM fibre to form the ring cavity. Since the C-SOA had integrated isolators, there was no need to include an external isolator in the SFRL cavity. The output spectrum (superimposed) of the two setups is given in Figure 6-11.

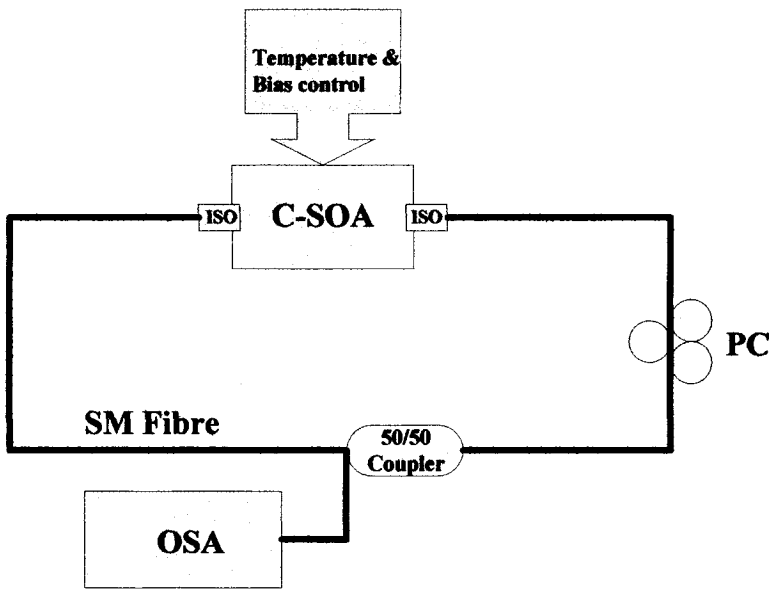

Figure 6-10 Experimental setup of C-band P-SFRL with the All SM fibre cavity. C-SOA: C-band SOA, ISO: Integrated C-band Isolators.

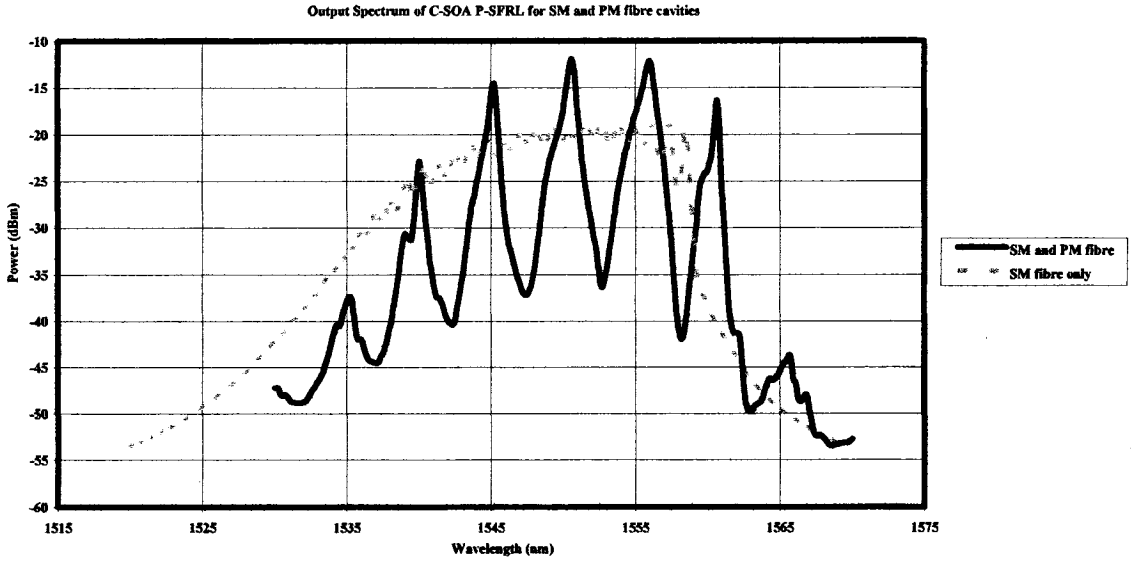

Figure 6-11 Output Spectrum of C-band P-SFRL. Grey curve represents setup in Figure 6-10 (All SM fibre cavity). Black curve is spectrum of setup in Figure 6-12 (SM + PM fibre cavity).

The spectra in Figure 6-11 show multiwavelength laser operation in the C-band, approximately between 1535 and 1565 nm. However, the spectrum of the all SM fibre C-band P-SFRL (grey curve) shows very broad linewidth compared to the C-band P-SFRL that uses a 1 m long PM fibre (black curve). The SM fibre does not maintain the polarization of the light travelling through it unlike the PM fibre. As a result, the all SM C-band P-SFRL has a much weaker polarization-dependant wavelength selection mechanism and its lasing wavelengths linewidths becomes very broad. In fact, it is actually very difficult to distinguish the individual lasing wavelengths and their linewidths actually merge to make them almost undistinguishable from each other for the all SM C-band P-SFRL (grey curve). Figure 6-11 highlights the important role of the PM fibre in ensuring that the oscillating modes in the SFRL cavity will experience different gains/losses based on their polarization states, this also helps with the reduction of their linewidths. Similar results were presented in [Zho'98].

The inclusion of the PM fibre in the ring cavity actually forms a Lyot Filter [Lee'04], [Ple'04], [Zho'02]. Such a filter has a comb like transmission spectrum with regularly spaced peaks. The spacing of these transmission peaks $\Delta\lambda$ is given by:

$$\Delta\lambda = \frac{\lambda^2}{B_{PM} L_{PM}} \qquad \textbf{6. 19}$$

Where

- $\Delta\lambda$ is the comb filter spacing,
- B_{PM} is the beat length of the PM fibre, ~ $3\text{x}10^{-4}$ at 1550 nm,
- L_{PM} is the length of the PM fibre.

For the 1m PM fibre used in setup 6-12, and assuming lasing in C-band and taking the 1550 nm wavelength as a reference, the comb spacing of a 1m PM Lyot filter is approximately 8.008 nm. All further experiments were carried out with the 1m PM fibre in the SFRL cavity setup shown in Figure 6-12 below.

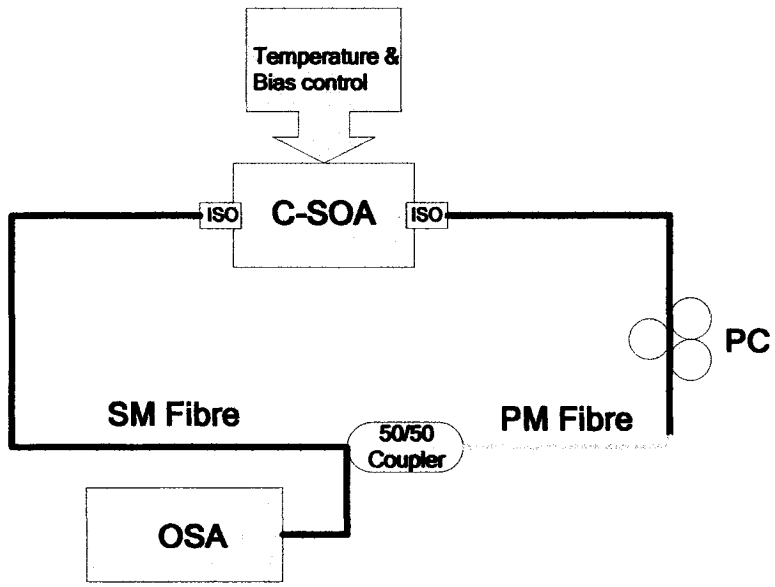

Figure 6-12 Experimental setup of C-band P-SFRL with the SM and PM fibres. C-SOA is designed for C-band operation, ISO: Integrated C-band Isolators.

Figure 6-13 shows the output power vs. bias current for the C-band P-SFRL. The threshold of our laser is approximately 30 mA and its output power is approximately 9 dBm at 250 mA bias.

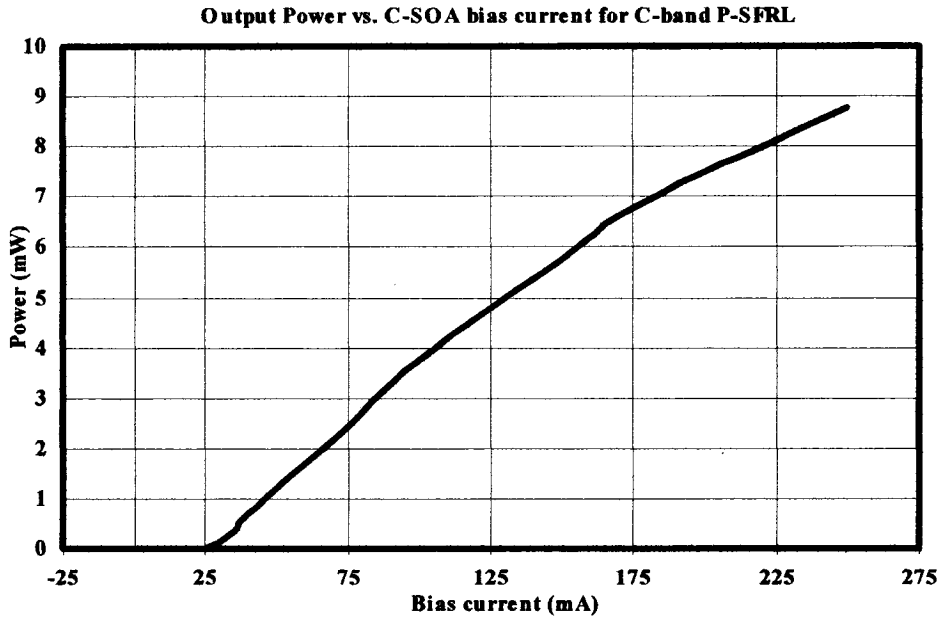

Figure 6-13 Output power vs. C-SOA bias current for C-band P-SFRL.

We adjusted the PC to observe the effect of the C-SOA's PDG on the output spectrum of the C-band P-SFRL. As previously stated in section 6.2.1, the C-SOA had a PDG of approximately 0.6 dB in the C-band. Figure 6-14 shows the output spectrum of the C-band P-SFRL for two different and arbitrary PC settings.

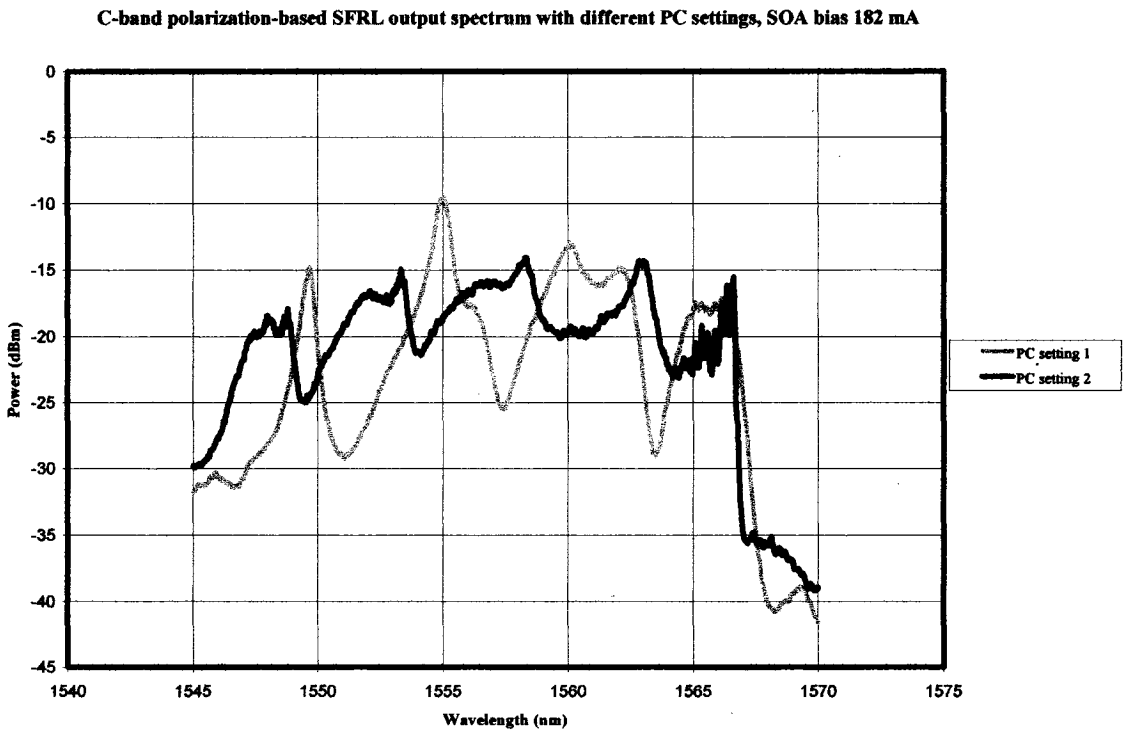

Figure 6-14 Output Spectrum of C-band P-SFRL for two different PC settings.

Figure 6-14 illustrates the role the C-SOA's PDG as a competitive wavelength-dependant selection mechanism. It is important to note however, the relatively large linewidth of the lasing wavelengths (irrespective of which PC setting is used). This is primarily due to the low PDG gain of the C-SOA. This is similar to results reported in [Zho'98]. If we desire a narrower linewidth, we need to use a SOA with a high PDG. Such high PDG serves as an additional wavelength-dependant gain/loss mechanism [Zho'98].

6.3.3 S-band P-SFRL experiment

A SOA available from Kamelian for S-band operation (1460 nm – 1530 nm) was used for the next series of experiments. It had a high PDG of approximately 1.5-2 dB in the S-band. Its PDG in the C-band was approximately 0.6 dB. Figure 6-15 shows the experimental setup for the S-band P-SFRL. The S-band SOA, referred to thereafter as S-SOA, had no integrated isolators and as a result we used an external isolator in the cavity. Figure 6-16 shows the ASE spectrum for the S-SOA under different bias current levels.

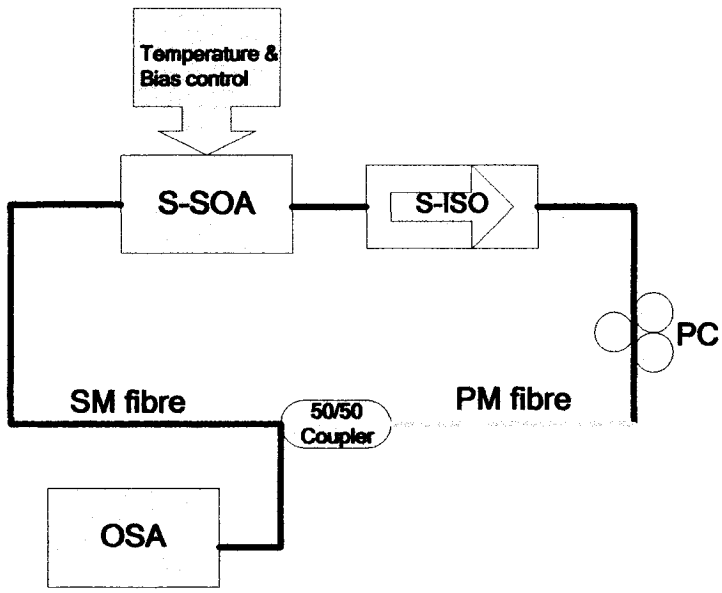

Figure 6-15 Experimental setup for S-band P-SFRL. S-SOA is designed for S-band operation, S-ISO: S-band isolator.

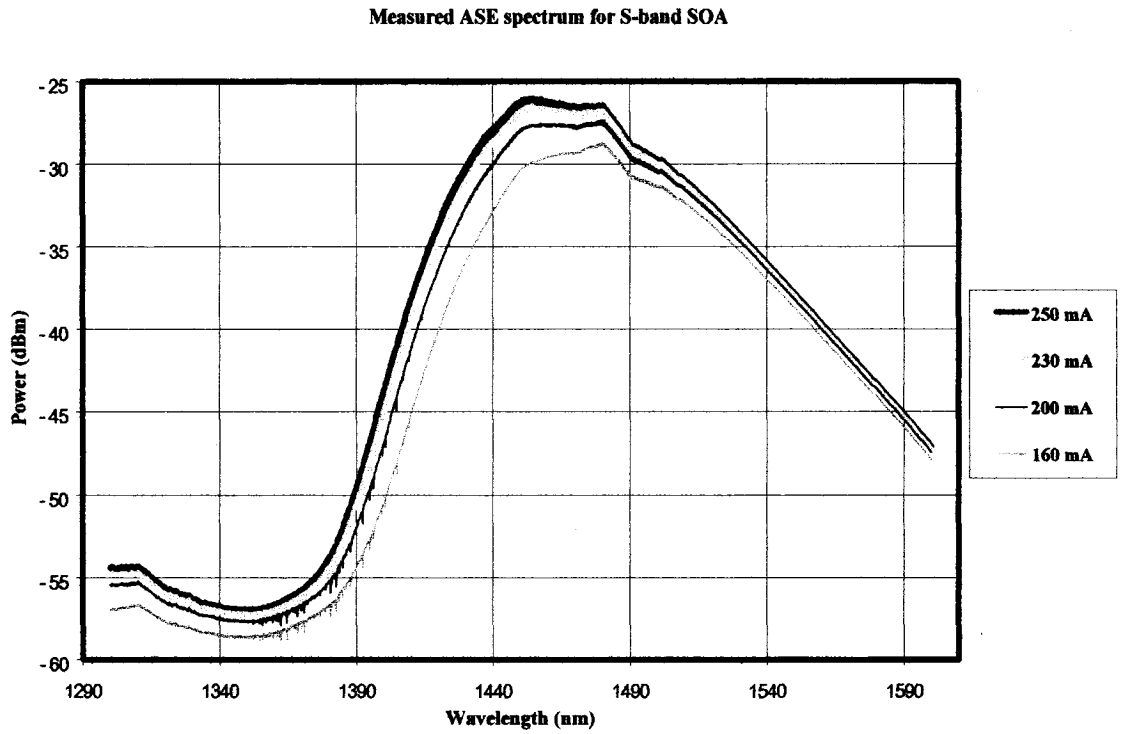

Figure 6-16 Measured ASE spectrum for S-SOA.

The S-SOA is optimized for operation (i.e. amplification) in the S-band. This can be deduced from its ASE spectrum (Figure 6-16) which also shows that the ASE power is highest in the 1440–1490 nm range (compare with ASE power produced in the C-band, 1535-1565 nm). As a result, one would expect a P-SFRL that uses the S-SOA as the gain medium (Figure 6-16) to operate or lase in the S-band, most likely in the range with highest ASE power, namely 1440-1490 nm. This can also be explained from the competitive optics point of view, the longitudinal modes of the P-SFRL that happen to lie in the 1440-1490 nm range have the highest initial powers compared to other longitudinal modes. Viewing the SFRL (and its variant, the P-SFRL) as a Winner-Take-All competitive optics system (sections 4.2.1 and 6.1), we would expect that the longitudinal modes with the highest initial powers (those lying in the 1440-1490 nm) would win the competition for the S-SOA gain and suppress the lasing of other longitudinal modes and become the output of the P-SFRL.

Figure 6-17 however, shows the output spectrum of the P-SFRL setup of Figure 6-15. Clearly, we have multiwavelength operation that is similar to that of the C-band P-SFRL setup of Figure 6-12. I.e. even though we used a S-SOA as the gain medium, our P-SFRL setup still lases in the C-band range, contrary to the earlier prediction of S-band lasing.

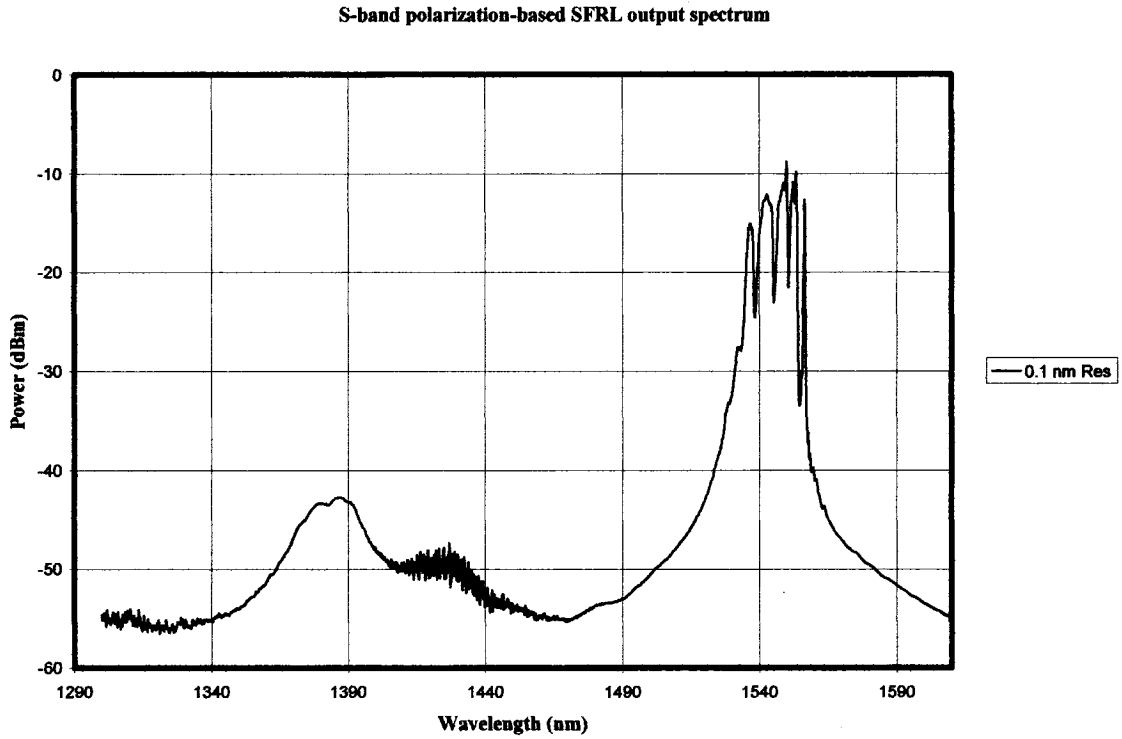

Figure 6-17 Output Spectrum of S-band polarization-based SFRL in Figure 6-15

This result, is in fact, still *consistent* with the theory of the P-SFRL as a WTA competitive optics structure. The analysis given in the last paragraph does not consider *all* possible competitive mechanisms that occur simultaneously in the P-SFRL and influence its output state.

The ASE curve for the S-SOA (Figure 6-16) shows that it is capable of producing ASE in the C-band and therefore produce C-band wavelength/longitudinal modes in the SFRL. Furthermore, the fibre used in the experimental setup (especially the SM fibre) has lower attenuation in the C-band range compared to the S-band. The S-band isolator used had an operating wavelength of 1460-1580 nm and therefore allowed both S and C-band signals to

pass through. All of these factors combined to produce a system (the SFRLs setups described so far, using either S or C-SOAs) that has a *natural tendency to favour lasing in the C-band* since its these longitudinal modes/wavelengths that experience *the lowest loss possible in the SFRL* and as a result still win the overall competition for the SOA gain and suppress the lasing of other wavelengths/longitudinal modes (such as those in the S-band). Therefore, even though the S-SOA produces S-band longitudinal modes that have higher powers than C-band longitudinal modes, the other aforementioned factors in the P-SFRL system present the C-band longitudinal modes with a lower overall loss. Therefore, the C-band longitudinal modes become the output of the P-SFRL system. This is also consistent with viewing the P-SFRL as a WTA competitive system.

We also obtain similar results if we replace the external S-band isolator in figure 6-15 with a C-band isolator (which has an operating range of 1535-1560 nm). This is also expected since the C-band isolator is optimized for C-band wavelengths and therefore the P-SFRL still lases in the C-band. Figure 6-18 shows the insertion loss of the C and S-band isolators used in the experiments.

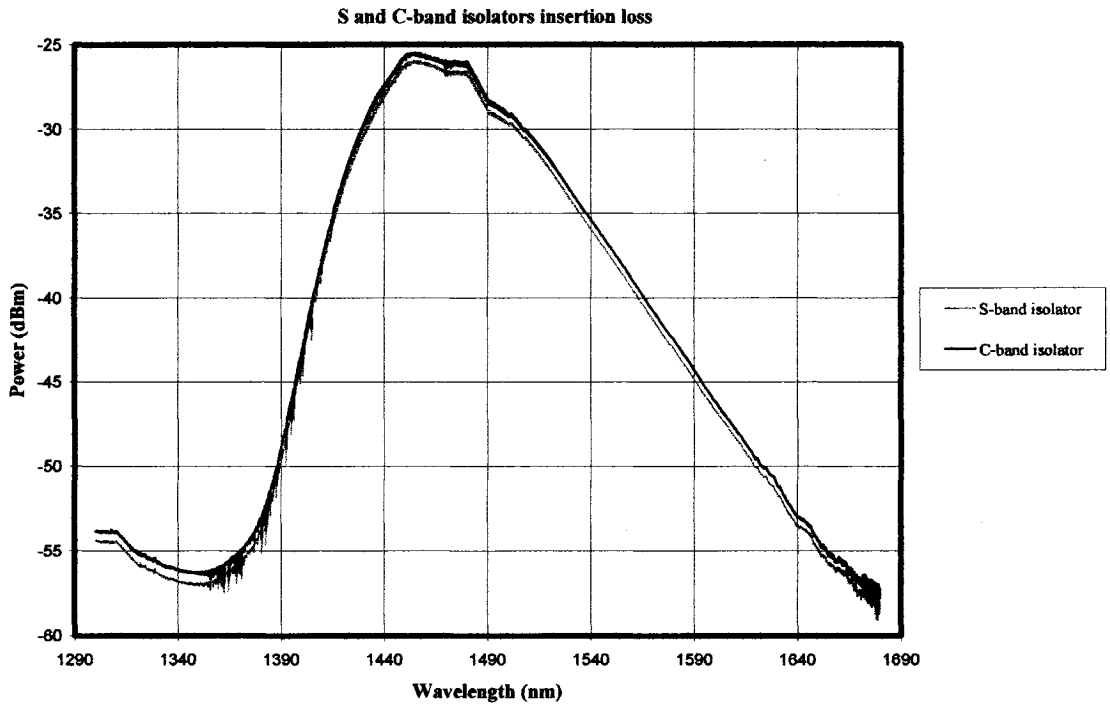

Figure 6-18 S and C-band isolators insertion loss.

For the P-SFRL to operate in the S-band, we must setup our system to *favour S-band lasing* by presenting S-band longitudinal modes/wavelengths with a lower loss than the C-band longitudinal modes/wavelengths (or alternatively, present C-band longitudinal modes/wavelengths with higher losses compared to those belonging to the S-band). The usual way to do this is to use an isolator that does not allow the C-band wavelengths to pass with ease (i.e. an isolator optimized for the 1460-1530 nm range only). Such an isolator was not available at BTI. However, observing the C-band isolator insertion loss and specs suggested that if we place the isolator in the reverse direction, it would present the C-band wavelengths with a much larger attenuation than those belonging to the S-band (since the C-band isolator had an operating range of only 1535-1560 nm, i.e. does not cover the S-band). Figure 6-19 shows the insertion loss of the C-band isolator when its in the normal and reverse directions using an ASE source. As we can see, the C-band wavelengths are signficantly attenuated compared to the S-band wavelengths.

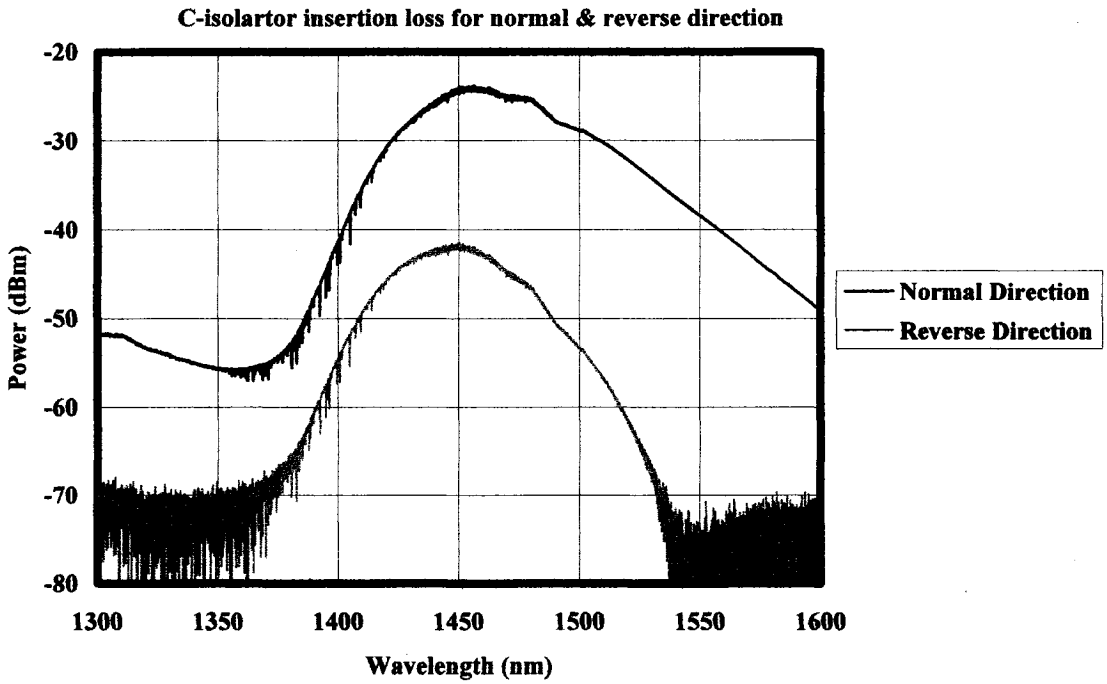

Figure 6-19 C-band isolator normal and reverse direction insertion loss.

If we setup our P-SFRL with the C-band isolator in reverse, we create a new system which presents the C-band longitudinal modes with much greater attenuation compared to all other longitudinal modes (especially those belonging to the S-band). As a result, C-band longitudinal modes will no longer be the winners of the gain competition and the S-band longitudinal modes will take their place (since they have been the 'runner ups' of the competition in all of the previous experiments). Figure 6-20 shows the experimental setup of the new P-SFRL while Figure 6-21 shows its output spectrum.

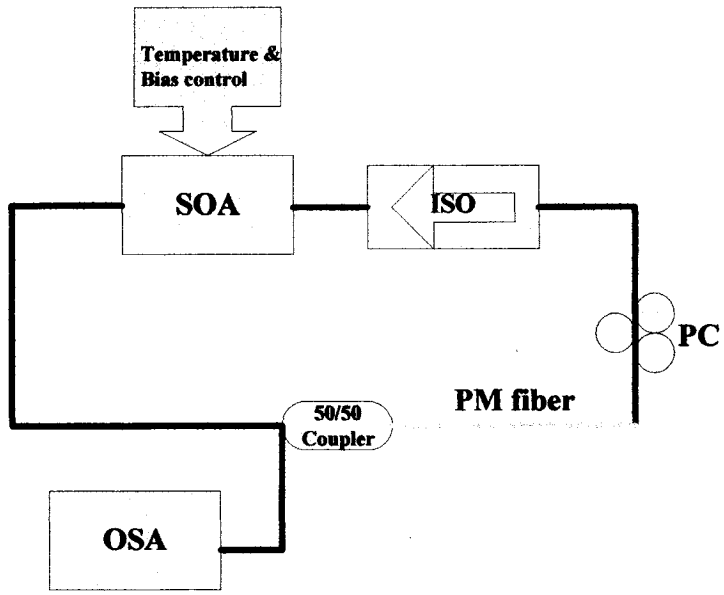

Figure 6-20 Modified S-band P-SFRL experimental setup. SOA is designed for S-band operation, ISO: C-band isolator.

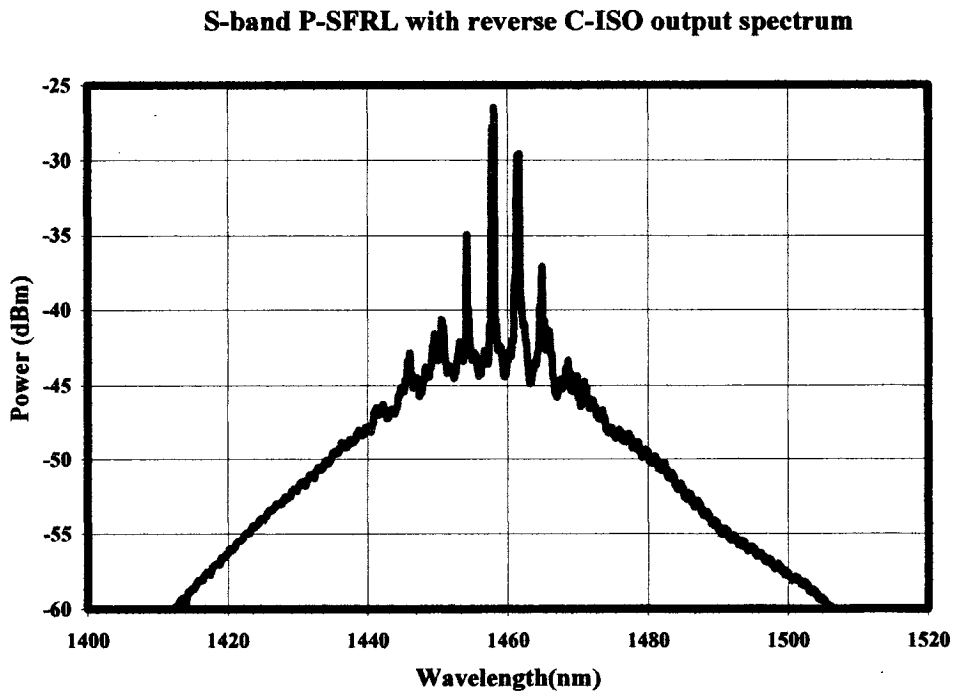

Figure 6-21 Output spectrum of modified S-band P-SFRL setup shwon in Figure 6-20.

Figure 6-21 demonstrates that the P-SFRL does indeed lase (multiwavelength operation) in S-band range, specifically in the 1440-1490 nm range (where the S-SOA produces ASE with highest power, Figure 6-16). Furthermore, the linewidth of the lasing longitudinal modes is much narrower compared to those of C-band P-SFRL of Figure 6-12 which uses the C-SOA (its output spectrum is shown in Figure 6-14). This is because the S-SOA has a higher PDG (1.5 – 2 dB) compared to C-band SOA (0.6 dB). As a result, the P-SFRL utilising the S-SOA has stronger polarization-dependant gain/loss wavelength selection mechanisms compared to the P-SFRL that use the C-SOA. This leads to significant enhancement in the P-SFRL's linewidth. This confirms the results presented in [Xu'02] and [Zho'98]. Figure 6-22 shows another OSA trace (0.02 nm resolution) of the modified S-band P-SFRL to confirm its narrow linewidth.

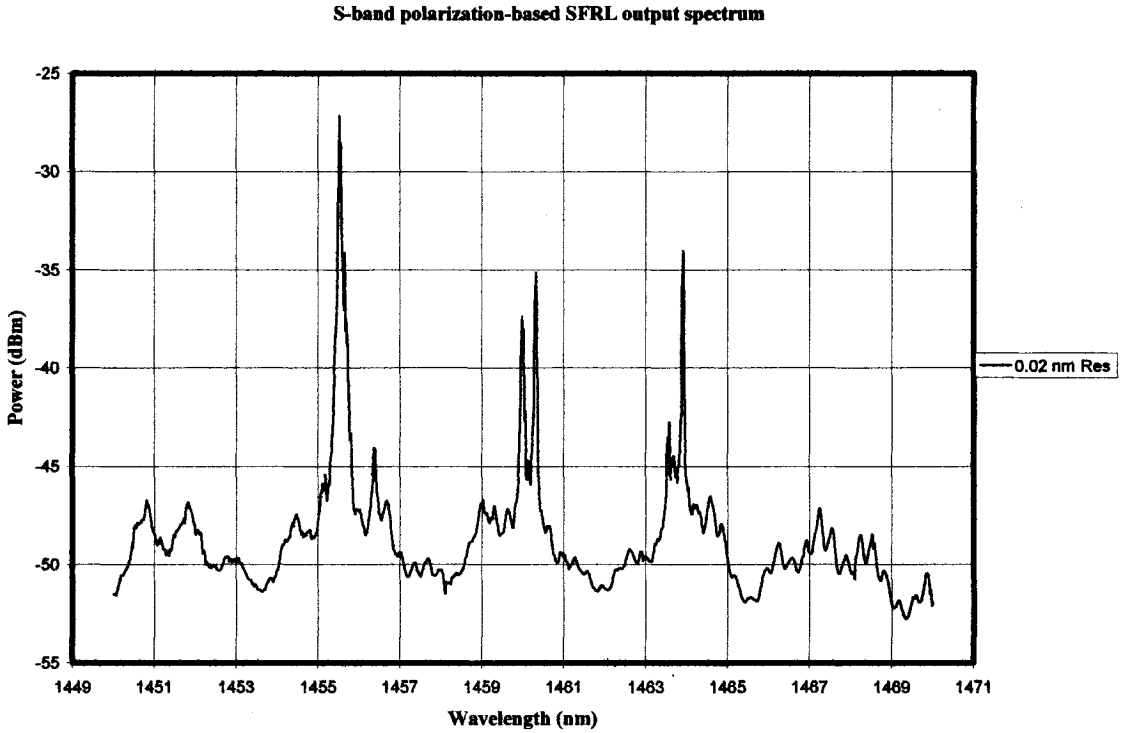

Figure 6-22 Output spectrum of modified S-band P-SFRL of Figure 6-20, 0.02 nm resolution.

Figure 6-23 shows the output spectrum for the modified S-band P-SFRL with different PC settings. This confirms the possibility of tuning the P-SFRL output based on the setting of the PC. The PC functions as another polarization-dependant gain/loss competitive mechanism. By changing the PC settings, different longitudinal modes of the P-SFRL will experience different gains/losses and become the output of the P-SFRL. Note that the longitudinal modes that lase are defined by the Lyot Filter transmission spectrum (section 6.3.2, Equation 6-19). Figure 6-24 shows the output power vs. S-SOA bias current for the modified S-band P-SFRL setup in Figure 6-20. This proves that the modified setup is indeed lasing but as expected its output power is very low. This is only due to the fact that the C-isolator is placed in reverse which, even though allows the modified P-SFRL setup to lase in the S-band, still presents a very large loss in the system. This can easily be avoided by using a dedicated S-band isolator, i.e. an isolator rated for the 1430-1530 nm range. Unfortunately we did not have access to such an isolator however, the C-band P-SFRL setup (which are similar in overall operation to the modified S-band P-SFRL setup) demonstrated high output powers ~ 9mW. We can expect similar output powers if we use a proper S-band isolator in our modified S-band P-SFRL setup.

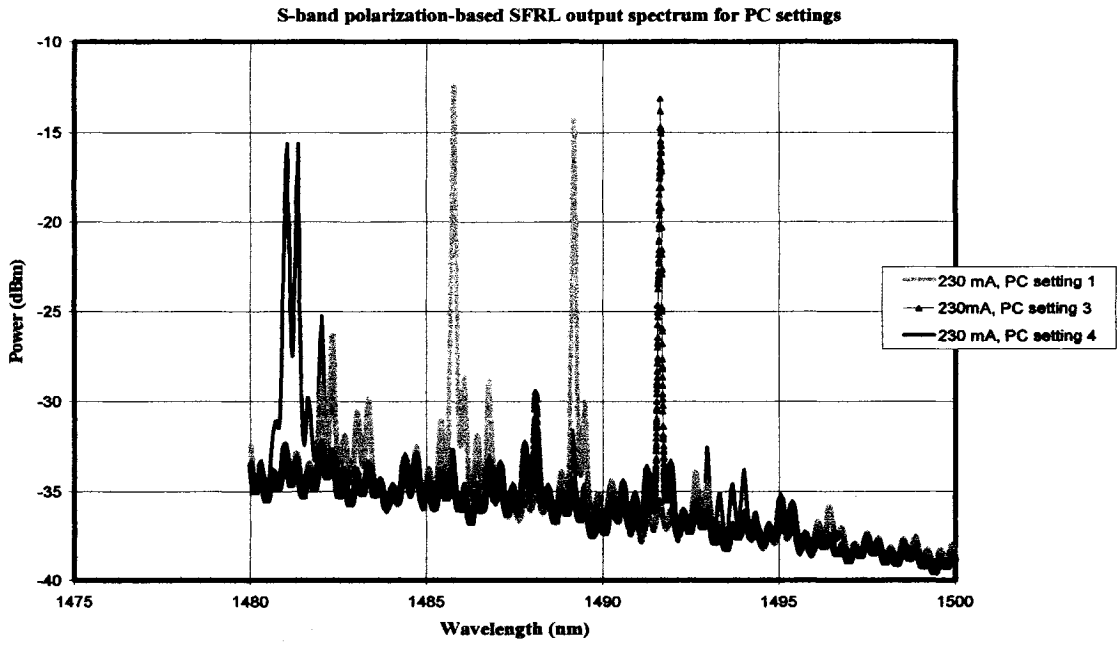

Figure 6-23 Output spectrum of modified S-band P-SFRL in Figure 6-20 for different PC settings

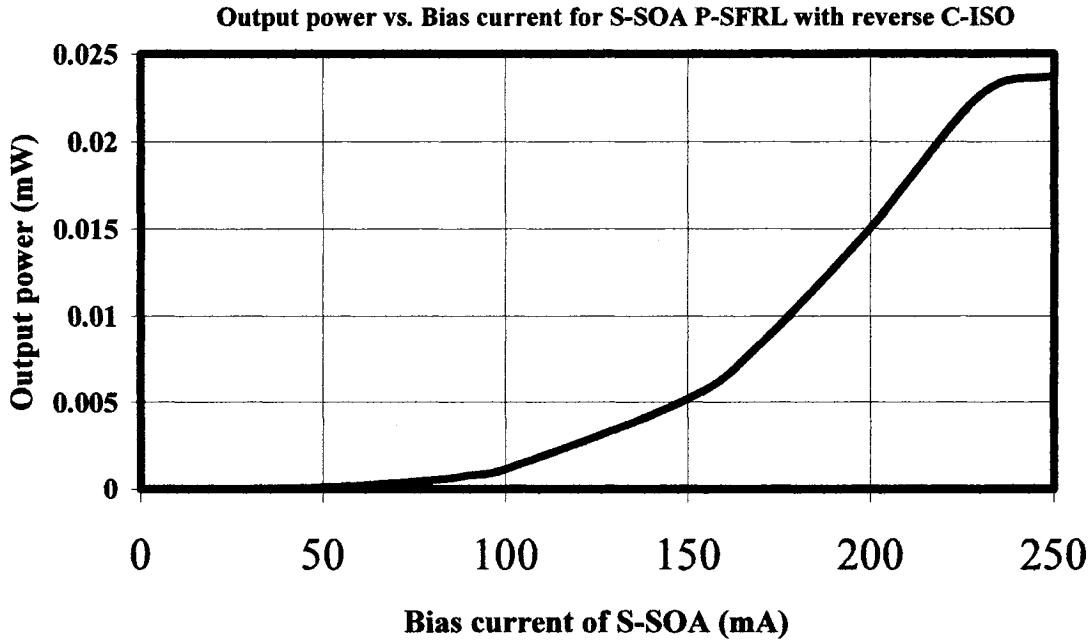

Figure 6-24 Threshold plot of modified S-band P-SFRL setup in Figure 6-20

6.4 Putting it all together, SFRLs as competitive optics systems.

Our investigation of the competitive interactions of the P-SFRL reveals several different and simultaneously occurring polarization dependant gain/loss competitive mechanisms. In essence, the P-SFRL is a WTA competitive optics system with various competitive mechanisms and their interactions define the output state of the P-SFRL. The longitudinal modes that experience the lowest overall loss are selected by the aforementioned competitive mechanisms to be the winners of the competition for the gain of the SOA and thus become the final output of the P-SFRL WTA system. The situation is also similar in F-SFRL but the selection 'rules' are not based on the polarization of the longitudinal modes but on weather the modes lie within the transmission bandwidth of the filtering element used. Table 6-2 gives a comparison between the F-SFRLs and P-SFRLs.

F-SFRL	P-SFRL
• Competition facilitated by a dedicated filter.	• Competition based on polarization of λs.
• Filter BW is usually small enough to support allow only one lasing wavelength.	• Often several λs can lase, multiwavelength operation.
• Has better immunity to environmental perturbations, primarily due to the presence of the filter. More stable output.	• Sensitive to environmental perturbations.
• Uni- and bi-directional operation possible.	• Uni- & bi-directional operation possible.
• External injection possible.	• Generally requires more components (PM fibre, linear polarizer, Polarization Controllers (PC)).
• Integration potential.	• Large SOA PDG (i.e. cheaper SOA) an advantage.

Table 6-2 Comparison between F-SFRLs and P-SFRLs

We identified five competitive mechanisms that select the output longitudinal modes of the P-SFRL: 1) 1) Optical fibre's birefringence and the corresponding transmission spectrum of the Lyot filter formed by using PM fibre in the ring cavity, 2) Attenuation levels of the optical fibre used (SMF-28 presents lowest attenuation to C-band wavelengths), 3) PC settings, 4) SOA' PDG and finally 5) PDL of passive components in the ring. Finally, Table 6-3 compares the C-SOA and S-SOA used in this work.

C-SOA	S-SOA
• Optimized for amplifying C-band signals: 1535-1565 nm range.	• Optimized for amplifying S-band signals: 1460-1530 nm range.
• Mounted on evaluation board with external C-band isolators.	• Mounted on evaluation board, no external isolators.
• Low PDG in C-band, ~0.6 dB.	• High PDG in S-band, 1.5-2 dB. • Low PDG in C-band, ~0.6 dB
• ~10 dBm output saturation power.	• >15 dBm output saturation power.

Table 6-3 Comparison between C and S-SOA used in experimental work.

6.5 Conclusion

In this chapter, a number of experiments were carried out to investigate the competitive optics nature of SFRLs. In particular, P-SFRL were investigated whose output is dependant on the various polarization-based wavelength selection mechanism present within the SFRL cavity. The experimental results confirm the competitive nature of the SFRL and help further the case for the competitive optics paradigm in saturated gain media (primarily SOA). Several different competitive mechanisms were discussed and demonstrated in the experiments and their various effects were investigated. It is interesting to note that an SOA with a high PDG (often considered a major disadvantage and an undesirable feature for DWDM systems) can be taken advantage of to create very narrow linewidth P-SFRL. It is important to note that the main disadvantage of P-SFRL is their stability since any environmental disturbances such as bending of the fibre (particularly SM fibre which has no polarization marinating capability) and temperature variations can significantly affect the output of the P-SFRL. This can be mediated by using only PM fibre or alternatively, integrating the SFRL which will minimise the environmental disturbances and stabilize its the output.

Chapter 7 Conclusions and Outlook

7.1 Summary

In Chapter 1, we carried out a general analysis of impairments facing current and future photonic technologies, and identified several all-optical enabling technologies for the next generation of photonic networks that can overcome these impairments. These key, all-optical technologies include new optical amplifiers, cascadable all optical logic, efficient and inexpensive 3R regeneration, wavelength conversion, and optical memory. An overview of the state of the art of these technologies was presented.

In Chapter 2, the Semiconductor Optical Amplifier (SOA) was introduced and its importance and role in current and future photonic networks was illustrated. The SOA was shown to be a fundamental optical device in the realisation of the key all-optical technologies which require an optical device exhibiting strong nonlinear behaviour. A brief comparison between bulk, Quantum Well, and Quantum Dot SOA properties was given and it was shown that QD-SOA devices possess superior properties over other SOA designs. It was argued that QD-SOA represent the next generation of SOA devices and could be deployed in future photonic networks with ultra-high data rates. The fundamental role of the rate equation model of the SOA was highlighted and a brief comparison between some of the most common SOA models was provided. The SOA model used in some of the simulations in this work was described.

Chapter 3 provided a detailed survey of some of the all-optical enabling technologies identified in Chapter 1. The amplet amplifier structure was described and compared with traditional Optical Amplifiers (OA). A comprehensive description of the main nonlinear phenomena in the SOA (XGM, XPM, and FWM) was given and some all-optical logic applications were presented. A general survey of promising 3R regeneration and wavelength conversion schemes was also presented.

Chapter 4 introduced the concept and general principle of competitive optics. The Lotka-Volterra coupled differential equations model was introduced to describe the mode competition that takes place in a competitive optics systems and circuits. Two schemes, Winner-Take-All (WTA) and Voting-Paradox (VP), were introduced as typical examples of competitive systems with decision-making capabilities. Simulations of these systems were carried out to illustrate their different modes of operation. A brief description of competitive systems in saturated gain media (in our case, SOA) was given and contrasted with equivalent implementations in photorefractive media. The similarities between the implementation in the two different gain media were highlighted.

Chapter 5 introduced the Semiconductor Ring Laser (SRL) and illustrated its importance as a basic all-optical competitive optics device. The principle of operation and a simple dynamical model of the SRL were described. A modified Lotka-Volterra model was presented to describe the SRL as a competitive optics system. To illustrate the principles and application of competitive optics in saturated gain media, some SRL-based applications were described and simulated using VPIcomponentMaker™: Active Photonics and MATLAB. The simulated applications included all-optical wavelength conversion and cascaded SRL circuits. The simulation results from the VPIcomponentMaker™: Active Photonics and MATLAB were compared and the role of Relaxation Oscillations and ASE noise on the output of the circuits was highlighted.

Chapter 6 presented several experimental investigations of SFRL in particular those based on polarization competition between the cavity modes. The role of the various polarization-based competitive mechanisms was investigated. In particular, it was found that the presence of PM fibre and high SOA PDG were necessary to ensure stable and narrow linewidth lasing.

7.2 Outlook and Future Work

The work presented here provides further proof of the applicability of competitive optics all-optical signal processing schemes. Using gain competition as the fundamental competitive

phenomena in SOA, we were able to illustrate important and fundamental all-optical signal processing applications through simulations.

The work presented here also supports the concept of the SRL as an all-optical competitive device that can serve as a basic unit in the realisation of important all-optical signal processing functions. The SRL can be made into a very compact and very low power structure called the micro-ring laser, which can be easily integrated [Hil'04]. It is therefore, quite feasible to construct sophisticated all-optical devices using arrays of (coupled/uncoupled) SRLs to perform important signal processing functions in future photonic circuits. For example, one can envision the construction of a multi-state all-optical flip-flop circuit based on multiple coupled micro-SRLs [Liu'03].

QD-SOA can further enhance the capabilities of SRL. Issues, such as the pattern effect, which plague bulk and to a lesser extent MQW SOA are very negligible in QD-SOA [Sug'02]. Furthermore, QD-SOAs can support much higher data rates (~ 160 Gbit/s) and therefore are much more attractive for deployment in future photonic networks [Sug'02].

Important issues remain however, that need to be addressed. The overshoot at the output of the SRL can have a detrimental effect on the performance of the signal processing circuits especially if these circuits are cascaded. Many research results have been reported in technical literature with the aim of reducing and suppressing RO in lasers and to a lesser extent in SOA. In the future, it is quite feasible to be able to utilise some of that research to reduce the SRL-SOA overshoot due to RO.

Further experimental work needs to be carried out to investigate some of the temporal properties of SFRL (particularly polarization-based ones) and to better optimize their performance.

7.3 Conclusion

Competitive optics has been proven to be a powerful all optical signals processing method in photorefractive material, dynamic gratings and SOAs. Simulations, presented in this work, of SRL-based devices utilising competitive optics principles via gain competition (Cross Gain Modulation) have proven their strong potential for wide-scale applications in future photonic networks: as wavelength converters and cascadable devices. Furthermore, SRL-based devices can be used as logic gates, 2R and 3R regenerators, and memory elements.

QD-SOA offers considerable advantages over traditional Bulk and MQW SOA and offers new all-optical functional possibilities, such as greater bandwidth, pattern-free operation, support of higher data rates, and lower threshold currents. These advantages will further the penetration of QD-SOA based competitive optics circuits into current and future photonic networks.

Bibliography

[Adm'85] M. J. Adams, "Analysis of semiconductor laser optical amplifiers," Proc IEE Part J, Optoelectron, vol. 132, pp. 58-63, Feb 1985.

[Agr'95] G. P. Agrawal, Semiconductor Lasers: Past, Present, and Future. New York: American Institute of Physics, 1995.

[And'91] D. Anderson, "Photorefractive flip-flop," Optics letters. Vol. 16, pp 250-252, Feb 1991.

[And'90] D. Z. Anderson, "Competitive and cooperative dynamics in nonlinear optical circuits," (invited chapter) in An Introduction to Neural and Electronic Networks (S. V. Sonneteer, L. J. Davis and C. Lau, Eds., Academic Press, 1990), pp. 349-362.

[Bah'01] A. Bhardwaj, "All-Optical Logic Circuits based on the Polarization Properties of Non-Degenerate Four-Wave Mixing," Ph.D. thesis, California Institute of Technology, Pasadena, California 2001.

[Ben'91] C. Benkert, "Controlled competitive dynamics in a photorefractive ring oscillator: "Winner-takes-all" and the "voting-paradox" dynamics," Physical Review A, vol. 44, pp ,Oct 199.

[Ber'01] J. Bernerd, "Semiconductor Optical Amplifiers," pp. 36-38, Spie OE magazine.

[Bog'03] Antonella Bogoni, "Effective model for the design of ultrafast all optical signal processors based on SOAs," IEEE photonics tech letters, vol 15, pp, Nov 2003.

[Cal'05] N. Calabretta, "Optical signal processing based on self-induced polarization rotation in a semiconductor optical amplifier," J. of Lightwave Technology, vol. 22, pp. 372-381, Feb 2001.

[Che'04] H. Chen, "Dynamics of widely tunable single-frequency semiconductor fiber ring laser,", Physics Letters A, vol. 320, pp. 333-337, 2004.

[Cho'02] K.K. Chow, "Widely tunable all-optical wavelength converter using a fiber ring cavity incorporating a semiconductor optical amplifier," Optics Communications, vol. 203, pp. 101-106, Mar 2002.

[Con'01] M. J. Connelly, "Wideband SOA steady state numerical model," IEEE journal of QE, vol. 37, pp 439-447, Mar 2001.

[Con'02] M. J. Connelly, Semiconductor Optical Amplifiers. Dordrect, The Netherlands: Kluwer, 2002.

[Con'02] M. J. Connelly, Semiconductor Optical Amplifiers. Dordrect, The Netherlands: Kluwer, 2002.

[Con'02a] M. J. Connelly, "Wideband dynamic numerical model of a tapered buried ridge stripe semiconductor optical amplifier gate," IEE Proceedings - Circuits, Devices and Systems. Vol. 149, pp. 173-178. Jun 2002.

[Dam'01] V. B. Damilao, "Two-beam coupling modules for photorefractive optical circuits", Applied Optics, vol. 40, pp. 3365-3370, Jul 2001.

[Dom'00] R. Dommelen, "All-optical logic using SOA wavelength converters," Dalhousie University, Halifax, Oct 2000.

[Fer'05] Marcio Fertais, Optiwave Corporation, private communication.

[Gav'03] G. Gavioli, "Novel, High-Stability 3R All-Optical Regenerator based on Polarization Switching in A Semiconductor Optical Amplifier," in Proc IOOC-ECOC, 2003.

[Hab'00] T. Haber, "Tunable erbium-doped fibre ring laser precisely locked to the 50-GHz ITU frequency grid," IEEE Photonics Technology Letters, vol. 12, pp.1456-1458, Nov. 2000.

[Hal'98] K. L. Hall, "100-Gbitsbitwise logic," Optics Letters, vol. 23, pp 1271-1273, 1998.

[Hal'03] T. J. Hall, "Active photonic microprocessors," private communication.

[Ham'01] S. A. Hamliton, "Overview of 100 Gbit/s All-Optical Packet Processing Effort at MIT Lincoln Laboratory," MIT Lincoln Laboratory, Optical communications Technology group.

[Hen'85] I. D. Henning, "Performance predictions from a New optical amplifier model," IEEE journal of Quantum Electronics, vol. 21, Jun 1985.

[Hil'01] M. T. Hill, "All-optical Flip Flop based on coupled ring laser Diodes," IEEE journal of quantum electronics, vol. 37, pp. 405-413, Mar 2001.

[Hil'01a] M. T. Hill, "Fast Optical Flip-Flop By Use of Mach-Zehnder Interferometers," Microwave and Optical Technology Letters, vol. 31, pp. 411-415, Dec 2001.

[Hil'02] M. T. Hill, "All fibre-optic neural network using coupled SOA based ring lasers," IEEE transactions on neural networks, vol. 13, pp 1504-1513, Nov 2002

[Hil'04] M. T. Hill, "A fast low-power optical memory based on coupled micro-ring lasers," Nature, vol. 432, pp. 206-209, Nov 2004.

[Kam'03] Kamelian Ltd, "Semiconductor Optical Amplifiers (SOAs) as Power Boosters, Applications Note No. 0001," Kamelian Ltd technical articles, pp. 1-11, Jan 2003.

[Lan'76] R. Lang, "Suppression of relaxation oscillation in the modulated output of semiconductor lasers,", IEEE journal of Quantum Electronics, pp. 194-199, Mar 1976.

[Led'00] N. Ledentsov, "Quantum-Dot Heterostructure Lasers," IEEE journal of selected topics in quantum electronics, vol. 6, pp. 439-451, May/June 2000.

[Lee'03] Chung Chiu Lee, "Suppression of Pulse Shape Distortion Caused by Frequency Drif in a Harmonic Mode-Locked Semiconductor Ring Laser," IEEE Photonics Technology Letters, vol. 15, pp. 685-660, May 2003.

[Lee'04] K. L. Lee, "Optically controlled Sagnac loop comb filter," Optics Express, vol. 12, pp. 6335-6340, 2004.

[Lin'04] G. Lin, "Dynamics of optical backward-injection-induced gain-depletion modulation and mode locking in semiconductor optical amplifier fibre lasers," Optics express, vol. 12, pp. 2017-2026, May 2004.

[Liu'02] Y. Liu, "All-optical buffering in all-optical packet switched cross connects," IEEE Photonics Technology Letters, vol. 14, pp. 849-851, Jun 2002.

[Liu'03] Y. Liu, "All-Optical Buffering Using Laser Neural Networks," IEEE Photonics Technology Letters, vol. 15, pp. 596-598, Apr 2003.

[Liu'03a] L. Yiu, "Three-State All-Optical Memory Based on Coupled Ring Lasrs," IEEE Photonics Technology Letters, vol. 15, pp. 1461-1463, Oct 2003.

[Lot'25] A. J. Lotka, Elements of Physical Biology, Baltimore, Baltimore,1925.

[Low'88] A. J. Lowery, "New inline wideband dynamic semiconductor laser amplifier model," Proc. Inst. Elect. Eng., pt. J, vol. 135, pp. 242-250, (month) 1988.

[Lu'04] Z. Lu, "A large dynamic-range self-adjusting output-power laser devise," Microwave and Optical technology letters, vol 43, pp. 532-535, Dec 20 2004.

[Mør'03] J. Mørk, "The Dynamics of Semiconductor Optical Amplifiers: Modeling and Applications," Optics and Photonics news, vol. 14, pp 42-48, Jul 2003.

[Mor'93] S. Ruiz-Moreno, "Practical method for modelling the nonlinear behaviour of a travelling wave semiconductor optical amplifier," IEE proc, J, vol. 140, pp , Feb 1993.

[Nie'00] M. L. Nielsen, "A transfer function approach to the small signal response of saturated SOAs," Journal of lightwave technology, vol. 18, pp, Dec 2000.

[Nip'00] "All-optical 3R that retains input wavelength using Sagnac Interferometer integrated with Parallel- Amplifier Structure (SIPAS)". White paper by Nippon Telegraph and Telephone Corporation, 2000.

[Num'04] T. Numai, Fundamentals of Semiconductor Lasers. New York, Springer-Verlag, 2004.

[Occ'02] L. Occhi, "Semiconductor Optical Amplifiers made of Ridge waveguide Bulk InGaAsP/InP: Experimental Characterisation and Numerical Modelling of Gain, Phase, and Noise," PhD thesis, Eidgenössische Technische Hochschule Zürich.

[Ple'04] N. Pleros, "SOA-Based Multi-Wavelength Laser Sources," Fiber and Integrated Optics, vol. 23, pp. 263–274, 2004.

[Pen'02] C. Peng, "Theoretical analysis of actively mode-locked fibre ring laser with semiconductor optical amplifier," Optics communication, vol. 209, pp. 181-192, Aug 2002.

[Pen'92] E. T. Peng," Properties of an external-cavity travelling-wave semiconductor ring laser," Optics Letters, vol. 17, pp 55-57, Jan 1992.

[Sar'01] Bernd Sartorius, "3R All optical Signal Regeneration," in Proc. IOOC-ECOC, 2001.

[Sor'03] M. Sorel, "Operating Regimes of GaAs–AlGaAs Semiconductor Ring Lasers: Experiment and Model," IEEE journal of quantum electronics, vol. 39, pp. , Oct. 2003

[Spi'03] L. Spiekman, "Optical amplification for metro: EDFA/EDWA amplets and semiconductor technologies," in Proc. OFC, 2003, pp 443.

[Stu'00] K. E. Stubkjaer, "Semiconductor Optical Amplifier-Based All-Optical Gates for High-Speed Optical processing," Invited Paper, IEEE journal on selected topics in Quantum Electronics, Vol. 6, pp , Nov/Dec 2000.

[Sug'02] M. Sugawara, "Quantum-dot semiconductor optical amplifiers for high-bit-rate signal processing up to 160 Gbit/s and a new scheme of 3R regenerators,". Measurement Science Technology, vol. 13, pp 1683–1691, (month) 2002.

[Sug'03] M. Sugawara, "Quantum-Dot Semiconductor Optical Amplifiers," in OFC 2003.

[Vol'31] V. Volterra, Lecons sur la Theorie Mathematiques de la Lutte our la Vie, Gautheir-Villars, Paris, 1931.

[VPI'05] VPIcomponentMaker : active photonics manual, version 6.5

[Won'00] W. M. Wong, "Dynamic model of tapered semiconductor lasers and amplifiers based on transmission-line laser modelling," IEEE Journal of Selected Topics vol. 6, pp 585-596, July-Aug. 2000.

[Wu'00] C. Wu, "High-repetition-rate optical pulse generation using a rational harmonic mode-locked fiber laser," IEEE journal of Quantum Electronics, vol. 36, pp. 145-150, Feb 2000.

[Xin'04] Z. Xinliang, "Tunable and self-probed wavelength conversion in an SOA-based fibre-ring laser," Microwave and Optical technology letters, vol. 41, pp. 237-241, May 2004.

[Xu'02] Lei Xu, "Optical Spectral Bistability in a Semiconductor Fiber Ring Laser Through Gain Saturation in an SOA,", IEEE photonics technology letters, vol. 14, pp. 149-151, Feb 2002.

[Xu'03] Q. Xu, "Theoretical analyses on short-term stability of semiconductor fibre ring lasers," IEEE journal of quantum electronics, vol 29, pp. 1260-1265, Oct 2003.

[Yao'05] J. Yao, "Investigation of a multiwavelength fiber ring laser that incorporates a semiconductor optical amplifier as a phase modulator," IEEE journal of Lightwave Technology, vol. 23, no. 8, pp. 2484-2490, August 2005.

[Yik'01] S. Yikai, "Simultaneous 3R regeneration, and wavelength conversion using a fibre-parametric limiting amplifier," in Proc OFC, 2001.

[Zha'01] K. J. Zhang, "Bandwidth-expandable erbium-doped fibre amplets," IEEE Photonics Technology Letters, vol. 13, pp 281-283, Apr 2001.

[Zha'04] S. Zhang, "Ring-Laser Optical Flip-Flop Memory With Single Active Element," IEEE Journal of Selected Topics in Quantum Electronics, vol. 10, Sep/Oct 2004.

[Zha'05] C. Zhao, "Tunable all-optical NOR gate at 10 Bb/s based on SOA fiber ring laser," Optics express, vol. 13, pp. 2793-2798, Apr 2005.

[Zha'05a] S. Zhang, "Multistate Optical Memory Based on Serially Interconnected Lasers," IEEE photonics technology letters, vol. 17, pp. 1962-1964, Sep 2005.

[Zho'98] D. Zhou, "A Widely tunable narrow linewidth semiconductor fiber ring laser." IEEE photonics technology letters, vol. 10, pp. 781-783, Jun 1998.

[Zho'02] Kejiang Zhou, "Comb filter based on an all polarization maintaining fiber loop and its applications," Applications of Photonic Technology 5, Proceedings of SPIE Vol. 4833, pp. 988-994, 2002.

[Zim'02] D.R. Zimmerman, "Amplets: application and technology," in Proc CLEO, 2002, pp 443 – 444.

[Zim'04] D. R. Zimmerman, "Amplifiers for the masses: EDFA, EDWA, and SOA amplets for metro and access applications," Journal of Lightwave Technology, vol.22, pp 63-70, Jan. 2004

[Zoi'00] K. Zoiros, "Experimental and theoretical studies of a high repetition rate fibre laser, mode-locked by external optical modulation," Optics communication, vol. 180, pp. 301-315, Mar 2000.

[Zoi'05] K. Zoiros, "Complete theoretical analysis of actively mode-locked fiber ring laser with external optical modulation of a semiconductor optical amplifier," Optics communication, vol. 254, pp. 310-329, Oct 2005.